SYNTHESIS AND CHARACTERIZATION OF DIPHOSPHINE LIGANDS AND DIPHOSPHINE SUBSTITUTED OSMIUM AND RUTHENIUM CLUSTERS

Srikanth Kandala, M.S.

Dissertation Prepared for the Degree of

DOCTOR OF PHILOSOPHY

UNIVERSITY OF NORTH TEXAS

August 2007

APPROVED:

Michael G. Richmond, Major Professor and
Chair of the Department of Chemistry
Martin Schwartz, Committee Member
Diana Mason, Committee Member
Sushama Dandekar, Committee Member
Sandra L. Terrell, Dean of the Robert B.
Toulouse School of Graduate Studies

Kandala, Srikanth, Synthesis and characterization of diphosphine ligand substituted osmium and ruthenium clusters. Doctor of Philosophy (Organic Chemistry), August 2007, 133 pp., 23 schemes, 16 tables, 30 figures, 117 references.

The kinetics for the bridge-to-chelate isomerization of the dppe ligand in $H_4Ru_4(CO)_{10}$(dppe) have been investigated by UV-vis and NMR spectroscopies over the temperature range of 308-328 K. The isomerization of the ligand-bridged cluster 1,2-$H_4Ru_4(CO)_{10}$(dppe) was found to be reversible by ^{31}P NMR spectroscopy, affording a K_{eq} = 15.7 at 323 K in favor of the chelating dppe isomer. The forward (k_1) and reverse (k_{-1}) first-order rate constants for the reaction have been measured in different solvents and in the presence of ligand trapping agents (CO and PPh_3). On the basis of the activation parameters and reaction rates that are unaffected by added CO and PPh_3, a sequence involving the nondissociative migration of a phosphine moiety and two CO groups between basal ruthenium centers is proposed and discussed.

The substitution of the MeCN ligands in the activated cluster 1,2-$Os_3(CO)_{10}(MeCN)_2$ by the diphosphine ligands dppbz proceeds rapidly at room temperature to furnish a mixture of bridging and chelating $Os_3(CO)_{10}$(dppbz) isomers and the ortho-metalated product $HOs_3(CO)_9[\mu$-$(PPh_2)C=C\{PPh(C_6H_4)\}C_4H_4]$. Thermolysis of the bridging isomer 1,2-$Os_3(CO)_{10}$(dppbz) under mild conditions gives the chelating isomer 1,1-$Os_3(CO)_{10}$(dppbz), molecular structure of both the isomers have been determined by X-ray crystallography. The kinetics for the ligand isomerization has been investigated by UV-vis and ^1H NMR spectroscopy in toluene solution over the temperature range of 318-343 K. On the basis of kinetic data conducted in the presence of added CO and the Eyring activation parameters, a non-

dissociative phosphine migration across one of the Os-Os bonds is proposed. Ortho metalation of one of the phenyl groups associated with the dppbz ligand is triggered by near-UV photolysis of the chelating cluster 1,1-$Os_3(CO)_{10}$(dppbz).

The triosmium cluster 1,2-$Os_3(CO)_{10}(MeCN)_2$ reacts with the diphosphine ligand 3,4bis(diphenylphosphino)-5-methoxy-2(5)H-furanone (bmf) at 25 ºC to give the bmf-bridged cluster 1,2-$Os_3(CO)_{10}$(bmf). Heating 1,2-$Os_3(CO)_{10}$(bmf) leads to an equilibrium with the chelating isomer 1,1-$Os_3(CO)_{10}$(bmf). The molecular structure of each isomer has been crystallographically determined, and the kinetics for the isomerization has been investigated by UV-vis and ^{1}H NMR spectroscopy. The reversible nature of the diphosphine isomerization has been confirmed by NMR measurements, and the forward (k_1) and reverse (k_{-1}) first-order rate constants for the bridge-to-chelate isomerization have been determined. Thermolysis of the 1,1-$Os_3(CO)_{10}$(bmf) cluster (>110 ºC) leads to regiospecific activation of C-H and P-C bonds, producing the hydrido clusters $HOs_3(CO)_9$[μ-PPh_2C=C{PPh(C_6H_4)} CH(OMe)OC(O)] and the benzyne clusters $HOs_3(CO)_8$(μ_3-C_6H_4)[μ-PPhC=C(PPh_2)CH(OMe)OC(O)]. The hydride and benzyne clusters, which exist as a pair of diastereomers, have been fully characterized in solution by IR and NMR spectroscopy, and the molecular structure of one benzyne cluster (major diastereomer) has been determined by X-ray crystallography.

ACKNOWLEDGEMENTS

Standing on the brink of completing my doctorate degree, I look back with deep respect and admiration towards my advisor, colleagues, friends and family members who supported and encouraged me through this critical period of my education.

My advisor Dr. Michael G. Richmond, distinguished and exemplary scientist, patiently guided me through this study, and I thank him for his unrelenting support, and advice to me in all aspects of my work. His cheerful and candid suggestions and comments about my work and research were a constant inspiration to work harder and achieve better results.

I also owe my success in the completion of this substantial, but exhausting task, to the other members of my committee, Dr. Martin Schwartz, Dr. Susama Dandekar and Dr. Diana Mason, for their critical view of my work, and invaluable pointers and comments. Prof. William H. Watson, Texas Christian University and Dr. Xiaping Wand, University of North Texas, are acknowledged for all of the reported X-ray data in this dissertation.

Guanmin Wu and Dr. Bhaskar Poola are accomplished and admirable seniors, whose professionalism I emulated in my lab work. Their suggestions and training groomed me to develop technical skills, work ethics, and enthusiasm for my work. The completion of this dissertation was possible due to the generous efforts, friendship, and backing of my colleagues Tau Chen, Shih-Huang Huang, and Kevin Phan who also provided a lively lab environment and valuable research discussions.

My close friends Kiran Dittakavi, Praveen Nalla, Aakriti Tandon, Sreekar Marpu and especially Ushasree Kaipa were always optimistic and reassuring about my

success in an academic career while at UNT. Their proximity and friendship helped me maintain a good state of mind while going through this crucial period of time.

My family has provided me with constant love, affection, encouragement and financial support. They have inculcated in me deep moral values, and a spirit to fight till I achieve my goals. Their love has been the driving force of my life and work, miles away from home. I am indebted to my parents, K. Srinivasa Chary and Vijaya Lakshmi, for believing in me and giving me the opportunity to pursue my Ph.D. in the U.S. My dear brother Sridhar, and my sister, Sridevi, have been my companions, and helped me sail smoothly through all my trials and tribulations during this time. My family stood by me and my efforts, no matter what. I am deeply moved and honored to dedicate my work to my family members.

Finally I wish to thank Robert A. Welch Foundation for their financial support.

TABLE OF CONTENTS

LIST OF TABLES

Page

LIST OF FIGURES

Page

LIST OF SCHEMES

CHAPTER 1

INTRODUCTION

Transition-metal organometallic chemistry lies at the interface between classical organic and inorganic chemistry since it involves the interaction between inorganic metal ions and organic molecules and organic functional groups. The field of organometallic chemistry deals with compounds containing a metal-carbon bond(s) and has rapidly increased in importance over the past few decades since the landmark discoveries of ferrocene, Wilkinson's catalyst, Ziegler's catalyst and the Wacker process.[1] Organometallic compounds, particularly those containing transition metals, have found many applications in homogeneous catalysis, reagents that are capable of promoting novel organic transformations, and as precursors for the construction of solid-state devices, in addition to playing crucial roles in biological systems.[2]

Organometallic compounds are generally very labile and their reactivities are high. Hence, these organometallic compounds may be exploited by taking advantage of their high reactivity. In recent years, numerous applications that employ organometallic compounds in organic synthesis have been uncovered and a growing number of scientists continue to pursue research in this area.

The general acceptance of new metal-assisted reactions in a typical organic laboratory is rather low. Some of the apparent reasons are a lack of understanding and familiarity with the concepts of organometallic chemistry. It will become necessary for synthetic chemists to understand the underlying reactions in the coordination sphere of metal atoms, fundamental metal modified

transformations and ligand modified metal fragments. Different types of ligands coordinate with transition metals and depending on the coordination reactivity of these ancillary ligands, the stability and reactivity of the associated metals may change dramatically. Well-defined, stepwise kinetic studies and stoichiometric model reactions are necessary to elucidate a specific catalytic cycle.

In 1884, Ledwing Mond's work led to an important advancement in the refining of nickel. He discovered that the nickel valves used in the production of soda ash were consumed by carbon monoxide.[2] This led Mond to study the reaction between Ni powder and CO, which afforded the volatile compound, $Ni(CO)_4$, the first known metal carbonyl. Now, metal carbonyls are one of the most common and well-studied metal-ligand systems. Carbon monoxide is an unsaturated ligand and is a strong π-acceptor. The CO HOMO, which is defined by a lone electron pair that is largely localized on the carbon atom, donates its pair of electrons to the LUMO of the metal (empty $M(d_\sigma)$ orbital) and the metal HOMO (filled $M(d_\pi)$ orbital) back donates a pair of electrons to the LUMO on the CO. The result is that the carbon becomes more positive on coordination and the oxygen becomes more negative. This translates into a polarized CO ligand on coordination and this metal-induced polarization chemically activates the ligand, making the carbon more sensitive to nucleophilic and the oxygen more sensitive to electrophilic attack.[3] The reaction in Scheme 1.1 gives a carbene-like intermediate. This reaction is of importance because it represents a rare way in which a tightly bound CO may be removed under mild conditions. This, in turn,

generates an open or vacant coordination site at the metal center and facilitates the facile substitution of a CO group by an incoming ligand.

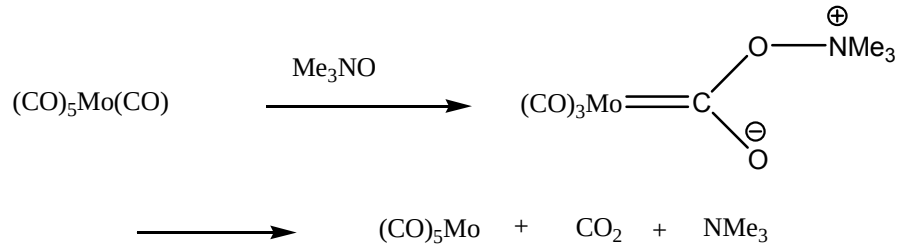

Scheme 1.1 Nucleophilic attack at a carbon atom in a metal carbonyl.

Carbon monoxide has a high tendency to bridge two or more metals. There are many examples in literature where a CO ligand simultaneously bridges two metal centers.[4] The electron count of the ligand remains unchanged on going from terminal to bridging group. A terminal CO ligand donates two electrons to one metal and when it acts as a bridging group between two metals, it donates one electron to each metal. Cotton has studied semi-bridged carbonyls in which the CO ligand is neither fully terminal nor fully bridged but intermediate between the two.[4] This is one of the many cases in organometallic chemistry where a stable species is intermediate between two bonding types. Triply bridged and even quadruply bridged CO ligands are also known.[4c] One of the earliest known examples of a cobridged compound is the tricobalt cluster $(Cp^*Co)_3(\mu_3\text{-}CO)_2$, where the CO ligands cap each triangular cobalt face in a triply bridged fashion.

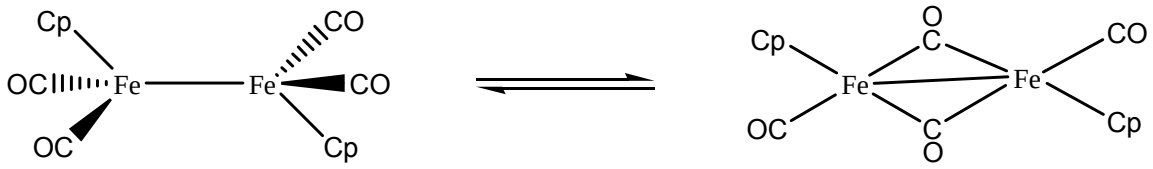

Figure 1.1 CO exchange mechanism.

Besides metal carbonyls, organometallic compounds with σ-bound ligands such as alkyls, aryls, halides and hydrides have been extensively studied. In addition to σ-bound one-electron donor ligands, there exist many examples of π-bound ligands. The first π-bonded organometallic compound that was synthesized was Zeise's salt $K[PtCl_2(ethylene)].H_2O$, which was originally prepared from the reaction of $PtCl_2$ and ethylene, and shown to contain a π-coordinated ethylene ligand.[4-7]

1.1. Metal Clusters

Cluster compounds are molecules containing three or more metal atoms connected by direct metal-metal bonds. Rather than forming chains like carbon, metal clusters tend to agglomerate so as to form a maximum number of M-M bonds whose close-packed structures resemble the motif exhibited by elemental metals. Early interest in the study of cluster chemistry stemmed from the fact that polynuclear clusters were proposed to serve as solution-soluble models for heterogeneous and alloy catalysts.[8] Cluster compounds contain a metal-metal framework that facilitates the coordination of the ancillary ligands to more than one metal center. Multi-metal substrate binding can modify the chemical reactivity of a ligand in a way not possible in mononuclear complexes, leading to multicenter activation and multicenter reactions (Scheme 1.2).[9]

Metal clusters can also act as electron reservoir compounds with charge-donating and charge-accepting properties.[10] Such clusters have a much lower ionization energy than that of an isolated atom and also have a higher electron affinity than most simple mononuclear compounds. Multinuclear metal clusters

contain a greater number of accessible redox states than their mononuclear counterparts and many of them exhibit multiple reversible redox states. Depending on the metal(s), the ligand(s), and redox stability, the metal framework may remain intact or undergo polyhedral fragmentation upon oxidation/reduction. Metal clusters can act as storehouses for the release and uptake of catalytically active fragments, while the breaking of M-M bonds can provide coordinatively unsaturated sites for the activation and coordination of incoming organic substrates. Some cluster compounds have been reported to be efficient catalysts for different types of reactions such as isomerization, hydrogenation, and hydroformylation of alkenes.[11] For example, the catalytic hydrogenation activity displayed by tetranuclear ruthenium carbonyl systems containing chiral diphosphine auxiliaries have been investigated.[11] The ability of a metal cluster to activate more than one substrate would be useful in designing specific catalysts with site-specific activations. An important factor in all these reactions is the nature of the metal-metal bonds in the cluster, structural geometry of the cluster, and nature of the ancillary ligands.

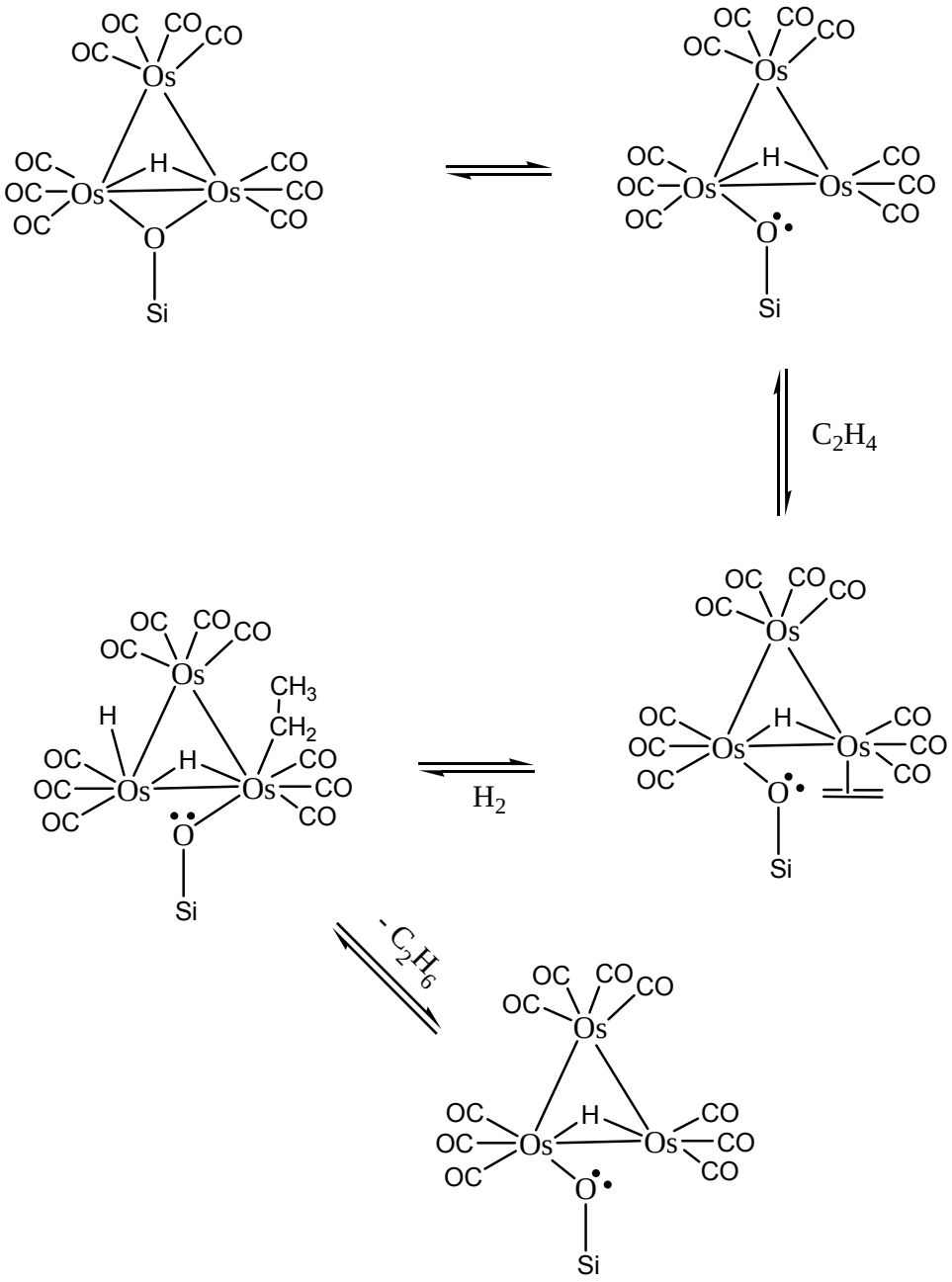

Scheme 1.2 Hydrogenation of ethylene by the silica-supported triosmium cluster.

1.2. Phosphine Ligands

Among the many ligands that can bind to transition metals, tertiary phosphines, PR_3, are important because they constitute one of the few series of ligands in which the steric and electronic properties of the ligand can be altered in a periodic and systematic fashion by varying the nature of the R-group. Transition-metal complexes and clusters have a high coordination affinity for a variety of monodentate, bidentate, and polydentate phosphine ligands. The use of phosphine ligands is necessary for nearly all homogeneous catalysis employing precious metals.[12] The choice of the right ancillary ligand can influence the shielding and steric properties of catalysts, electron density at the metal center(s), and the reactivity of the participating species in a catalytic cycle. Therefore, a wide range of phosphine ligands have been designed and investigated for their catalytic efficacy. Several metal catalysts containing mono- and bidentate phosphine ligands have been shown to be successful in Heck, Suzuki, and Buchwald-Hartwig cross-coupling reactions.[13] Among the common monodentate ligands, triarylphosphines, tricyclohexylphosphine, tri(tert-butyl)phosphine and trimethylphosphine continue to receive the bulk of the attention. Chiral monodentate phosphines have established their position as some of the most effective ligands in asymmetric homogeneous catalysis.[14] Figure 1.2 shows some common monodentate and bidentate phosphine ligands.

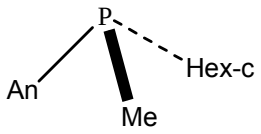

(S)-CAMP

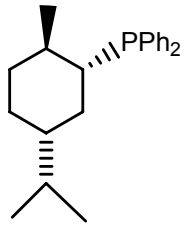

neomethyldiphenylphosphine [NMDPP]

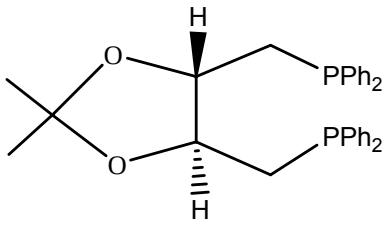

(S,S)-DIOP

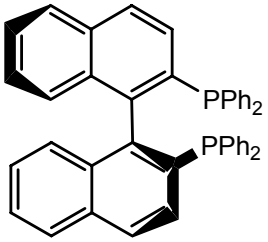

(S)-2,2'-bis(diphenylphosphino)-
1,1'-binaphthyl [(S)-BINAP]

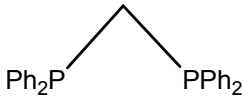

bis(diphenylphosphino)methane [dppm]

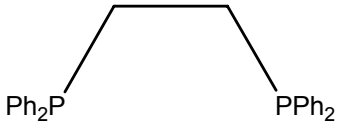

1,2-bis(diphenylphosphino)ethane [dppe]

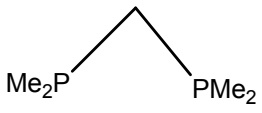

bis(dimethylphosphino)methane [dmpm]

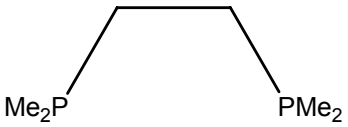

1,2-bis(dimethylphosphino)ethane [dmpe]

Figure 1.2 Common mono- and bidentate phosphine ligands.

Many phosphine-metal complexes have found broad application in catalytic reactions, especially in the reactions that involve oxidative addition, insertion, and reductive elimination steps. Tertiary phosphine ligands usually remain coordinated to transition-metal complexes throughout a catalytic cycle because of their high affinity for the metal, especially with late transition metals,

and they can stabilize low-valent metal intermediates, allowing the high activity of the catalyst to be maintained. The phosphine ligands used in homogeneous catalysis are often modified in order to influence the activity and selectivity of the actual or working catalyst. Thus, one of the most exciting and challenging subjects in the research of new catalytic systems is the development of new, diverse, and stable phosphine ligands that will influence the reaction efficiency in terms of catalytic activity and enantioselectivity.

The reactivity of phosphine ligands with multinuclear metal carbonyl clusters has been explored extensively with respect to the bonding mode(s) adopted by a phosphine ligand upon coordination.[15-18] In recent years, a wide range of clusters that possess simple terminal, edge-bridged, and face-capped phosphine ligands have been prepared from the reaction of tertiary phosphines with metal clusters.[19-20] These studies involving the reaction of metal clusters with different phosphine ligands have led to a greater understanding of the factors responsible for facile P-C bond formation and cleavage, and metal skeletal transformations. Considerable recent efforts have been devoted to the stability assessment of phosphine ligands bound to polynuclear carbonyl clusters.[4,21,22]

1.3. Substitution Chemistry of Metal Clusters – Phosphine Ligands

The ligand substitution chemistry of multinuclear metal carbonyl complexes using phosphine ligands has been studied extensively. Ligand substitution studies at multimetal clusters are not only of academic interest but also of prominence in providing a detailed description on the working of

homogeneous catalysts. For example, dicobalt octacarbonyl has been reported as catalytic precursor for hydroformylation reactions, while the cluster compound $Ru_3(\mu_3\text{-NPh})(CO)_{10}$ has been shown to catalyze the coupling of CO and alkynes to yield maleimide derivatives.[23] Recently, it has been suggested that the Pauson-Khand reaction employing methylidynetricobalt nonacarbonyl clusters most likely proceed through an intact polynuclear species.[24] Kinetic measurements of ligand substitution processes are also useful in defining the reactivity of intermediates that result from ligand dissociation and can provide useful information regarding the substitution chemistry of metal clusters. Mechanistic information provided by kinetic measurements can afford invaluable information necessary for the design of new and selective homogeneous catalysts.

1.3.1 Triosmium Dodecacarbonyl Clusters - Monodentate Phosphines

Phosphine-substituted triosmium clusters are among the most studied derivatives of osmium carbonyl clusters. Simple substituted triosmium clusters such as $Os_3(CO)_{12-X}L_X$ (L= monodentate phosphine ligand) and their subsequent reactions to give cluster- and ligand-fragmentation products have been known for years.[26-27] The initial studies on these substitution reactions were conducted by thermal and photochemical methods. Typically, these reactions are not specific with respect to the nature of the end product, with mono-, bis-, tris- and sometimes higher forms of the ligand-substituted cluster formed.[25]

In the late 1970's new methods to prepare mono- and bis-substituted cluster products from the parent cluster $Os_3(CO)_{12}$ and its conversion to the activated cluster compounds $Os_3(CO)_{11}(NCMe)$, $Os_3(CO)_{10}(NCMe)_2$ and $Os_3(CO)_{10}(\mu^4\text{-}C_6H_8)$ were successfully demonstrated. These activated complexes provide a convenient platform for the preparation of a variety of substitution products. A simple synthetic scheme for the preparation of the MeCN-activated species is outlined below (scheme 1.3).[28]

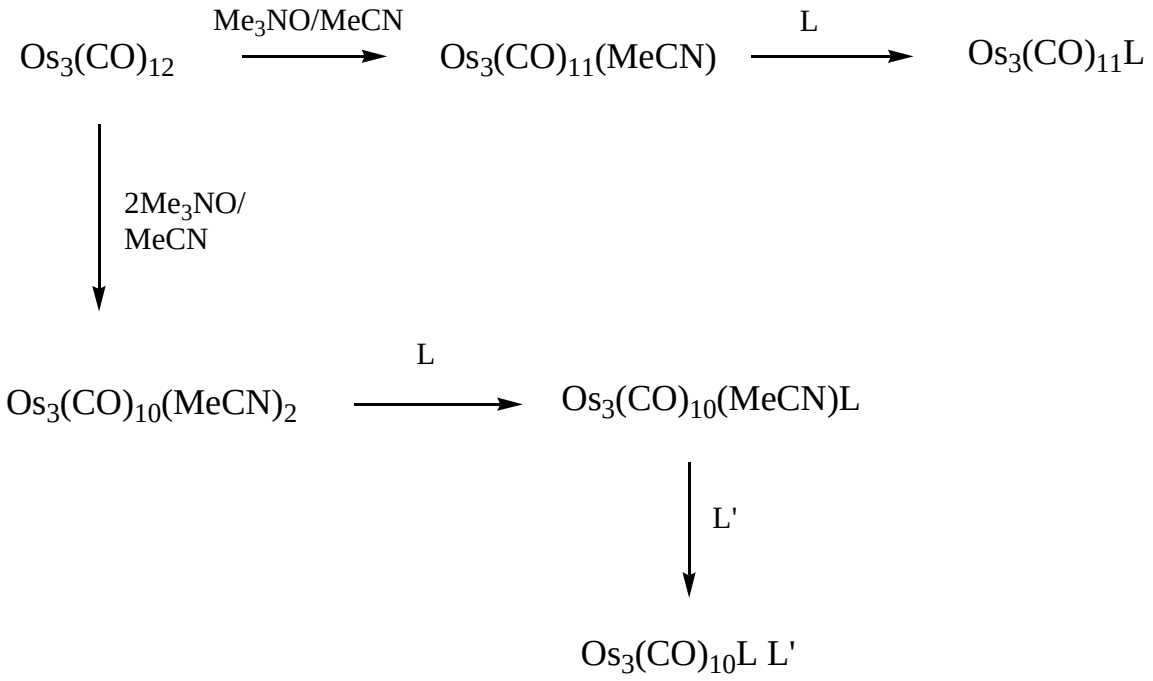

Scheme 1.3 Synthesis of active precursors and their conversion to substituted triosmium clusters.

Since these initial studies, the substitution chemistry and subsequent reactivities and reaction mechanisms of mono- and bis-substituted ligand derivatives of $Os_3(CO)_{12}$ have been studied extensively. One of the most interesting kinetic studies dealing with the substitution of CO by monodentate tertiary phosphine ligands with a triosmium cluster was published by Pöe and

Sekhar.[29] It was shown that at high temperature and low concentrations of PBu_3, $Os_3(CO)_{12}$ undergoes substitution by a ligand-independent path, forming $Os_3(CO)_{11}(PBu_3)$, $Os_3(CO)_{10}(PBu_3)_2$, and finally $Os_3(CO)_9(PBu_3)_3$ in quantitative yield via the stepwise dissociation of CO from $Os_3(CO)_{12}$ and the resulting PBu_3-substituted products. When the reaction was performed using a high concentration of PBu_3 and at low temperature, cluster fragmentation and formation of the mononuclear complexes $Os(CO)_4(PBu_3)$ and $Os(CO)_3(PBu_3)_2$ were observed with none of the expected triosmium product $Os_3(CO)_9(PBu_3)_3$. Presumably, the fragmentation reaction takes place by the formation of the ring-opened intermediate $Os_3(CO)_{11}(PBu_3)$, whose structure is displayed in figure 1.3.

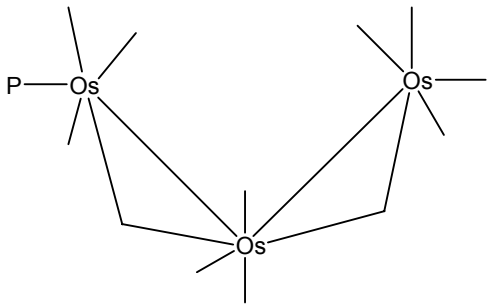

Figure 1.3 Possible intermediate in the reaction of $Os_3(CO)_{11}(PBu_3)$ with PBu_3.

A variety of monodentate phosphine ligand substituted triosmium clusters have been prepared in high yield from $Os_3(CO)_{11}(MeCN)$. The phosphine ligands in the resulting product exclusively occupy an equatorial coordination site in the cluster $Os_3(CO)_{11}P$ product.

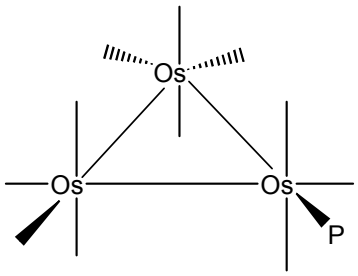

Figure 1.4 Molecular structure of $Os_3(CO)_{11}P$.

Within the family of $Os_3(CO)_{11}P$ clusters, the carbonyl ligands are fluxional in solution due to the labilizing influence of the phosphine ligand. Two mechanisms have been proposed to explain the dynamic axial-equatorial exchange of the ancillary CO groups in these clusters. The mechanism with the lowest energy barrier is depicted in Scheme 1.4, where the carbonyl exchange takes place via a bridging intermediate with two carbonyls bridging the Os_A-Os_B edge and perpendicular to triosmium plane. The position of phosphine ligand is unchanged in this process. The opening of the doubly bridged μ-CO intermediate leads to scrambling of the six co-planar carbonyl ligands. The other possible perpendicular plane along Os_A-Os_C edge is blocked by phosphine ligand.

A second mechanism, having a higher energy barrier, involves the pair-wise exchange of carbonyl groups at the phosphine-substituted osmium center. In this mechanism, the phosphine ligand rotates in a restricted trigonal twist from one equatorial position to other equatorial position (scheme 1.5), which in turn serves to promote the equilibration of an axial CO group and the unique equatorial CO group at that particular osmium center. This mechanism leads to equilibrium between the two conformations with the phosphine ligand occupying different equatorial positions at the same osmium atom. In the case of

monophosphine derivatives, these two exchange products are structurally and spectroscopically indistinguishable.

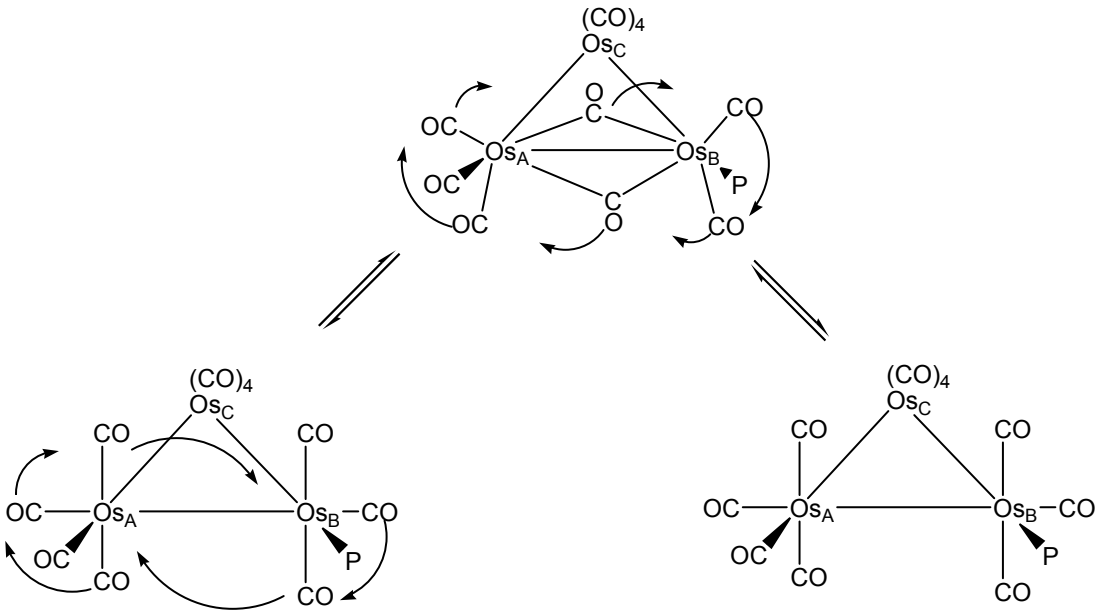

Scheme 1.4 In-plane carbonyl ligand exchange in $Os_3(CO)_{11}P$.

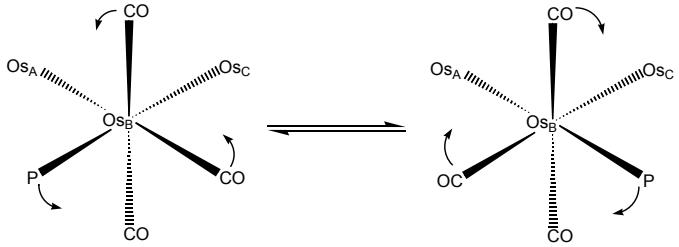

Scheme 1.5 Trigonal-twish mechanism of carbonyl exchange.

$Os_3(CO)_{10}(MeCN)_2$ typically reacts with two equivalents of a monodentate phosphine ligand (PR_3) to give the corresponding bisphosphine-substituted derivative.[30] Four isomers may be formed as a result of the different equatorial coordination sites that exist in the product. More highly substituted derivatives of triosmium clusters have been synthesized by employing small cone angle ligands

and by conducting the reaction at elevated temperatures, using ultraviolet irradiation activation, or by a combination of both thermal and photochemical reactions.

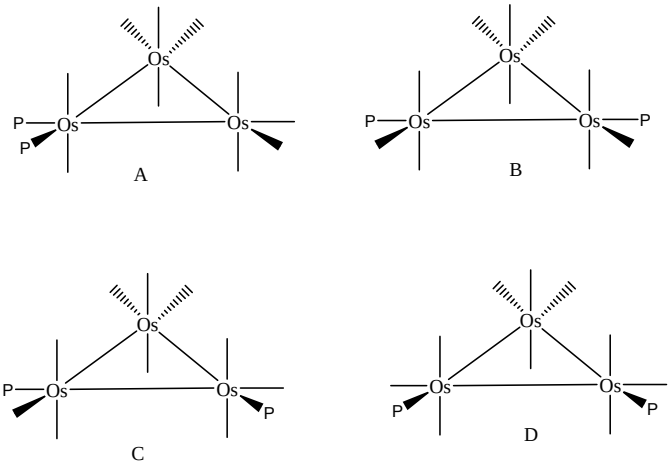

Figure 1.5 Isomers of $Os_3(CO)_{10}P_2$.

1.3.2. Hydrido Ruthenium Clusters – Monodentate Phosphines

The coordination chemistry of the tetranuclear ruthenium cluster $H_4Ru_4(CO)_{12}$ with different phosphine ligands has been studied in great detail over the years.[31] The reactions of $H_4Ru_4(CO)_{12}$ with various phosphines, phosphites and their derivatives has been found to generally yield Ru_4 clusters that contain 60 valence electrons and tetrahedral Ru_4 frames. Some of the phosphine derivatives have been tested as catalyst precursors for the hydrogenation of olefins and aldehydes.[32] In one of the studies reported by Bianchi et al., tetrasubstituted tetraruthenium clusters with phosphines containing ester groups provided evidence for the functionalization of the initial ligand.[32a] The tetrasubstituted ruthenium clusters, $Ru_4H_4(CO)_8[P(CH_2OCOR)_3]_4$, which possess different R-groups, undergo ester hydrogenation under mild conditions with the formation of corresponding alcohols on heating in presence of hydrogen

gas.[33] The synthesis and substitution chemistry of the tetraruthenium hydride cluster $H_4Ru_4(CO)_{12}$ with the monodentate phosphine ligands PPh_3, $P(OEt)_3$, $P(OMe)_3$, PMe_2Ph, $P(C_6F_5)_3$, and the functionalized phosphines $P(CH_2OCOR)_3$ have been studied over the years and found to yield mono- to tetrasubstituted products $H_4Ru_4(CO)_{12-x}P_x$ (where x = 1-4), depending upon the mode of cluster activation. All of the structurally characterized tetrahedral ruthenium clusters from these substitution reactions show a similar pattern of four long and two short metal-metal bonds. The long Ru-Ru bonds in these substituted clusters are attributed to those Ru-Ru bonds bridged by the four hydride ligands. In polymetallic systems, the common coordination modes exhibited by hydride groups are terminal, edge- or face-bridging, with interstitial hydride groups observed in rare cases.[34] Usually rapid intramolecular rearrangements of these hydride groups about the cluster polyhedron are observed in fluid solution. Aime et al. have examined the dynamics of several monosubstituted tetraruthenium cluster derivatives. There they confirmed the presence of two isomers for the monosubstituted cluster $Ru_4H_4(CO)_{11}[P(OEt)_3]$ in solution at low temperature. Aime et al. concluded that there is a rapid hydride and CO exchange taking place in solution, as shown in Scheme 1.6.[34]

In another important observation by Wong and co-workers,[41] the functionalized monodentate ligand tri(2-furyl)-phosphine was found to react with the tetraruthenium cluster $H_4Ru_4(CO)_{12}$ to afford a range of new cluster products containing μ-phosphide, and μ_3- and μ_4-phosphinidene ligands with no cluster fragmentation to lower nuclearity species.

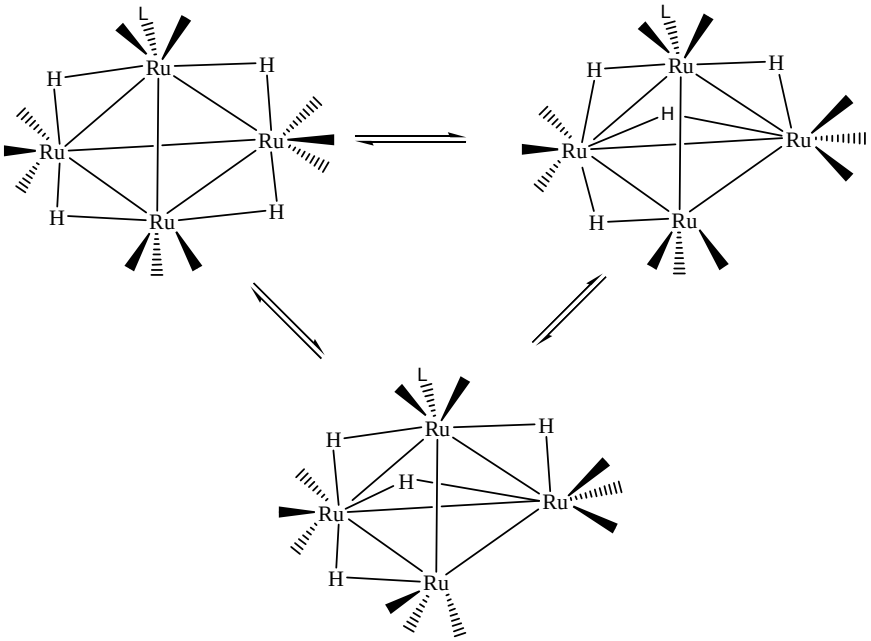

Scheme 1.6 Hydride fluxionality in the monosubstituted ruthenium cluster $H_4Ru_4(CO)_{11}[P(OEt)_3]$.

1.3.3 Osmium and Ruthenium Clusters containing Bidentate Phosphines

Deeming and co-workers have extensively investigated the synthesis and reactivity of triosmium clusters with many of the commonly available simple diphosphine ligands of the series $Ph_2P(CH_2)_nPPh_2$ (where n = 1-4).[35-37] The structures and names of some of these common diphosphine ligands are shown in Figure 1.2. Diphosphine-substituted triosmium clusters with the ligand coordinated across an osmium-osmium bond furnishes a bridged diphosphine cluster, also referred to as the 1,2-isomer, while the coordination of the P-P ligand to a single osmium metal center yields the chelated isomer, also referred

to as the 1,1-isomer. The structures of the generic bridging and chelating isomers of $Os_3(CO)_{10}$(P-P) are shown below.

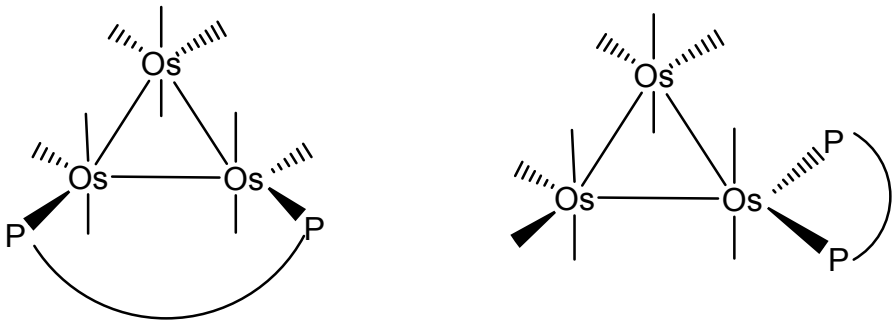

Bridging Chelating

Figure 1.6 Bridging and chelating isomers of $Os_3(CO)_{10}$(P-P).

The reaction between the labile triosmium cluster 1,2-$Os_3(CO)_{10}(MeCN)_2$[50] and the simple diphosphine ligands $Ph_2P(CH_2)_nPPh_2$ such as dppm (n=1), dppe (n=2), dppp (n=3) and dppb (n=4) was found to furnish the corresponding $Os_3(CO)_{10}$(diphosphine) clusters, which exist as the 1,2-isomer (bridging) and/or the 1,1-isomer (chelating) depending on the nature of the diphosphine ligand employed. The 1,1-isomer predominates in the case of the dppe and dppp ligand substituted clusters, while the 1,2-isomer is observed as the major product in the case of the dppb ligand. The reaction of 1,2-$Os_3(CO)_{10}(MeCN)_2$ with the shorter chain dppm ligand furnishes the 1,2-isomer exclusively with none of 1,1-isomer observed. Presumably, both ring strain in the formation of the four-membered ring and steric favorability associated with the bridging system account for the isomer selectivety in the reaction using the dppm ligand. In comparison, there are a few examples for the formation of chelating isomers using the dppm ligand in the metal cluster systems,[38-39] with bridging isomers being more common. In this class of clusters, the wide angle between equatorial sites of triosmium clusters is

expected to promote the selective formation of the bridged isomer. The tendency of diphosphines to act as bridging and chelating ligands was studied by comparing the yields of each isomer from the respective reactions. It was confirmed that dppe acts predominantly as chelating ligand, and that the chelating tendency decreases as the chain length of diphosphines increases. It has been observed that $Ph_2P(CH_2)_5PPh_2$ acts selectively as a bridging ligand in the vast majority of cluster systems investigated.[40] The fluxional behavior of the CO groups in the ligand-bridged and ligand-chelated triosmium clusters is similar to that of monodentate clusters. In the case of diphosphine-substituted clusters, there is only one vertical plane for an axial-equatorial exchange of the carbonyl groups (Scheme 1.7).

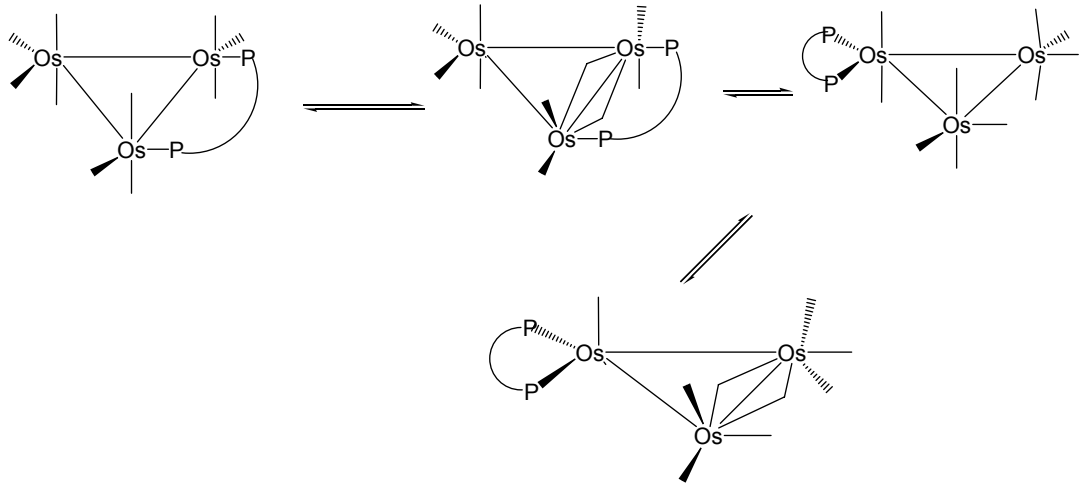

Scheme 1.7 Carbonyl exchange in the triosmium clusters 1,1- and 1,2-$Os_3(CO)_{10}$(P-P).

The 1,2-isomer has one osmium atom and the 1,1-isomer has two osmium atoms associated with a possible restricted trigonal twist as the rotation around remaining osmium atoms is blocked by the equatorial phosphine ligands. While

carbonyl ligands can rapidly migrate around the metal atoms in these clusters, no evidence existed for the intramolecular phosphine transfer about the cluster core until recently. This is probably due to the inertness of the triosmium system and negligible rates associated with the phosphine migration in the bridging and chelating isomers that would promote the overall isomerization a phosphine group between adjacent metal clusters.

The CO substitution chemistry in $H_4Ru_4(CO)_{12}$ by bidentate phosphine ligands has also been extensively studied over the years with respect to the coordination mode adopted by the diphosphine relative to the Ru_4 polyhedron. The fluxional behavior and exchange pathways exhibited by the bridging hydride groups,[42] and the catalytic hydrogenation activity displayed by systems containing a chiral diphosphine auxiliary have also been investigated.[43] Unlike the substitution chemistry displayed by triosmium clusters using the simple diphosphine ligands dppm, dppp, and dppb, the tetraruthenium cluster $H_4Ru_4(CO)_{12}$ undergoes reaction with the same diphosphine ligands to give ligand-bridged tetraruthenium products. No evidence for the chelation of a diphosphine ligand to a single ruthenium cluster in these clusters has been reported.[44] The fact that only the bridging isomer has been observed in this particular class of cluster may be attributed to the unfavorable energy requirements involved in the formation of the chelating isomer. The trimethylamine N-oxide mediated substitution of $H_4Ru_4(CO)_{12}$ cluster with 1,2-bis(diphenylphosphino)ethane yielded the bridging isomer as the kinetically formed product. Heating led to the isomerization and formation the chelating

isomer.[45] This diphosphine isomerization represents the first unequivocal paradigm for the coordinative flexibility of a diphosphine ligand in a metal cluster compound. This will be discussed in detail in Chapter 2. The coordination chemistry of the $H_4Ru_4(CO)_{12}$ cluster with the chiral diphosphine ligands 2,2-dimethyl-[4,5-bis(diphenylphosphino)-methyl]1,3-dioxane and 1,2-bis(2-methoxyphenyl)(phenylphosphino)ethane yielded a bridging isomer and chelating isomer, respectively, both of which exhibit a six-membered metallocycle ring.

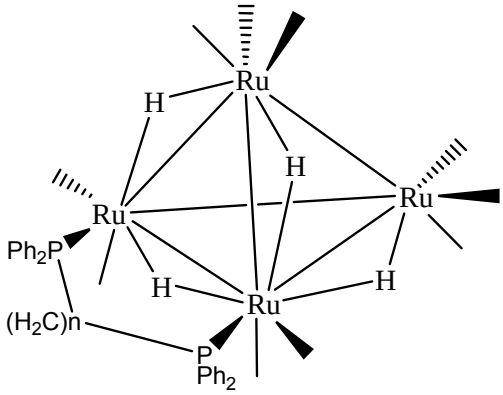

Figure 1.7 Tetraruthenium clusters with bridging diphosphine ligands (n = 1, 3, and 4).

It is apparent that the vast majority of diphosphine ligands possess a saturated backbone that connects the phosphorus atoms. As was discussed earlier, steric and electronic factors play a very important role in the structure and chemical properties of these phosphine-substituted clusters. The reaction between phosphine ligands having an unsaturated backbone and metal clusters may yield substituted clusters having properties different from those derived from the ligands dppm and dppe, etc. Richmond et al., has had a long-standing interest in the study of the substitution reactivity of phosphine-substituted metal

clusters containing unsaturated P-C=C-P backbones. With the introduction of different substituents at the carbon atoms that comprise the unsaturated back bone, many new types of diphosphine ligands may be synthesized and investigated for their chemical reactivity upon coordination to the metal cluster.

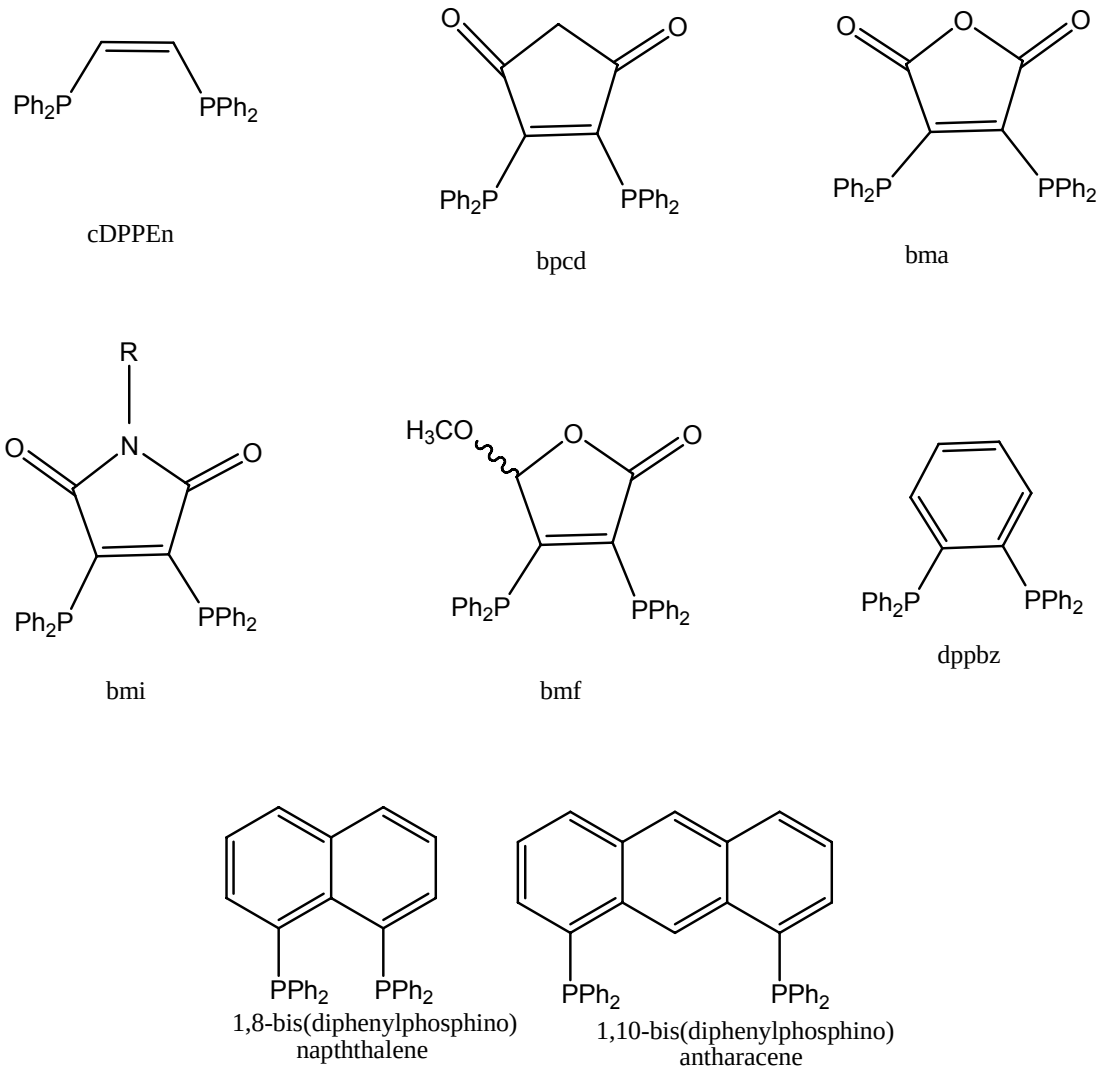

Figure 1.8 Rigid diphosphine ligands.

The growing interest in the study of the coordination chemistry of bidentate ligands with aromatic backbones stems from the high catalytic activity and stability of metal complexes containing these ligands.[46b] The aromatic

backbone of such ligands confirms rigidity to a metal cluster since the coordinated atoms are fixed to a plane. Some important diphosphine ligands that contain unsaturated and aromatic backbones are listed in Figure 1.8.

Table 1.1 Abbreviations and names of bidentate diphosphine ligands.

Abbreviations	Name
cDPPEn	(Z)-1,2-bis(diphenylphosphino)ethane
bpcd	4,5-bis(diphenylphosphino)-4-cyclopentene-1,3-dione
bma	2,3-bis-(diphenylphosphino)maleic anhydride
bmi	2,3-bis(diphenylphosphino)maleimide
bmf	3,4-bis(diphenylphosphino)-5-methoxy-2(5H)-furanone
dppbz	1,2-bis(diphenyphosphino)benzene
dppn	1,8-bis(diphenylphosphino)naphthalene
BINAP	2,2'-bis(diphenylphosphino)-1,1'-binapthyl

The presence of a carbon-carbon double bond that serves to link two phosphorus atoms yields a four-atom backbone (P-C-C-P), whose atoms are constained to a planar or near planar geometry. The simplest diphosphine ligand with a unsaturated backbone is (Z)-1,2-bis(diphenylphosphino)ethene (cDPPEn). Bruce and coworkers initially examined the substitution chemistry of the triosmium cluster $Os_3(CO)_{12}$ with cDPPEn. A product having the composition $Os_3(CO)_{10}$(cDPPEn) was obtained and characterized in solution by IR and ^1H NMR spectroscopy.[46] Later a detailed mechanistic study on bridging to chelating ligand isomerization and C-H and P-C bond activation was carried out by Richmond's group.[47]

In order to better understand the reactivity of rigid bidentate ligands that are bound to a metal cluster, Richmond et al., have explored the substitution chemistry of the triruthenium cluster $Ru_3(CO)_{12}$ with the ligand bpcd. Thermolysis of $Ru_3(CO)_{12}$ with bpcd affords the fragmentation products that are displayed in Scheme 1.8. It was observed that the initial substitution product, 1,1-$Ru_3(CO)_{10}$ (bpcd), undergoes fragmentation at ambient temperature in the dark to give two bimetallic fragmentation products, $Ru_2(CO)_6$(bpcd) and $Ru_2(CO)_6$[μ-C=C(PPh_2)C(O)CH_2 C(O)](μ$_2$-PPh_2).[48] The bpcd ligand chelates to one ruthenium atom and the alkene moiety of the ancillary bpcd ligand donates a pair of electrons to the adjacent ruthenium atom resulting in the donor-acceptor complex $Ru_2(CO)_6$(bpcd). Photolysis of $Ru_2(CO)_6$(bpcd) promotes P-C bond cleavage to give the phosphido complex $Ru_2(CO)_6$[μ-C=C(PPh_2)C(O)CH_2 C(O)](μ$_2$-PPh_2).

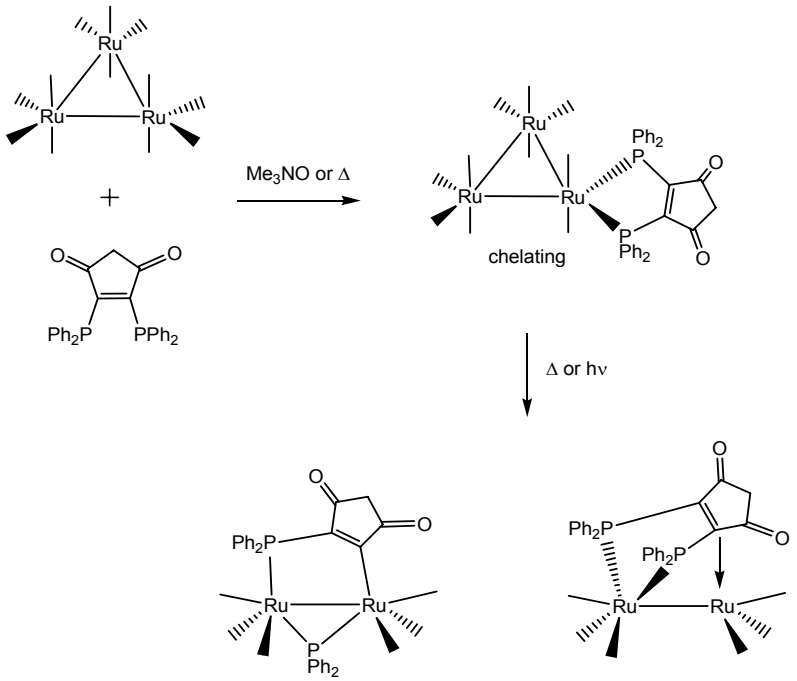

Scheme 1.8 Reaction leading to and fragmentation of the triruthenium cluster 1,1-$Ru_3(CO)_{10}$(bpcd).

The coordination chemistry of bpcd with the octahedral hexaruthenium carbide cluster $Ru_6(C)(CO)_{17}$ has yielded some interesting results. Reaction of $Ru_6(C)(CO)_{17}$ with bpcd leads to the coordination of the two phosphorus atoms to adjacent ruthenium atoms and the coordination of the alkene bond of the ligand to a third ruthenium center. Here the bpcd ligand donates six electrons to the cluster and caps one of the eight triangular faces of the octahedral cluster. This reactivity exhibited by the ancillary bpcd ligand is unique to this genere of unsaturated diphosphine ligands.[49]

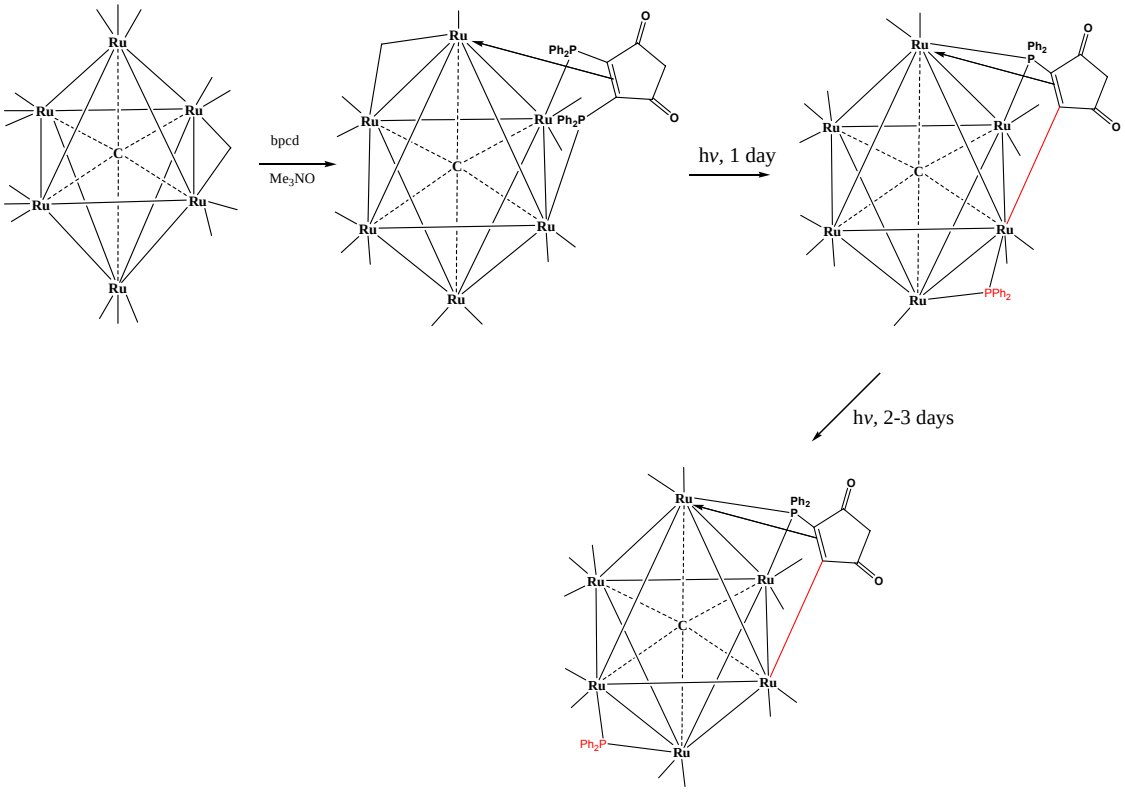

Scheme 1.9 Substitution chemistry of a hexaruthenium cluster with bpcd.

The face-capped bpcd product $Ru_6(C)(CO)_{14}$(μ-bpcd) that is depicted in scheme 1.9 undergoes P-C bond cleavage upon optical excitation. The simple rigid diphosphine ligand cDPPEn reacts with $Ru_6(C)(CO)_{17}$ under analogous reaction conditions to yield the face-capped product $Ru_6(C)(CO)_{14}$(μ-cDPPEn). This later cluster was found to be inert to near-UV irradiation. This shows a marked difference in the reactivity of these rigid bidentate ligands with the change in the substituents on the P-C-C-P backbone. In another observation made by Bruce and coworkers,[50] the reaction between $Os_3(CO)_{12}$ and 1,8-bis(diphenylphosphino)naphthalene (dppn) yielded P-C and C-H bond cleavage products with no evidence observed for the bridging or chelating isomers of $Os_3(CO)_{10}$(dppn).

Presented in this dissertation are the reactions of diphosphine ligands with various osmium and ruthenium clusters. In-depth mechanistic studies on the ligand isomerization and the stepwise, regiospecific C-H and P-C bond activation chemistry of the new ligand-substituted osmium and ruthenium clusters are reported.

1.4 Chapter References

1. Crabtree, R.H. *The Organometallic Chemistry of the Transition Metals*, Wiley Weinheim, 1998.
2. Beller, M.; Bolm, C. *Transition Metals For Organic Synthesis,* Wiley-VCH, Weinheim, 1998.
3. (a) Hurlburt, K.P.; Rack, J.J.; Luck, S.J.; Dec, S.F.; Webb, J.D.; Anderson, O.P.; Strauss, S.H. *J. Am. Chem. Soc.* **1994**, *116*, 10003 (b) Howard,

W.A.; Parkin, G.; Rheingold, A.L. *Polyhedron* **1995**, *14*, 25. (c) Dyson, P.J.; McIndoe, J.S. *Transition Metal Carbonyl Cluster Chemistry*; Gardon and Breach Sciences Publishers: Amsterdam, The Netherlands, 2000; Chapter 1.

4. (a) Cotton, F.A. *Prog. Inorg. Chem.* **1976**, *21*, 1. (b) Canuto, C.H.; Masic, A.; Rees, N.H.; Heyes, J.S.; Gobetto, R.; Aime, S. *Organometallics* **2006,** *25*, 2248 (c) Hepp, A.F.; Blaha, J.P.; Lewis, C.; Wrighton, M.S. *Organometallics* **1984**, *3*, 174.
5. Baird, M.C.; Osbon, J.A.; Wilkinson, G. *Chem. Commun*. **1966**, 129.
6. Winter, M.J. *Adv. Organomet. Chem.* **1989**, *29*, 101.
7. Schnokel, H. *Angew. Chem., Int. Ed.* **1992**, *31*, 638.
8. (a) Mingos, D.M.P. *Pure Appl. Chem.* **1991**, *63,* 807; (b) King, R.B. *Encyclopedia of Inorganic Chemistry*, Wiley, New York, 1994; p. 3348.
9. Choplin, A.; Besson, B.; Basset, J. *J. Am. Chem. Soc.* **1988**, *110*, 2783.
10. (a) Lemoine, P. *Coord. Chem. Rev*. **1988**, 83, 169. (b) Lemoine, P. *Coord. Chem. Rev*. **1982**, 47, 56; (c) Drake, S.R. *Polyhedron* **1990**, 9, 455.
11. (a) Muetterties, E.L.; Krause, M.J. *Angew. Chem., Int. Ed. Engl*. **1983**, 22, 135. (b) Laine, R.M. *J. Mol. Catal*. **1982**, 14, 137. (c) Smith, A.K.; Basset, J.M. *J. Mol. Catal*. **1977**, 2, 229. (d) Süss-Fink, G.; Neumann, F. in *The Chemistry of the Metal-Carbon Bond*, Hartley, F. R (ed.), Vol. 5, Wiley, New York. 1989; Chapter 7, p 231. (e) Homanen, P.; Persson, R.; Haukka, M.; Pakkanen, T.A.; Nordlander, E. *Organometallics* **2000**, *19*,

5568. (f) Matteoli, U.; Menchi, G.; Frediani, P.; Bianchi, M.; Piacenti, F. *J. Organomet. Chem.* **1985**, *285*, 281.

12. Blase, H.U; Indolese, A.; Schnyder, A. *Science* **2000,** *78*, 1336.
13. Wolfe, J.P. *Angew. Chem*. **1999,** *111*, 2570.
14. Jacobson, E.N.; Pfaitz, A.; Yamamoto, H. *Comprehensive Asymmetric Catalysis*; Springer; New York, **1999**; Vols. 1-3
15. Deeming, A.J.; Donovan-Mtuzi, S.; Kabir, S.E. *J. Organomet. Chem.* **1984**, *276*, C65; **1987**, *333*, 253.
16. Cartwright, S.; Clucas, J.A.; Dawson, R.H.; Foster, D.F.; Smith, A.K. *J. Organomet. Chem.* **1986**, *302*, 403.
17. Poe, A.J.; Sekhar, V.C., *J. Am. Chem. Soc.* **1884**, *106*, 5034.
18. Deeming, A.J.; Stchedroff, M. *J. Chem. Soc. Dalton Trans.* **1998***,* 3819.
19. (a) Huttner, G.; Knoll, K. *Angew. Chem., Int. Ed. Engl.* **1987**, *26*, 743. (b) O'Neill, M.E.; Wade, K. *Metal Interactions with Boron Clusters*; Grimes, R.N., Ed.; Plenum Press: New York,1982. (c) Johnson, B.F.G., Ed.; *Transition Metal Clusters*; Wiley: NewYork, 1980. (d) Vahrenkamp, H. *Adv. Organomet. Chem.* **1983**, *22*, 169. (e) Adams, R.D.; Horvath, I.T. *Prog. Inorg. Chem.* **1985**, *33*, 127.
20. (a) Ang, H.G.; Ang, S.G.; Du, S.; Sow, B.H.; Wu, X. *J. Chem. Soc., Dalton Trans.* **1999**, 2799. (b) Süss-Fink, G.; Godefroy, I.; Be´guin, A.; Rheinwald, G.; Neels, A.; Stoeckli-Evans, H. *J. Chem. Soc., Dalton Trans.* **1998**, 2211. (c) Wang, W.; Enright, G.D.; Carty, A.J. *J. Am. Chem. Soc.* **1997**, *119*, 12370.

21. (a) Lugan, N,; Lavigne, G.; Bonnet, J.J. Inorg. Chem. **1987**, *26*, 585. (b) Bergounhou, C.; Bonnet, J.J.; Fompeyrine, P.; Lavigne, G.; Lugan, N.; Mansilla, F. *Organometallics* **1986**, *5*, 60.

22. a) Ang, H.G.; Ang, S.G.; Du, S. *J. Chem. Soc., Dalton Trans.* **1999**, 2963. (b) Chi, Y.; Carty, A.J.; Blenkiron, P.; Delgado, E.; Enright, G.D.; Wang, W.; Peng, S.-M.; Lee, G.-H. *Organometallics* **1996**, *15*, 5269. (c) Clarke, L. P.; Davies, J.E.; Raithby, P.R.; Shields, G.P. *J. Chem. Soc., Dalton Trans.* **2000**, 4527.

23. (a) Han, S.H.; Geoffroy, G.L.; Rheingold, A.L. *Organometallics*, **1987**, *6*, 2380. (b) Han, S.H.; Geoffroy, G.L.; Rheingold, A.L. *Organometallics*, **1986**, *5*, 2561.

24. (a) Stefani, A.; Consiglio, G.; Botteghi, C.; Pino, P. *J. Am. Chem. Soc.* **1977***, 99,* 1058. (b) Sugihara, T.; Yamaguchi, M. *J. Am. Chem. Soc.* **1998**, *120*, 10782.

25. (a) Hughes, A.K.; Wade, K. *Coord. Chem. Rev* **2000**, *197*, 191. (b) Housecroft, C.E.; Wade, K.; Smith, B.C. *J. Chem. Soc., Chem. Commun*. **1978**, 765.

26. (a) March, J. *Advanced Organic Chemsitry,* McGraw-Hill: New York **1977**: p237. (b) Pearson, J. *J. Am. Chem. Soc*. **1963**, *85*, 3533. (c) Hancock, R. D.; Martell, A.E. *Chem. Rev.* **1989**, *89*, 1875.

27. (a) Izatt, R.M.; Pawlak, K.; Bradshaw, J.S. *Chem. Rev.* **1995**, *95*, 2529. (b) Lehn, J.M. *Pure Appl. Chem.* **1994**, *66*, 1961.

28. (a) Johnson, B.F.G.; Lewis. J.; Pippard, D. *J. Organomet. Chem.* **1978**, *145*, C4. (b) Tachikawa, M.; Shapley, J.R. *J. Organomet. Chem.* **1977,** *124,* C19.

29. Poe, A.J.; Sekhar, V.C.; *Inorg. Chem.* **1985**, *24*, 4376.

30. Leong, W.K.; Liu, Y. *J. Organomet. Chem.* **1995**, *584*, 174.

31. Pomeroy, R.K.; Abel, E.W.; Stone, F.G.A.; Wilkinson, G. *Comprehensive Organometallic Chemistry II, Vol. 7.* Pergamon press, Oxford, **1995**, 845.

32. (a) Bianchi, M.; Menchi, G.; Matteoli, U.; Piacenti, F. *J. Organomet. Chem.* **1993**, *451*, 139. (b) Bhaduri, M.; Sharma, K.; Mukesh, D. *J. Chem. Soc., Dalton Trans.* **1993**, 1191.

33. Mario, B.; Piero, F.; Antonella, S. *Organometallics* **1997,** *16*, 482.

34. Aime, S.; Botta, M.; Gobetto,R.; Milone, L.; Oscilla, D.; Gellert, R.; Rosenberg, E. *Organometallics* **1995**, *14*, 3693.

35. (a) Claucas, J.A.; Dawson, R.H.; Dolby, P.A.; Harding, M.M.; Pearson, K.; Smith, A.K. *J. Organomet. Chem.* **1986**, *311*, 153. (b) Deeming, A.J.; Donovan-Mtunzi, S.; Hardcastle, K.I.; Kabir, S.E.; Henrick, K.; McPartlin, M. *J. Chem. Soc., Dalton Trans.* **1988**, 579. (c) Deeming, A.J.; Hardcastle, K.I.; Kabir, S.E. *J. Chem. Soc., Dalton Trans.* **1988**, 825.

36. Azam, K.A.; Hursthouse, M.B.; Kabir, S.E.; Malik, K.M.A.; Mottalib, M.A. *J. Chem. Crystallogr.* **1999**, *29*, 813.

37. Brown, M.P.; Dolby, P.A.; Harding, M.M.; Mathews, A.J.; Smith, A.K. *J. Chem. Soc., Dalton Trans.* **1993**, 1671.

38. Tachikawa, M.; Shapley, J.R.; Haltiwanger, R.C.; Piperpont, C.G. *J. Am. Chem. Soc.* **1976**, *98*, 4651.

39. Evans, J.; Gracey, L.R.; Webstar, M. *J. Organomet. Chem.* **1982**, *240*, C61.

40. Kabir, S.E.; Miah, A.; Nesa, L.; Uddin, K.; Hardcastle, K.I.; Rosenberg, E.; Deeming, A.J. *J. Organomet. Chem.* **1995**, *492*, 41.

41. Wong, W.-Y.; Ting, F.-L.; Lin, Z. *Organometallics*, **2003**, *22*, 5100.

42. (a) Puga, J.; Arce, A.; Braga, D.; Centritto, N.; Grepioni, F.; Castillo, R.; Ascanio, J. *Inorg. Chem.* **1987**, *26*, 867. (b) Bruce, M.I.; Horn, E.; Shawkataly, O.B.; Snow, M.R.; Tiekink, E.R.T.; Williams, M.L. *J. Organomet. Chem.* **1986**, *316*, 187.

43. (a) Homanen, P.; Persson, R.; Haukka, M.; Pakkanen, T.A.; Nordlander, E. *Organometallics* **2000**, *19*, 5568. (b) Matteoli, U.; Menchi, G.; Frediani, P.; Bianchi, M.; Piacenti, F. *J. Organomet. Chem.* **1985**, *285*, 281.

44. Puga, J.; Arce, A.; Braga, D.; Centritto, N.; Grepioni, F.; Castillo, R.; Ascanio, J. *Inorg. Chem.* **1987**, *26*, 867.

45. Churchill, M.R.; Lashewycz, A.R.; Shapley, J.R.; Richter, S.I. *Inorg. Chem.* **1980**, *19*,1277.

46. (a) Bruce, M.I.; Williams, M.L.; Skelton, B.W.; White, A.H. *J. Organomet. Chem.* **1986**, *306*, 115. (b) Grossman, O.; Azerraf, C.; Gelman, D. *Organometallics*, **2006**, *25*, 375.

47. Watson, W.H.; Wu, G.; Richmond, M.G. *Organometallics*, **2005**, *24*, 5431.

48. Shen, H.; Bott, S.G.; Richmond, M.G. *Organometallics*, **1995**, *14*, 4625.

49. Unpublished results from Dr. Richmond's research group.

50. Nicholls, J.N.; Vargas, M.D. *Inorg. Synth.* **1989**, *26*, 289.

CHAPTER 2
REACTION CHEMISTRY OF DIPHOSPHINE LIGANDS WITH TETRARUTHENIUM CLUSTER $H_4Ru_4(CO)_{12}$

The bridge-to-chelate isomerization of the dppe ligand in $H_4Ru_4(CO)_{10}$(dppe) was reported around twenty years ago by Shapley and Churchill, and their findings served as the first unequivocal paradigm for the coordinative flexibility of a diphosphine ligand in a metal cluster compound.[1-3] A subsequent study on the synthesis of the related clusters $H_4Ru_4(CO)_{10}[PhP_2(CH_2)_nPPh_2]$ containing the simple diphosphine ligands dppm, dppp, dppb (where n = 1, 3, 4,) has shown these diphosphine ligands to bridge a Ru-Ru bond in the tetrahedral Ru_4 cluster, with each derivative displaying idealized C_s symmetry. This reinforced the fact that the isomerization behavior was restricted to the ligand dppe, with all other diphosphine ligands exhibiting only bridging coordination to the tetraruthenium polyhedron.[4] Clearly the length of the carbon backbone associated with the diphosphine ligand serves as a variable in the isomerization reaction. The composition of the carbon chain that tethers the two phosphine centers in these ligands and its effect on the P-P ligand isomerization was also demonstrated by the synthesis and examination of $H_4Ru_4(CO)_{10}$(prophos). While the replacement of a hydrogen atom on the ethane bridge in dppe by a methyl group yields the structurally similar prophos ligand,[5] the corresponding 1,2-$H_4Ru_4(CO)_{10}$(prophos) cluster shows no evidence for diphosphine ligand isomerization to the chelated cluster 1,1-$H_4Ru_4(CO)_{10}$(prophos). This observation is of interest as it indicates that steric

effects within the carbon backbone of the diphosphine ligand also influence this particular transformation. Since then several other reports outlining analogous isomerization behavior in a variety of metal clusters have appeared in the literature.[6-10]

The unsaturated diphosphine ligand (Z)-$Ph_2CH=CHPPh_2$ (cDPPEn) is structurally identical to the dppe ligand except for the presence of its rigid unsaturated back bone. Despite this minor structural difference, the cDPPEn ligand has also been shown to participate in bridge-to-chelate isomerization reactions in other polynuclear systems.[11] Therefore it was deemed of interest to establish the substitution chemistry between unsaturated diphosphine ligands with $H_4Ru_4(CO)_{12}$. In addition, the introduction of different substituents at the carbon atoms of the P-C=C-P skeleton has the potential to furnish many new types of diphosphine ligands having a rigid unsaturated backbone. Such novel diphosphine ligands can be used to study the steric and electronic factors that affect the structure of a metal cluster, ligand fluxionality, and reactivity of diphosphine-substituted polynuclear cluster compounds. To explore the effect that the ancillary diphosphine ligand has on the reaction chemistry with respect to the ligand cDPPEn, the related ligand 2-(4-N,N'-dimethylaminobenzylidene)-4,5-bis(diphenylphosphino)-4-cyclopenten-1,3-dione (dbpcd) that bears a dimethylamino group has been synthesized by application of Knoevenagel condensation. The methyl groups associated with the NMe_2 group can serve as a suitable probe handle that will allow the isomerization progress of the isomerization reaction to be followed by ^1H NMR spectroscopy.

2.1 Results and Discussion

The synthesis of the novel diphosphine ligand 2-(4-N,N'-dimethylamino benzylidene)-4,5-bis(diphenylphosphino)-4-cyclopenten-1,3-dione (dbpcd) was achieved by condensation of bpcd with 4- N,N'-dimethyamino benzaldehyde. The phosphine ligand bpcd was synthesized via reaction of 4,5-dichloro-4-cyclo penten-1,3-dione with diphenyl(trimethylsilyl)phosphine.[12] 4,5-dichloro-4-cyclo penten-1,3-dione was synthesized by reducing hexachlorocyclopentadiene in the presence of Zn and HCl to yield 1,2,3,4-tetrachlorocyclopentadiene. Chlorination of 1,2,3,4-tetrachlorocyclopentadiene, followed by treatment with concentrated sulfuric acid, produces 4,5-dichloro-4-cyclopenten-1,3-dione.[12] Scheme 2.1 illustrates the synthesis of the starting bpcd ligand.

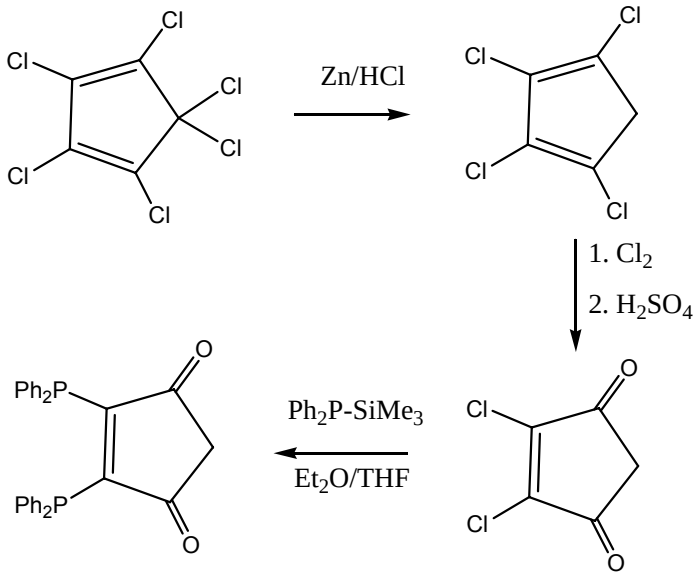

Scheme 2.1 Synthesis of the bpcd ligand from hexachlorocyclopentadiene.

Condensation of bpcd with 4-N,N'-dimethylaminobenzaldehyde was found to be sensitive to the reaction conditions. Good yields were achieved by employing a mixed-solvent system composed on of CH_2Cl_2 (DCM) and MeOH in

the presence of molecular sieves. The molecular sieves irreversibly remove the liberated water that accompanies the condensation reaction. It is believed that the presence of the protic solvent helps generate the enol derived from bpcd, which in turn functions as the active nucleophile in the condensation reaction. Carrying out the reaction according to the synthetic route depicted in Scheme 2.2, followed by column chromatography, affords 2-(4-N,N'-dimethylamino benzylidene)-4,5-bis(diphenylphosphino)-4-cyclopenten-1,3-dione (dbpcd) (**1**).

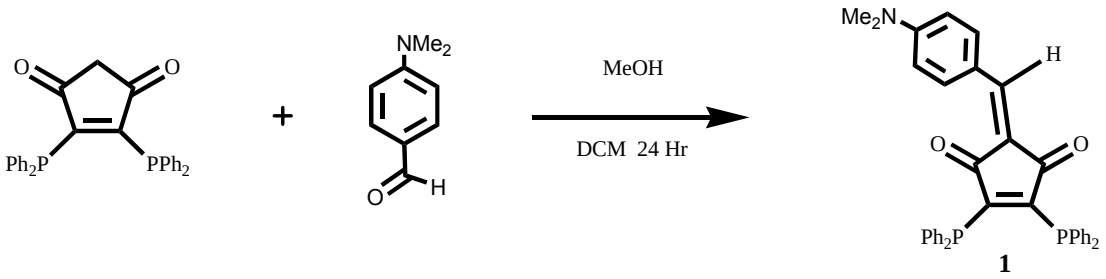

1

Mechanism:

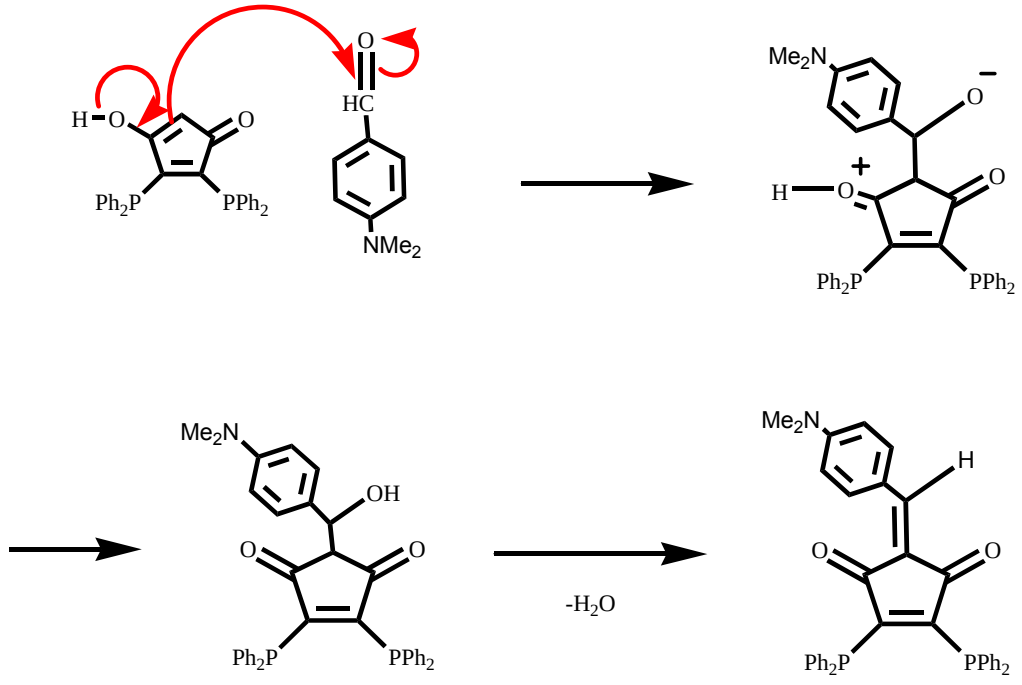

Scheme 2.2 Synthetic shcme for the preparation of 2-(4-N,N'-dimethylamino benzylidene)-4,5-bis (diphenylphosphino)-4-cyclopenten-1,3-dione.

2.2 Synthesis of the Diphosphine-Substituted Tetraruthenium Clusters $H_4Ru_4(CO)_{10}$(cDPPEn) (3) and $H_4Ru_4(CO)_{10}$(dbpcd) (4)

Ligand substitution in $H_4Ru_4(CO)_{12}$ by the unsaturated diphosphine ligands cDPPEn and dbpcd was achieved under a variety of different conditions to furnish the corresponding diphosphine-substituted clusters $H_4Ru_4(CO)_{10}$(P-P) (where P-P = cDPPEn, dbpcd). The parent cluster $H_4Ru_4(CO)_{12}$ (**2**) was activated towards ligand substitution by using the oxidative-decarbonylation reagent Me_3NO, thermolysis, and photochemistry. Treatment of $H_4Ru_4(CO)_{12}$ with two equivalents of Me_3NO in the presence of added ligand furnishes the chelating clusters **3** and **4** in moderate yields after chromatographic separation.

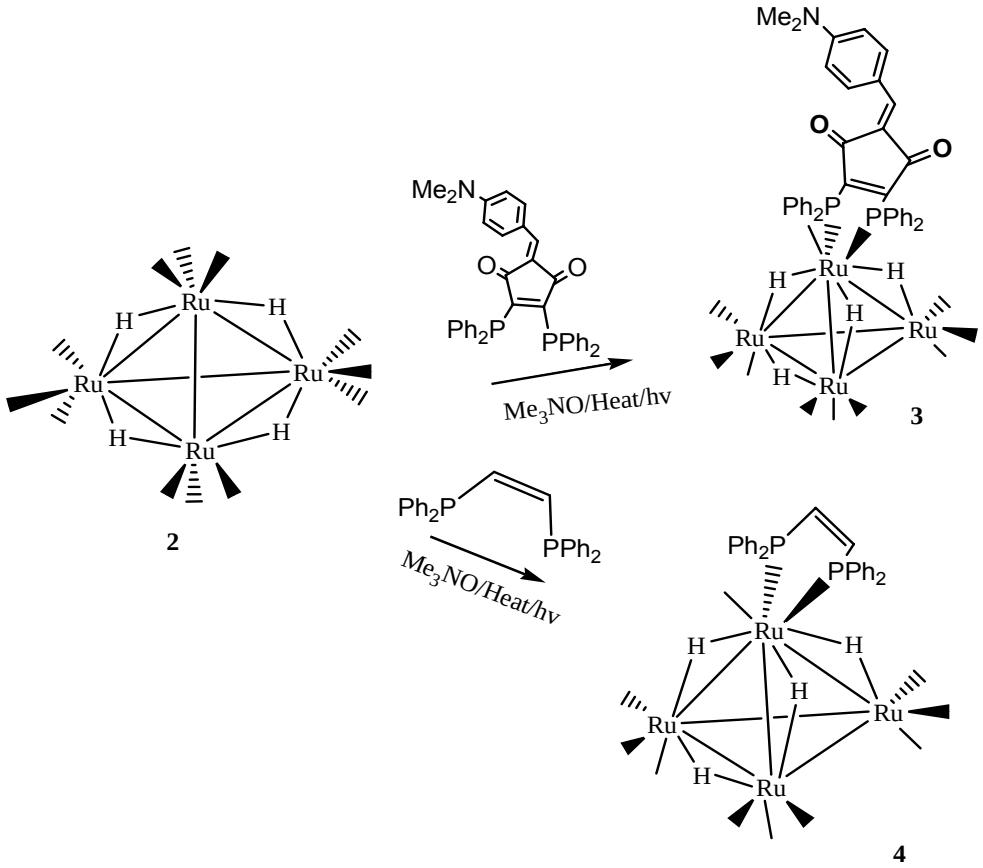

Scheme 2.3 Synthesis of the new diphosphine-substituted tetraruthenium clusters.

Both the cluster products were fully characterized in solution by IR and NMR spectroscopies. The IR spectrum of cluster **3** exhibits carbonyl stretching bands 2076 (s), 2047 (vs), 2024 (vs), 2007 (s), and 1975 (m) cm^{-1}. The ^1H NMR spectrum of cluster **3** exhibits an aromatic multiplet from δ 7.40-7.70 for the 24 aryl hydrogens, a singlet at δ 2.80 corresponding to 6 methyl hydrogens and two broadened high-field hydrides at δ -16.15 (3H) and -18.75 (1H). Cluster **4** displays carbonyl stretching bands for the ruthenium-bound CO ligands at at 2073 (s), 2044 (vs), 2021 (vs), 2003 (s) and 1985 (w) cm^{-1} that belong to the terminal Ru-CO ligands. The ^1H NMR spectrum shows a multiplet resonance from δ 6.95-7.58 for the 22 aryl and vinyl hydrogens and two high-field bridging hydride resonances at δ -15.34 and -18.70 in a 3:1 integral ratio. The IR data in the terminal carbonyl stretching region of both clusters suggest that the structures adopted by the clusters **3** and **4** show a common substitution pattern (*vide infra*), which is also supported by the ^1H NMR spectral data for the high-field bridging hydride ligand.

These data are contrasted with the related cluster $H_4Ru_4(CO)_{10}$(dppe), which shows both bridging and chelating isomers in common solvents such as $CHCl_3$ and toluene. The lack of observable bridge-to-chelate isomerization for the diphosphine ligands cDPPEn and 2-(4-N,N'-dimethylaminobenzylidene)-4,5-bis (diphenylphosphino)-4-cyclopenten-1,3-dione in these Ru_4 clusters suggests that the presence of a unsaturated backbone on the two-carbon ethene chain represents a sufficient enough condition to negate the formation and/or stabilization of diphosphine-bridged Ru_4 cluster. To better understand the

mechanism of isomerization in the case of the dppe substituted tetraruthenium cluster, a detailed study was carried out on $H_4Ru_4(CO)_{10}$(dppe). Herein kinetic data are presented that support a reversible, nondissociative diphosphine ligand pathway that involves the participation of an intermediate that possesses μ_2-dppe and μ_2-CO ligands.

2.3 The Isomerization Kinetics

The kinetics for the isomerization reaction shown in Scheme 2.4 were initially probed by ^{1}H and ^{31}P NMR spectroscopy using toluene-d_8 and $CDCl_3$ as solvents; however, the low solubility of the clusters in these solvents led to sensitivity problems that were remedied by a change to the solvent CD_2Cl_2. The higher solubility of both clusters in CD_2Cl_2 greatly facilitated the rate measurements by NMR spectroscopy. Heating a CD_2Cl_2 solution of freshly prepared bridging cluster (**5b**) under argon at 323 K revealed a smooth decrease in the ^{31}P bridging resonance at δ 35.50 and the formation of a new signal at δ 66.40 as shown in Figure 2.1. The peak positions of these ^{31}P resonances are in excellent agreement with the weighted-average chemical shift data calculated from the reported slow-exchange spectral data of the bridging and chelating isomers of $H_4Ru_4(CO)_{10}$(dppe).[2] The isomerization was clean and afforded an isomeric mixture of chelating and bridging isomers in a 94:6 ratio, respectively, after 30 hrs at 323 K, (ca. 10 half-lives). The fact that no mention of an equilibrium involving clusters **5b** and **5c** was made in the original report may be attributed to the aforementioned solubility problems that could easily complicate the observation of the small amount of the dppe-bridged cluster **5b** at equilibrium.

The disappearance of the bridging isomer and formation of the chelating isomer was monitored by ^{31}P NMR spectroscopy at regular intervals. Figure 2.2 depicts the bridge-to-chelate isomerization reaction as it approaches equilibrium in toluene-d_8 at 323 K. Non-linear regression analysis of the ^{31}P NMR data afforded the first-order rate constants (k_e) for the consumption of the bridging isomer and formation of chelating isomer.[13]

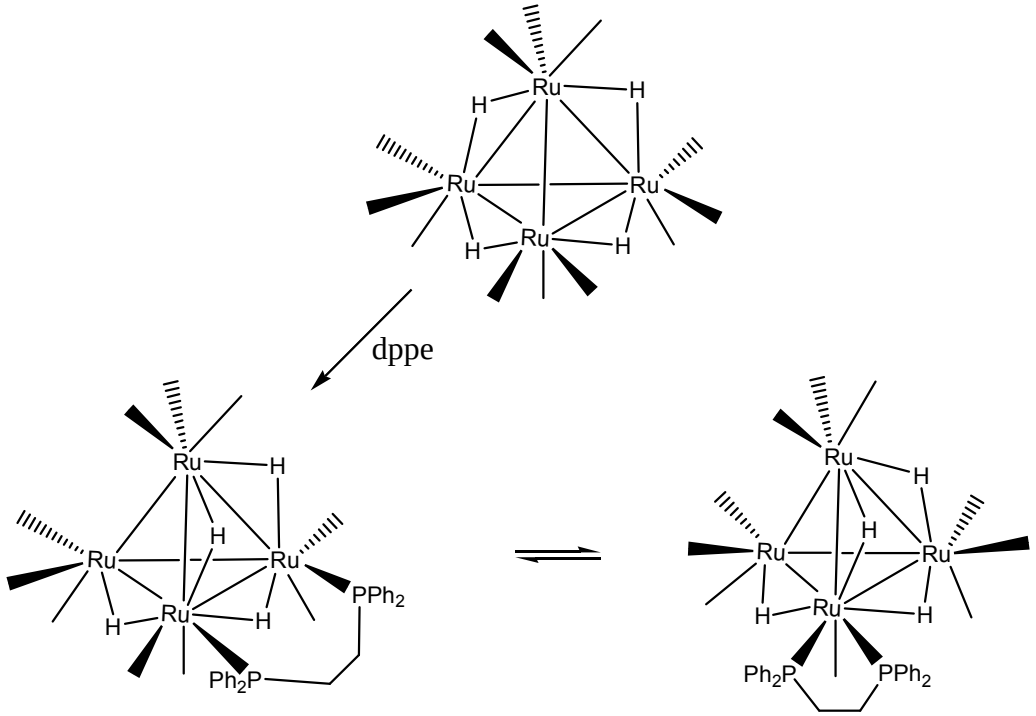

5b **5c**

Scheme 2.4 Reaction between dppe and $H_4Ru_4(CO)_{12}$ and isomerization of the ancillary dppe ligand.

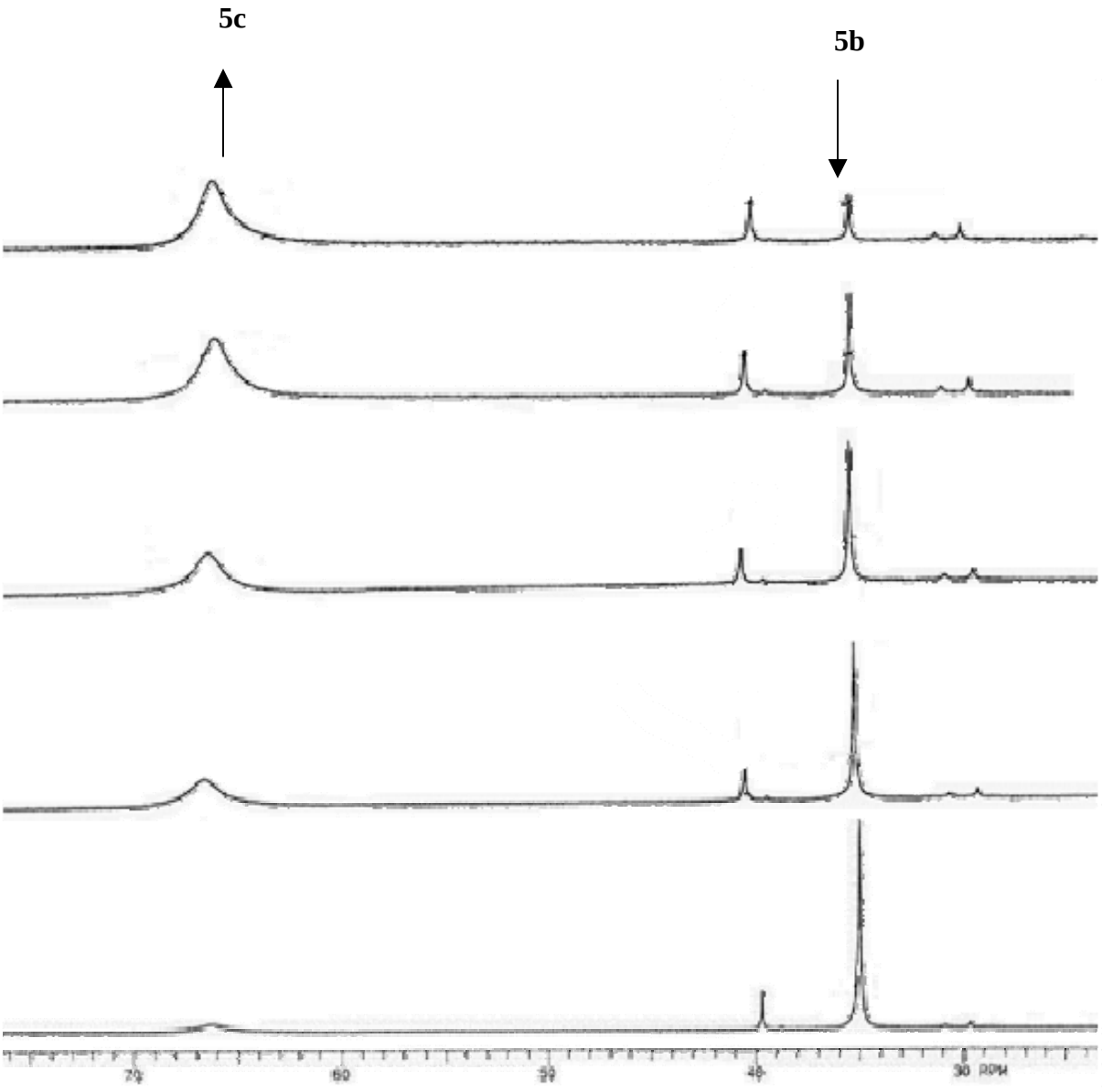

Figure 2.1 ^{31}P NMR spectral changes for the isomerization of **5b** to **5c** in CD_2Cl_2 at 323 K.

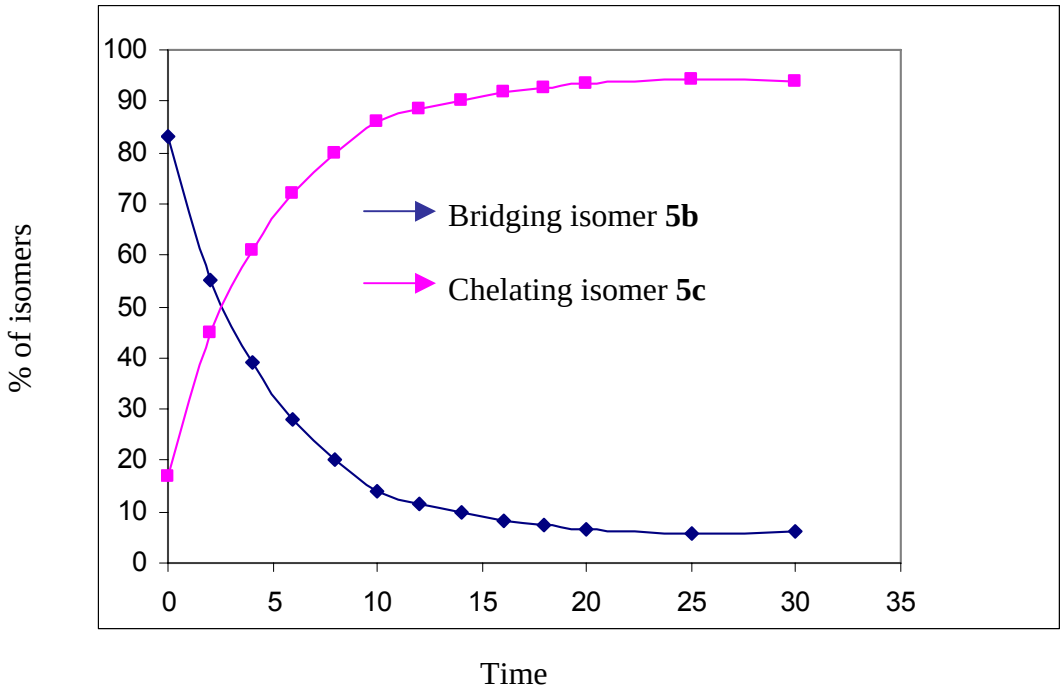

Figure 2.2 Plot of the cluster distribution of **5b** and **5c** versus time at 323 K.

The effect of added PPh_3 on the isomerization reaction was also studied by ^1H NMR spectroscopy in CD_2Cl_2 at 323 K by monitoring the rate of consumption of the bridging isomer. The progress of the reaction was monitored through the use of the hydride resonance at δ-17.15. This singlet represents the four rapidly exchanging hydride groups. The transformation from the bridging isomer to the chelating isomer was found to take place cleanly and without any evidence for the incorporation of PPh_3 into either isomer (Figure 2.3). The absence of PPh_3 incorporation into the end product rules out the long-lived unsaturated intermediate. Good first-order kinetics were found for over 4 half-

lives from the plot of ln[k/t] versus time, and the computed value of k_e [7.40(0.47) x 10^{-5} s^{-1}] from non-linear regression analysis agrees nicely with the rate obtained from the ^{31}P NMR experiment. The similarity in the k_e values and the absence of PPh_3 incorporation into the isomeric clusters **5a** and **5b** support a nondissociative, unimolecular isomerization of the dppe ligand. These computed rate constants to equilibrium were found to be identical within experimental error, with the average of these rates reported in Table 1.1, as well as the values for the forward (k_1) and reverse (k_{-1}) rate contributions.[1]

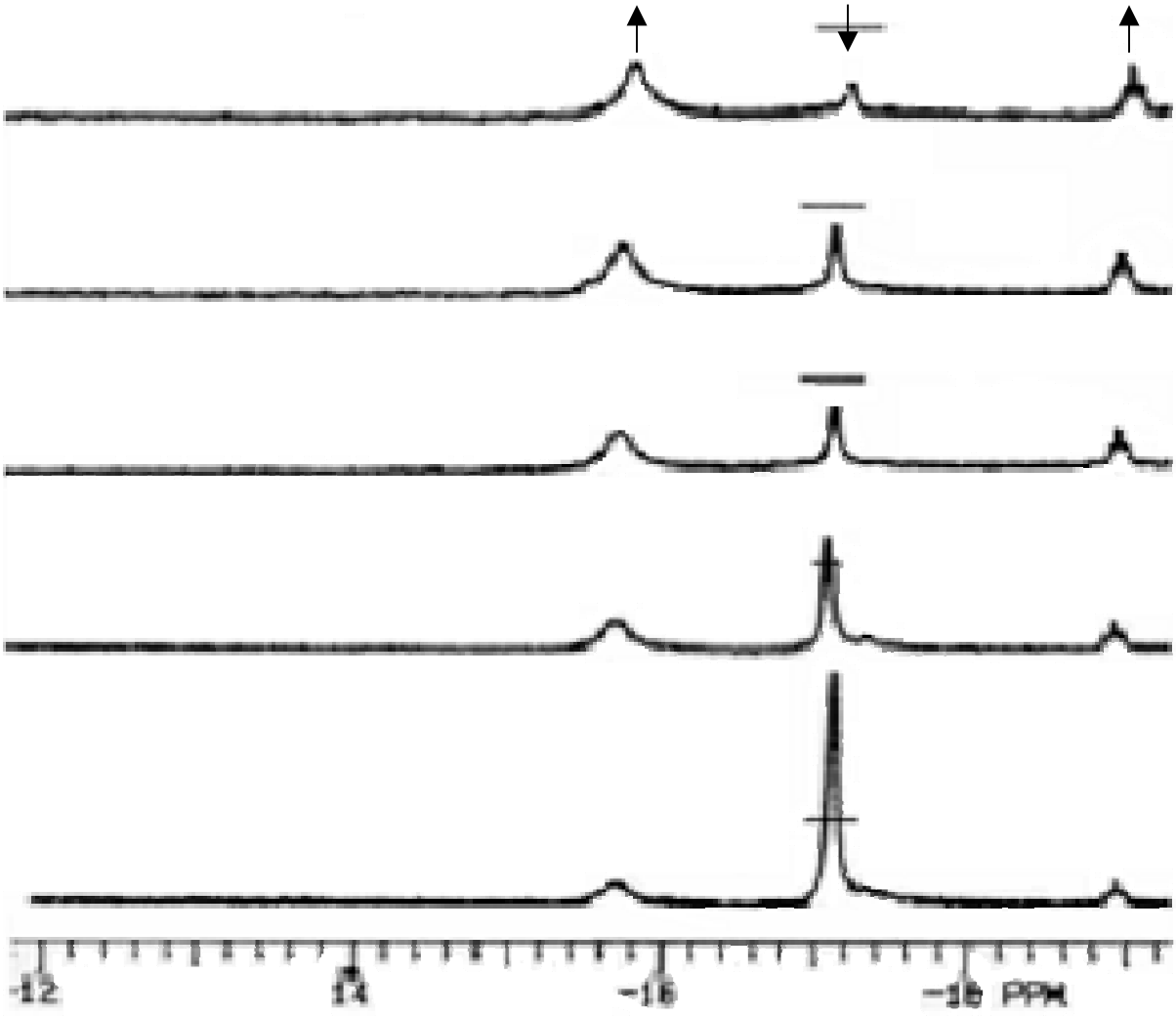

Figure 2.3 ^1H NMR spectral changes for the isomerization of **5b** to **5c** in

toluene-d_8 at 323 K in the presence of added PPh_3.

The equilibrium between **5b** and **5c** was more fully investigated by UV-vis spectroscopy over the temperature range of 308-328 K using toluene as the reaction solvent. Here the rate to equilibrium was measured by following the decrease in the 300 nm band belonging to **5b**. Figures 2.4 and 2.5 show the spectral changes that accompany the isomerization and non-linear regression analysis of these UV-vis data, respectively. Isosbestic points at 368 and 334 nm confirm that the isomerization is well-behaved and free from kinetic complications. As in the case of the NMR reaction carried out with added PPh_3, the presence of added CO (1 atm) in the UV-vis reaction afforded rates indistinguishable to those reactions conducted under argon (entries 2 and 3; entries 6 and 7-Table 2.1). The effect of solvent on the rate of the isomerization was also examined by running the UV-vis kinetic experiments in CH_2Cl_2 and THF (entries 4, 8, and 9-Table 2.1). These experiments showed no substantial solvent effect on the rate of isomerization.[14,15] This latter observation argues against the formation of a highly polarized intermediate or transition state.

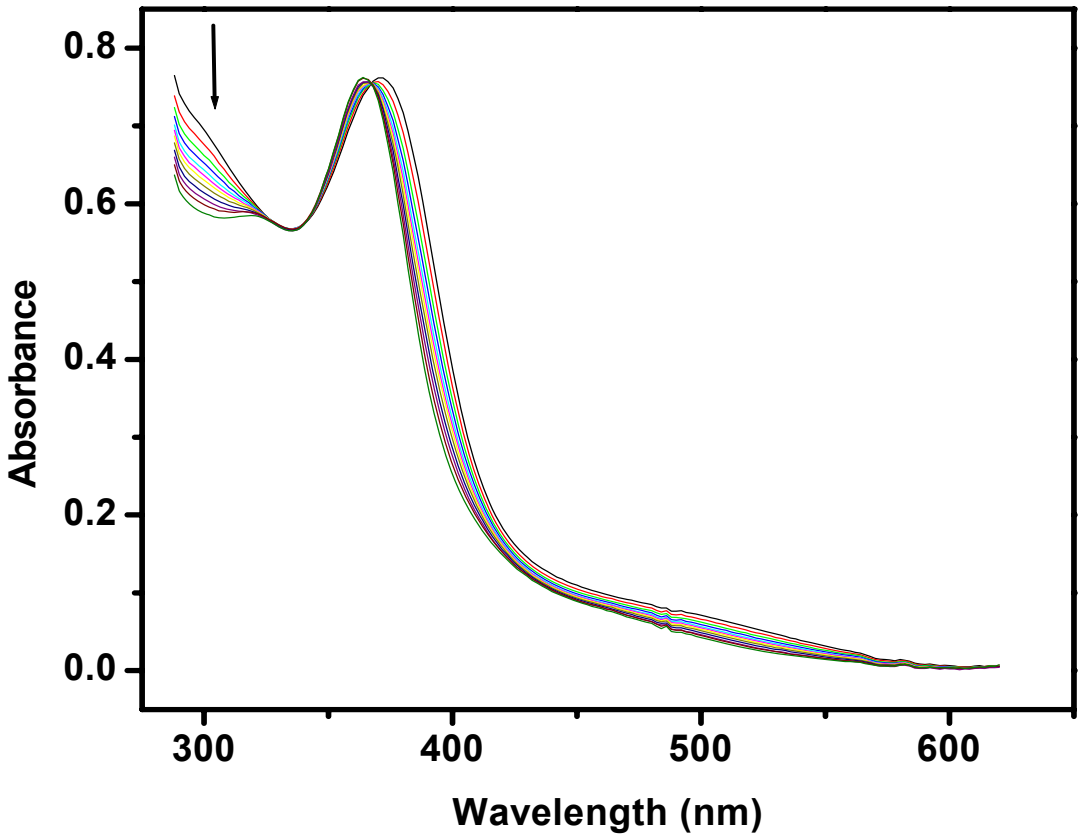

Figure 2.4 UV-vis spectral changes for the isomerization of **5b** to **5c** in toluene at 323 K.

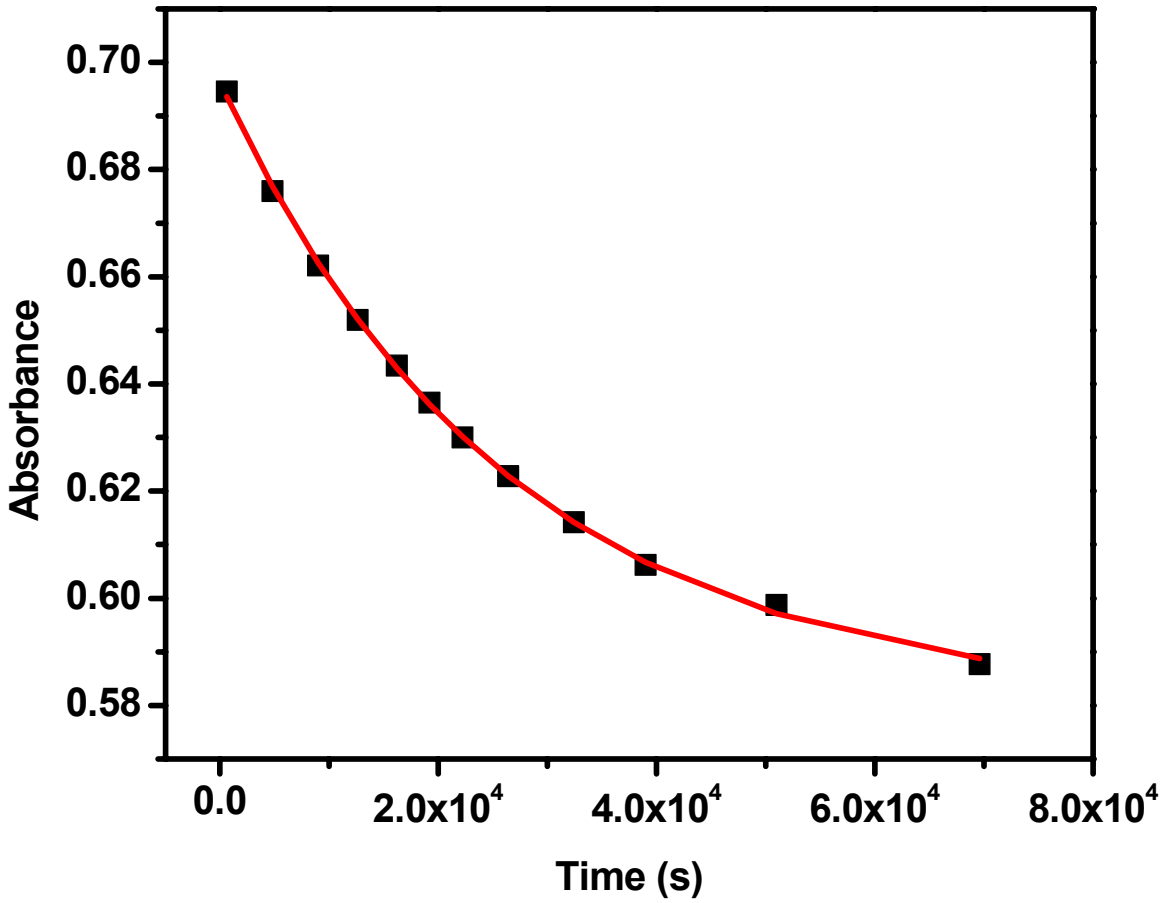

Figure 2.5 The absorbance decrease in the 300 nm band versus time curve for the experimental data (■) and the least-squares fit of k_e (——).

Table 2.1 Kinetic data for diphosphine isomerization in $H_4Ru_4(CO)_{10}$(dppe).[a]

Temp (K)	Solvent	10^5k_e (s^{-1})	10^5k_1 (s^{-1})[b]	10^5k_{-1} (s^{-1})	Method
308	toluene	1.78 ± 0.00	1.67 ± 0.04	0.11 ± 0.04	UV-vis
313	toluene	2.57 ± 0.09	2.42 ± 0.09	0.15 ± 0.09	UV-vis
313	toluene[c]	2.35 ± 0.04	2.21 ± 0.04	0.14 ± 0.04	UV-vis
313	DCM	1.95 ± 0.05	1.83 ± 0.05	0.12 ± 0.05	UV-vis
318	toluene	3.84 ± 0.03	3.61 ± 0.03	0.23 ± 0.03	UV-vis
323	toluene	4.95 ± 0.10	4.65 ± 0.10	0.3 ± 0.10	UV-vis
323	toluene[c]	4.30 ± 0.04	4.04 ± 0.04	0.26 ± 0.04	UV-vis
323	DCM	5.75 ± 0.11	5.41 ± 0.11	0.34 ± 0.11	UV-vis
323	THF	3.81 ± 0.07	3.58 ± 0.07	0.23 ± 0.07	UV-vis
323	DCM	5.88 ± 0.09	5.53 ± 0.09	0.35 ± 0.09	^{31}P NMR
323	DCM[d]	7.40 ± 0.47	6.90 ± 0.47	0.44 ± 0.47	^{1}H NMR
328	toluene	7.37 ± 0.07	6.93 ± 0.07	0.44 ± 0.07	UV-vis

[a]All kinetic data were collected under argon unless otherwise noted. [b]The quoted rate constants (k_e) represent the rate towards equilibrium, as determined by following the decrease in the 300 nm band (UV-vis), changes in the ^{31}P resonances for the bridging and chelating isomers (^{31}P NMR), or the decrease in the hydride resonance for the bridging isomer (^{1}H NMR). [c]Experiments conducted under 1 atm of CO. [d]Experiment conducted in the presence of 10 eq of PPh_3.

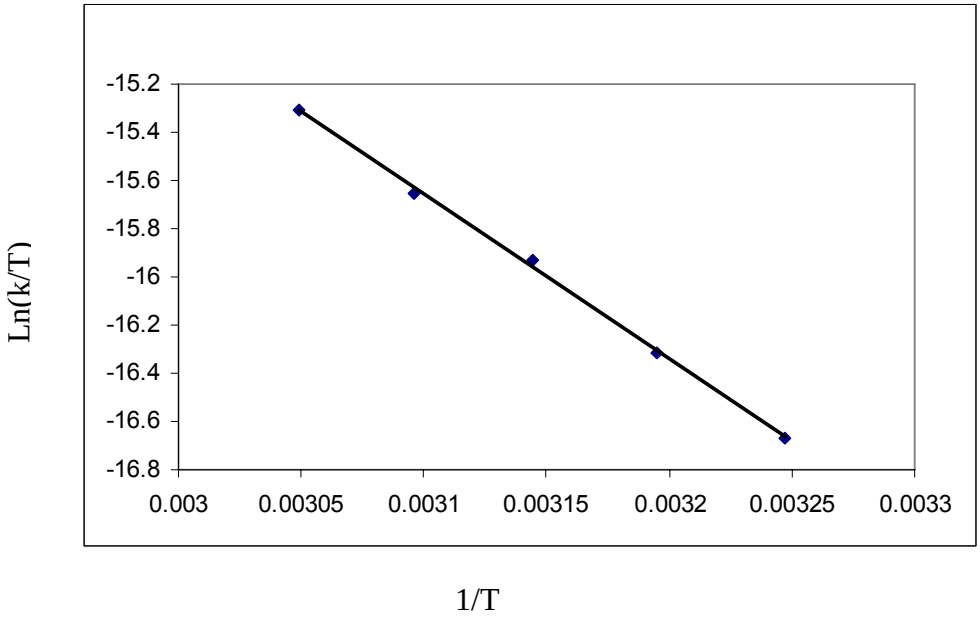

Figure 2.6 Eyring plot for the isomerization of **5b** to **5c.**

The Eyring activation parameters for the forward and reverse directions of the isomerization were calculated as $\Delta H^{\ddagger}$ = 13.2(9) kcal/mol and $\Delta S^{\ddagger}$ = -38(3) eu and $\Delta H^{\ddagger}$ = 13.0(8) kcal/mol and $\Delta S^{\ddagger}$ = -44(3) eu, respectively. These kinetic data support a nondissociative, intramolecular process that involves the migration of the dppe ligand across a ruthenium-ruthenium bond from **5b** to **5c** and **5c** to **5b**. A rate-limiting process involving the dissociative loss of CO, H_2, or release of one end of the dppe ligand from the Ru_4 cluster can be eliminated from consideration based on indistinguishable rates measured under argon, CO, and PPh_3, coupled with the large negative entropies of activation. The calculated values for $\Delta S^{\ddagger}$ are consistent with the proposed mechanism where one of the terminally bound PPh_2

moieties transforms into a bridging μ-PPh_2 moiety as it transits across a Ru-Ru bond in the equatorial plane defined by the basal ruthenium atoms.[16] Implicit in such a scenario is the simultaneous migration of CO ligands and an "opening up" of the bridging hydride groups. Scheme 2.4 illustrates a plausible scheme for the isomerization of the dppe ligand in $H_4Ru_4(CO)_{10}$(dppe). Given the documented edge-terminal-edge hydride mobility in both clusters **5b** and **5c**, a non-dissociative ligand isomerization involving two equatorially bound CO groups and one end of the dppe ligand would allow the permutation of these three ligands between the three ruthenium centers.[17] The transient terminal hydride groups at each ruthenium center that accompany the migration of the two CO groups and the PPh_2 moiety are not shown in the isomerization scheme. The presence of terminal hydride groups facilitates the overall migration of the phosphine and CO ligands by eliminating the two basally confined edge-bridged hydrides that would otherwise retard the proposed migratory path of the non-hydride ligands.

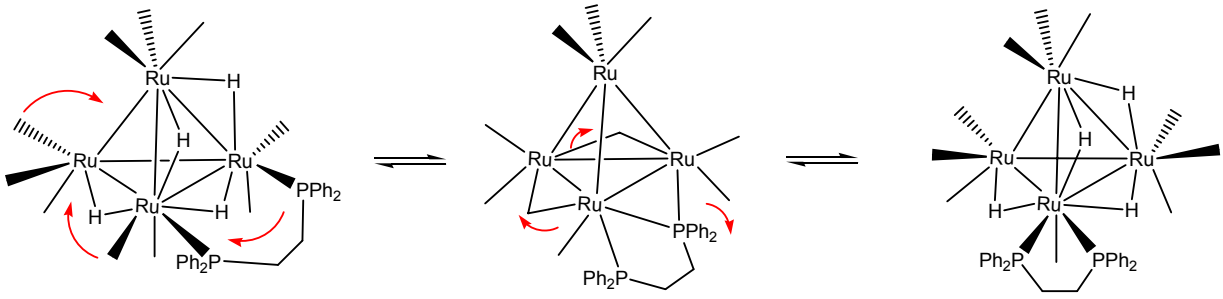

Scheme 2.5 Proposed non-dissociative ligand isomerization mechanism for the isomerization of **5b** to **5c**.

2.4. Conclusions

The lack of observable bridge-to-chelate isomerization for the prophos ligand in 1,2-$H_4Ru_4(CO)_{10}$(prophos) suggests that the presence of a single methyl group on the two-carbon ethane chain is sufficient to negate the isomerization reaction. This is understandable and expected if the atoms associated with the ethane backbone must adopt an eclipsed conformation during the transit of the diphosphine ligand across the ruthenium-ruthenium bond. Indirect proof for the importance of such subtle steric effects in the diphosphine isomerization reaction derives from the related clusters $H_4Ru_4(CO)_{10}$[(Z)-$Ph_2PCH=CHPPh_2$][7] and $H_4Ru_4(CO)_{10}$[dbpcd]. These two clusters exhibit only chelating diphosphine ligands irrespective of the methods used to activate the parent cluster. It is believed that the unsaturated C=C backbone that links the two phosphine centers promotes the bridge-to-chelate isomerization in the case of the unsaturated ligands (Z)-$Ph_2PCH=CHPPh_2$ and dbpcd through the elimination of the aforementioned eclipsing interactions in the saturated carbon bridges of dppe, prophos, and longer chain diphosphine homologues.

2.5 Chapter References

1. Churchill, M.R.; Lashewycz, R.A. *Inorg. Chem.* **1978**, *17*, 1950.
2. Churchill, M.R.; Lashewycz, R.A.; Shapley, J.R.; Richter, S.I. *Inorg. Chem.* **1980**, *19*, 1277.

3. Shapley, J.R.; Richter, S.I.; Churchill, M.R.; Lashewycz, R.A. *J. Am. Chem. Soc.* **1977**, *99*, 7384.
4. Puga, J.; Arce, A.; Braga, D.; Centritto, N.; Grepioni, F.; Castillo, R.; Ascanio, J. *Inorg. Chem.* **1987**, *26*, 867.
5. The diphosphine ligand prophos is also known as 1,2-bis(diphenyl phosphino)propane.
6. Evans, J.; Gracey, B. P.; Gray, L. R.; Webster, M. *J. Organomet. Chem.* **1982**, *240*, C61.
7. (a) Yang, K.; Smith, J.M.; Bott, S.G.; Richmond, M.G. *Organometallics* **1993**, *12*, 4779. (b) Bott, S.G.; Yang, K.; Richmond, M.G. *J. Organomet. Chem.* **2005**, *690*, 3067.
8. Laurenczy, G.; Bondietti, G.; Ros, R.; Roulet, R. *Inorg. Chim. Acta* **1996**, *247*, 65.
9. Sutin, K.A.; Kolis, J.W.; Mlekuz, M.; Bougeard, P.; Sayer, B.G.; Quilliam, M.A.; Faggiani, R.; Lock, C.J.L.; McGlinchey, M.J.; Jaouen, G. *Organometallics* **1987**, *6*, 439.
10. Adams, R.D.; Captain, B.; Fu, W.; Pellechia, P. J. *Inorg. Chem.* **2003**, *42*, 3111.
11. Watson, W.H.; Wu, G.; Richmond, M.J. *Organometallics* **2005**, *24*, 5431.
12. (a) Fenske, D.; Becher, H. *Chem. Ber.* **1974**, *107*, 117. (b) Fenske, D. *Chem. Ber.* **1979**, *112*, 363.
13. Watson, W.H.; Kandala, S.; Richmond, M.G. *J. Chem. Crystallogr.* **2006**, *36*, 813.

14. Espenson, J. H. *Chemical Kinetics and Reaction Mechanisms*, 2nd ed.; McGraw-Hill: New York, 1995.

15. The UV-vis data have also been treated in terms of a reversible equilibrium as were those data obtained from the ^{31}P NMR experiment.

16. For other unimolecular structural reorganizations that exhibit large, negative $\Delta S^{\ddagger}$ values, see: (a) Grynkewich, G.W.; Marks, T.J. *Inorg. Chem.* **1976**, *15*, 1307. (b) Sundararajan, G.; San Fillippo, J., Jr. *Organometallics* **1985**, *4*, 606.

17. (a) Pursiainen, J.; Pakkanen, T.A. *J. Organomet. Chem.* **1989**, *362*, 375. (b) Chen, C.C.; Chi, S.M.; Lee, G.H. *J. Chem. Soc., Dalton Trans.* **1993**, 1823. (c) Wang, J.C.; Chi, Y.; Peng, S.M.; Lee, G.H.; Shyu, S.G.; Tu, F.H. *J. Organomet. Chem.* **1994**, *481*, 143. (d) Horng, H.C.; Cheng, C.P.; Yang, C.S.; Lee, G.H. *Organometallics* **1996**, *15*, 2543.

CHAPTER 3

SUBSTITUTION CHEMISTRY OF 1,2-BIS(DIPHENYLPHOSPHINO)BENZENE AT TRIOSMIUM DODECACARBONYL CLUSTERS

The introduction of different substituents at the carbon atoms of P-C=C-P skeleton has the potential to furnish many new types of diphosphine ligands having a rigid unsaturated backbone.[1] Such novel diphosphine ligands can be used to study the steric and electronic factors that affect the structure, ligand fluxionality, and reactivity of diphosphine-substituted polynuclear organometallic compounds. Over the last several years, the Richmond group has explored the reactivity of the rigid diphosphine ligands 4,5-bis(diphenylphosphino)-4-cyclopenten-1,3-dione (bpcd), 2,3-bis-(diphenylphosphino)maleic anhydride (bma) and 3,4-bis(diphenylphosphino)cyclobutenedione (bpcbd) with polynuclear clusters (Figure 3.1).[1] Their investigations have included the study of the structural dynamics exhibited by such ligands and mechanistic examination on the degradation pathways that these diphosphine ligands participate in upon thermolysis and photolysis reactions.

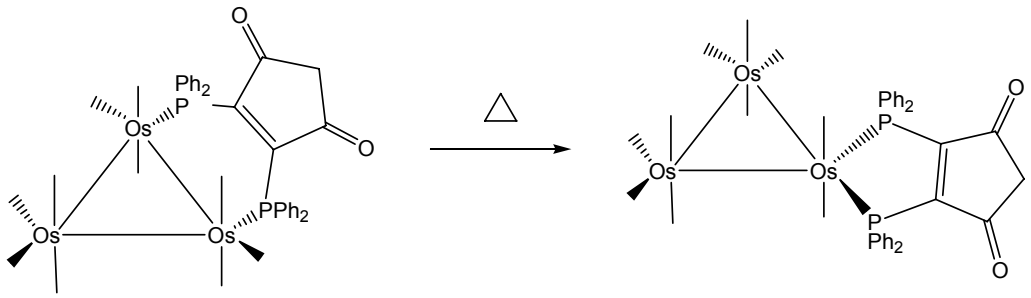

Figure 3.1 Diphosphine isomerization of the bpcd ligand in the triosmium cluster $Os_3(CO)_{10}$(bpcd).

The reaction between the diphosphine ligand bpcd and 1,2-$Os_3(CO)_{10}(MeCN)_2$ has been investigated and found to give 1,2-$Os_3(CO)_{10}$(bpcd) as the kinetic product of ligand substitution.[2] Thermolysis of the bridged cluster 1,2-$Os_3(CO)_{10}$(bpcd) is accompanied by a nondissociative, irreversible ligand isomerization to give the corresponding diphosphine chelated cluster 1,1-$Os_3(CO)_{10}$(bpcd). The isomerization kinetics and thermodynamics have been studied by UV-vis and NMR spectroscopic methods. Extended thermolysis of 1,1-$Os_3(CO)_{10}$(bpcd) furnished the C-H and P-C bond activation products $HOs_3(CO)_9[\mu\text{-}PhP(C_6H_4)C{=}C(PPh_2)C(O)CH_2C(O)]$ and $HOs_3(CO)_8(\mu_3\text{-}C_6H_4)[\mu\text{-}PPh)C{=}C(PPh_2)C(O)CH_2C(O)]$, respectively. These new hydride-bridged clusters were fully characterized by a combination of solution spectroscopic methods, X-ray crystallography and elemental analyses.

To explore the effect that an aromatic backbone has on the diphosphine ligand with respect to its reactivity upon coordination to the triosmium cluster "$Os_3(CO)_{10}$," the related ligand 1,2-bis(diphenylphosphino)benzene (dppbz) has been allowed to react with the triosmium cluster 1,2-$Os_3(CO)_{10}(MeCN)_2$. The resulting triosmium cluster products have been fully investigated. Presented here is the detailed discussion of the observed reactivity of the benzene-based diphosphine ligand in the cluster $Os_3(CO)_{10}$(dppbz).

3.1 Results and Discussion

3.1.1 Synthesis, Characterization, and X-ray Diffraction Structures of the Isomeric Clusters 1,2- and 1,1-$Os_3(CO)_{10}$(dppbz)

The substitution of the acetonitrile ligands in the activated cluster 1,2-$Os_3(CO)_{10}(MeCN)_2$ (**6**) by an equimolar amount of the unsaturated diphosphine ligand 1,2-bis(diphenylphosphino)benzene (dppbz) (**7**) proceeds rapidly at room temperature with complete consumption of the starting cluster (Scheme 3.1). ^{31}P NMR analysis of the crude reaction mixture revealed the presence of three products assigned to the clusters 1,2-$Os_3(CO)_{10}$(dppbz) **(8b),** 1,1-Os_3-$(CO)_{10}$ (dppbz) (**8c**) and $HOs_3(CO)_9[\mu$-$(PPh_2)C_6H_4C\{PPh(C_6H_4)\}]$ (**9**). The observed cluster distribution was in ca. 20%, 60% and 20%, respectively. TLC examination of the reaction mixture revealed only one spot for the three cluster products, necessitating the use of NMR spectroscopy to unequivocally establish the composition of the mixture.

Particularly diagnostic in the characterization of the mixture of products was the ^{31}P NMR spectroscopy. Here separate ^{31}P resonances were observed for clusters **8b**, **8c** and **9**. The singlet observed at δ 8.50 is in agreement with the proposed dppbz-bridged cluster **8b,** while the singlet reported at δ 26.50 is readily assigned to the chelating cluster **8c.** The two distinct doublets observed at δ 28.50 and δ 40.50 are characteristic of non-equivalent phosphine moieties typically found in related hydride clusters.[3] Attempts to obtain pure 1,2-

$Os_3(CO)_{10}$(dppbz) through repeated recrystallyzations and the use of shorter reactions times were not successful. In an important observation, lowering the reaction temperature to 0 °C led to the formation of bridging isomer **8b** as major product apart from the formation of chelating isomer **8c** and hydride cluster **9**. It was subsequently confirmed that stirring cluster **6** and dppbz at 0 °C for one hour in DCM yielded clusters **8b**, **8c**, and **9** in a 75:15:10 ratio. In another control experiment, the reaction vessel was covered with aluminum foil and the run in the dark at 0 °C. Here no change in the composition of the three clusters was found relative to the reaction conducted at 0 °C under laboratory light.

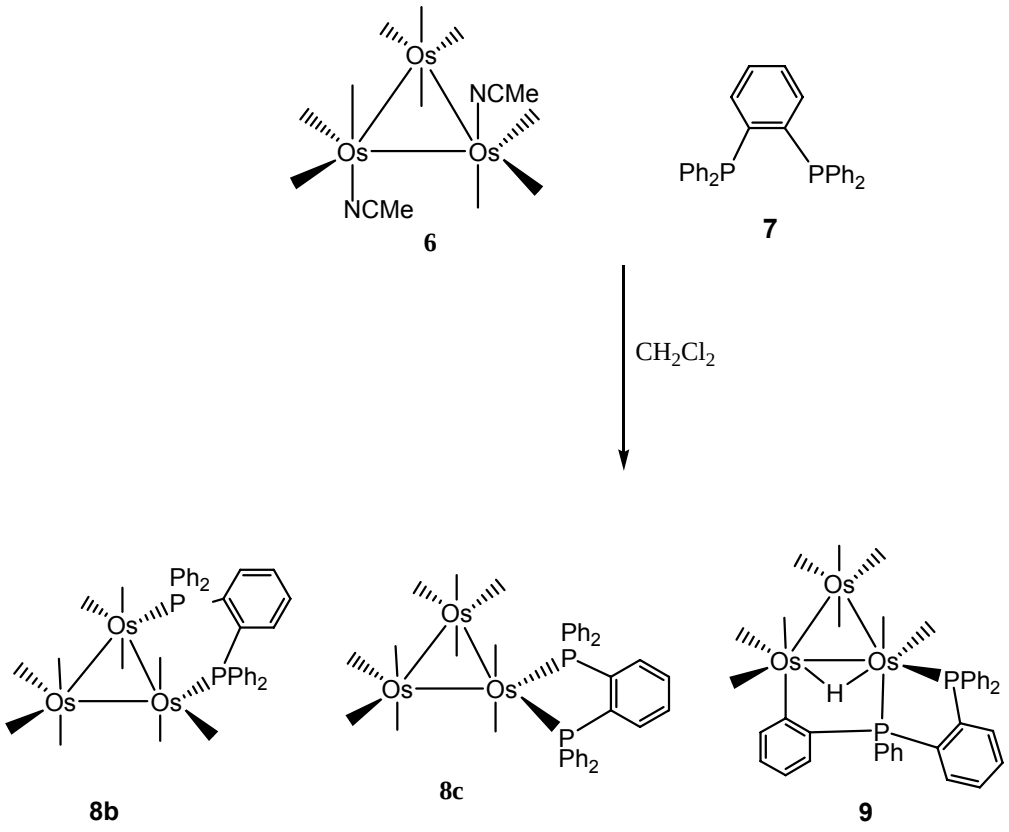

Scheme 3.1 Isolated products from the reaction of 1,2-$Os_3(CO)_{10}(MeCN)_2$ with dppbz.

The last control experiment indicates that a room-light promoted ortho

metalation of **8b** or **8c** may be eliminated as a route to cluster **9**. These control experiments suggest that clusters **8b, 8c,** and **9** originate from independent pathways. The amount of cluster **9** formed in the control experiments was not statistically different from the standard reaction between **6** and dppbz. Also, the thermal conversion of the bridging isomer **8b** to the chelating isomer **8c** at room temperature can be eliminated from consideration based on the extrapolated rate data from the isomerization studies on conversion of **8b** to **8c,** which place the half-life for this conversion at 298 K at over 5 days. From these kinetic data, it may be concluded that clusters **8b, 8c** and **9** observed in the initial synthetic reactions must arise from the direct or independent substitution sequence involving **6** and dppbz. The reactivity pattern observed in reaction between **6** and dppbz is similar to the bimodal substitution observed in the reaction of cluster **6** with the diphosphine ligand dmpe, which affords the two clusters 1,2-$Os_3(CO)_{10}$(dmpe) and 1,1-$Os_3(CO)_{10}$(dmpe) as a non-interconverting isomeric mixture.[4]

3.1.2 Thermolysis of the Triosmium Cluster Mixture

The initial 20:60:20 cluster mixture containing **8b**, **8c** and **9** was subjected to thermolysis in toluene in a sealed NMR tube under 1 atm of CO at 55 °C in a thermostated bath for 24 h. The extent of the reaction was monitored by ^{31}P NMR spectroscopy. The thermolysis of this particular cluster mixture was accompanied by the complete consumption of clusters **8b** and **9** and the formation of the chelating cluster **8c** in quantitative yield after 24 hrs. The ^{31}P NMR spectral changes and the graphical representation of changes in the concentration of

these clusters as a fur **8c** of time are represented in Figures 3.2 and 3.3.

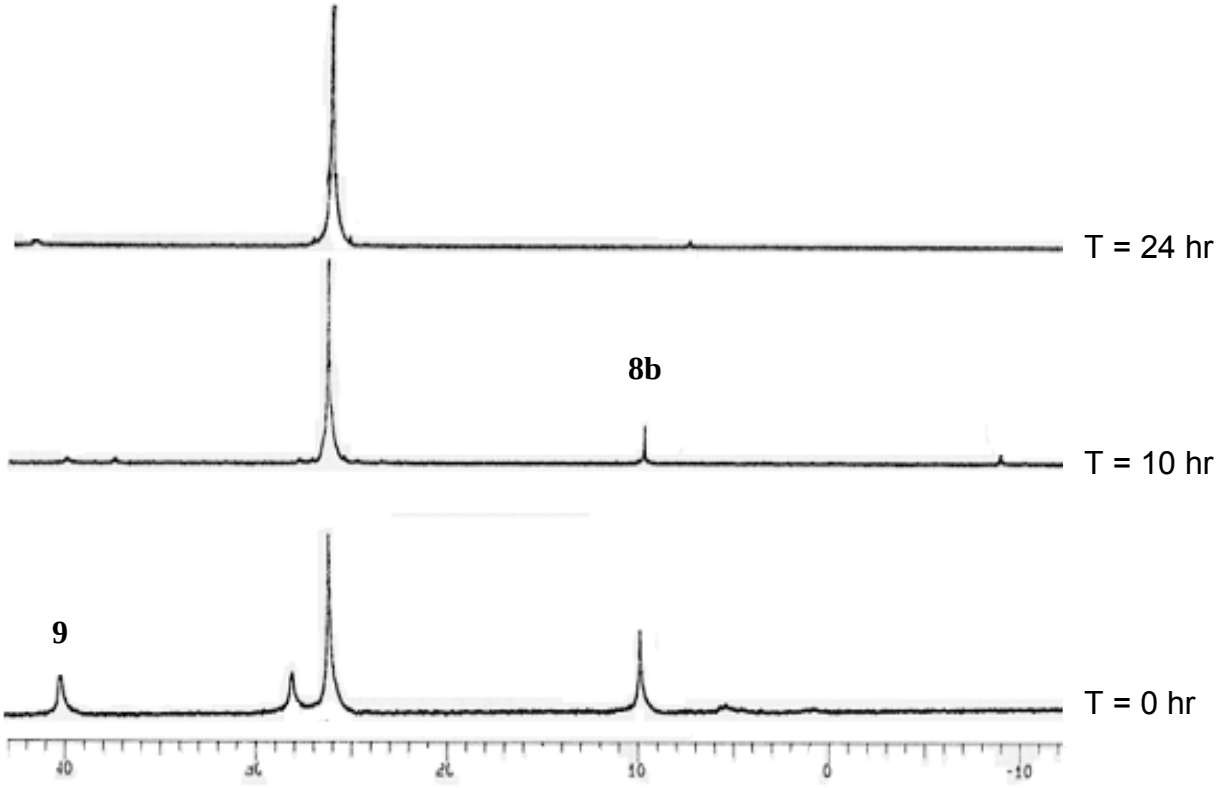

Figure 3.2 ^{31}P NMR spectral changes observed in the thermolysis of the initial mixture of clusters **8b**, **8c** and **9.**

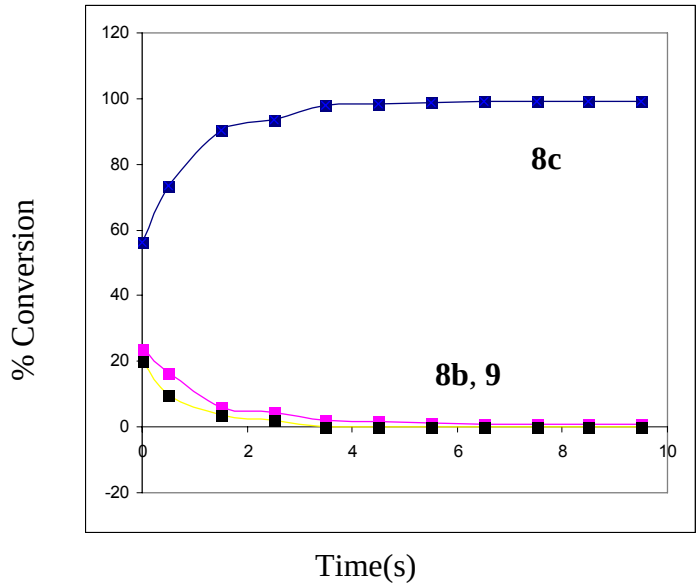

Figure 3.3 Plot of the cluster distribution (**8b**, **8c** and **9**) versus time during the

thermolysis at 50 °C.

These results parallel earlier research work on the isomeric osmium clusters $Os_3(CO)_{10}$(bpcd), where added CO suppressed the ortho-metalation reaction that affords the hydride cluster $HOs_3(CO)_9$[μ-(PPh_2)C=C{$PPh(C_6H_4)$}C(O)CH_2C(O)] but did not adversely affect the isomerization of the bridging to chelating transformation of the ancillary diphosphine ligand.[2]

The ^{1}H NMR spectrum at the end of thermolysis in $CDCl_3$ revealed only the presence of cluster **8c**. Here a multiplet corresponding to 24 aromatic hydrogens was observed at δ 6.50 - 7.80. The downfield singlet recorded at δ 26.50 in the ^{31}P NMR spectrum is in accord with the proposed structure for cluster **8c**. The IR spectrum of the chelating isomer exhibits terminal carbonyl stretching bands at 2095 (s), 2042 (s), 2012 (s), 1990 (m), 1974 (m), and 1956 (m) cm^{-1}.[5] The reaction of the activated cluster $Os_3(CO)_{10}(MeCN)_2$ with dppbz ligand at 0 °C yielded the dppbz-bridged triosmium cluster as major product (<75%) based on ^{31}P spectroscopy. The identity of clusters **8b** and **8c** was unequivocally established by single crystal X-ray crystallography. X-ray quality crystals of 1,2- and 1,1-$Os_3(CO)_{10}$(dppbz), the former which exists as the CH_2Cl_2 solvate, were successfully grown from a CH_2Cl_2 solution containing the respective cluster that had been layered with hexane. The X-ray data processing and collection parameters for 1,2-$Os_3(CO)_{10}$(dppbz) are listed in Table 3.1, with selected bond distances and angles given in Table 3.2. The molecular configuration and the numbering scheme of 1,2-$Os_3(CO)_{10}$(dppbz) are presented

in the thermal ellipsoid plot shown in Figure 3.4.

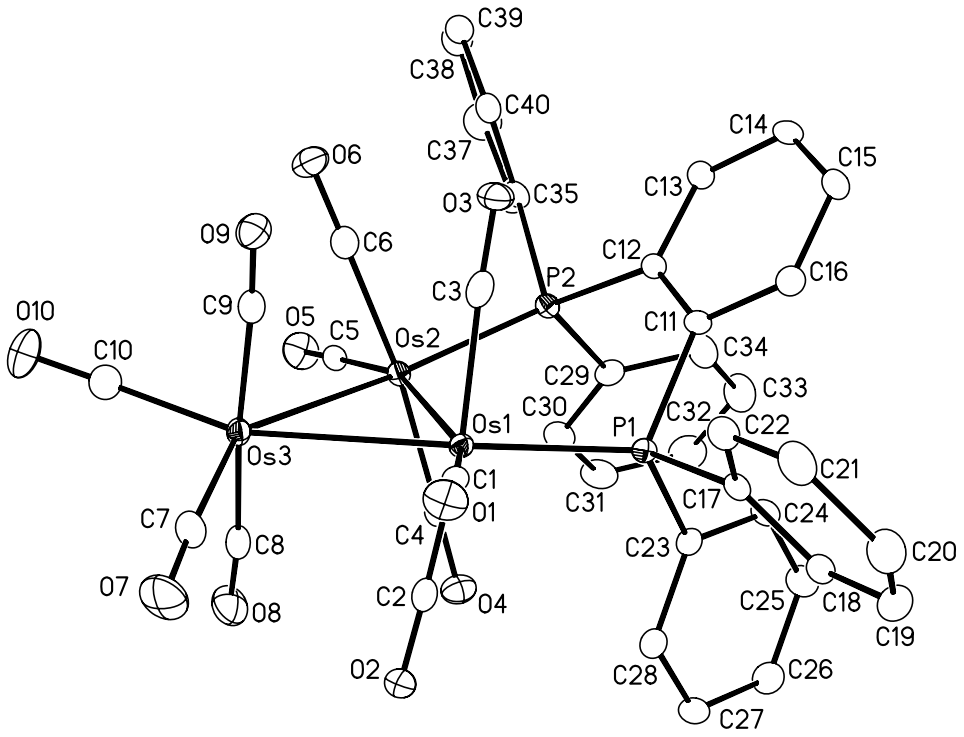

Figure 3.4 Thermal ellipsoid plot of the non-hydrogen atoms of 1,2-$Os_3(CO)_{10}$(dppbz) (**8b**) showing the thermal ellipsoids at the 50% probability level.

Table 3.1 Crystal data and structure refinement details for 1,2-$Os_3(CO)_{10}$ (dppbz).CH_2Cl_2.

Identification code	osdipbz-1	
Empirical formula	$C_{40}H_{24}O_{10}Os_3P_2$. CH_2Cl_2	
Formula weight	1382.06	
Temperature	100(2) K	
Wavelength	0.71073 Å	
Crystal system	Triclinic	
Space group	P-1	
Unit cell dimensions	a = 11.9406(3) Å	α= 86.09°.
	b = 13.2173(4) Å	α = 70.01°.
	c = 15.0648(4) Å	α = 66.42°.
Volume	2041.3(1) $Å^3$	
Formula units per cell (Z)	2	
Density (calculated)	2.249 Mg/m^3	
Absorption coefficient	9.581 mm^{-1}	
Reflections collected	24301	
Independent reflections	8375 [R(int) = 0.0176]	
Completeness to theta = 26.40°	99.9%	
Absorption correction	Semi-empirical from equivalents	
Max. and min. transmission	0.5971 and 0.4188	
Refinement method	Full-matrix least-squares on F^2	
Data / restraints / parameters	8375 / 0 / 523	
Goodness-of-fit on F^2	1.012	
Final R indices [I > 2σ(I)]	R1 = 0.0140, wR2 = 0.0322	
R indices (all data)	R1 = 0.0160, wR2 = 0.0328	
Δp(max), Δp(min) ($e/Å^{-3}$)	1.14 and -0.42	

Table 3.2 Selected bond lengths [Å] and bond angles [°] for 1,2-$Os_3(CO)_{10}$(dppbz).

Bond lengths

Os(1)-C(1)	1.891(3)	C(12)-C(13)	1.398(3)
Os(1)-C(2)	1.936(3)	C(11)-C(12)	1.423(3)
Os(1)-C(3)	1.941(3)	C(11)-C(16)	1.400(3)
Os(1)-P(1)	2.335(6)	Os(3)-C(10)	1.910(3)
Os(1)-Os(2)	2.856(1)	Os(3)-C(8)	1.949(3)
Os(1)-Os(3)	2.856(1)	Os(3)-C(9)	1.958(3)
Os(2)-C(5)	1.890(3)	C(12)-C(13)	1.398(3)
Os(2)-C(6)	1.940(3)	C(13)-C(14)	1.390(3)
Os(2)-C(4)	1.944(3)	C(14)-C(15)	1.376(4)
Os(2)-P(2)	2.328(6)	C(15)-C(16)	1.392(3)
Os(2)-Os(3)	2.882(1)	C(17)-C(18)	1.397(3)
Os(3)-C(7)	1.906(3)	C(18)-C(19)	1.395(4)
P(1)-C(23)	1.827(2)	P(1)-C(11)	1.858(2)
P(1)-C(17)	1.840(3)	P(1) ·· P(2)	3.607(1)

Bond angles

C(1)-Os(1)-Os(2)	159.29(7)	C(2)-Os(1)-Os(2)	95.24(7)
C(3)-Os(1)-Os(2)	79.68(7)	P(1)-Os(1)-Os(2)	95.56(1)
C(1)-Os(1)-Os(3)	100.40(7)	C(2)-Os(1)-Os(3)	77.92(7)
C(3)-Os(1)-Os(3)	94.73(7)	P(1)-Os(1)-Os(3)	155.38(1)
Os(2)-Os(1)-Os(3)	60.68(4)	C(5)-Os(2)-C(6)	90.08(1)
C(5)-Os(2)-C(4)	93.23(1)	C(6)-Os(2)-C(4)	170.82(1)
C(5)-Os(2)-P(2)	94.34(8)	C(6)-Os(2)-P(2)	93.86(8)
C(4)-Os(2)-P(2)	94.42(8)	C(5)-Os(2)-Os(1)	163.79(7)
C(6)-Os(2)-Os(1)	95.06(7)	C(4)-Os(2)-Os(1)	79.53(7)
P(2)-Os(2)-Os(1)	100.62(1)	C(5)-Os(2)-Os(3)	106.99(7)
C(6)-Os(2)-Os(3)	76.20(7)	C(4)-Os(2)-Os(3)	94.64(7)
P(2)-Os(2)-Os(3)	156.26(1)	Os(1)-Os(2)-Os(3)	59.72(3)
C(7)-Os(3)-C(10)	100.51(1)	C(7)-Os(3)-C(8)	92.55(1)

The thermal ellipsoid plot of 1,2-$Os_3(CO)_{10}$(dppbz) confirms that the diphosphine ligand is attached to the triosmium frame by way of coordination to the Os(1) and Os(2) atoms. The Os-Os bond distances range from 2.856(4) Å [Os(1)-Os(2)] to 2.882(4) Å [Os(2)-Os(3)] and display a mean distance of 2.862 Å. The Os-Os distances are normal relative to those distances found in other simple polynuclear osmium clusters.[6-8] The ten terminal carbonyl groups may be considered as linear with standard distances and angles. The observed distortion of the axial CO groups in 1,2-$Os_3(CO)_{10}$(dppbz) from idealized D_{3h} to D_3 symmetry is a feature commonly found in many structurally characterized phosphine-substituted triosmium and triruthenium clusters.[9] The two Os-P bond lengths of 2.339(6) Å [Os(1)-P(1)] and 2.329(6) Å [Os(2)-P(2)] are in excellent agreement with the average Os-P bond distances reported for a variety of phosphine-substituted osmium compounds.[10,11] Coordination of the diphosphine ligand across the Os(1)-Os(2) bond leads to a significant stretching of the dppbz ligand that leads to ground-state destabilization relative to chelating isomer 1,1-$Os_3(CO)_{10}$(dppbz). The internuclear P(1) ··· P(2) bond distance of 3.607(1) Å found for 1,2-$Os_3(CO)_{10}$(dppbz) is ca 0.53 Å longer than the corresponding distance reported for free ligand, whose structural data are available upon request of the author.[12] The remaining bond distances and angles are unexceptional and require no comment.

Single crystals of 1,1-$Os_3(CO)_{10}$(dppbz) were grown from a concentrated solution of CH_2Cl_2 of the chelating isomer that has been layered with hexane. The X-ray data processing and collection parameters for 1,1-$Os_3(CO)_{10}$(dppbz) are

listed in Table 3.3, with selected bond distances and angles reported in Table 3.4. The molecular configuration and the numbering scheme for 1,1-$Os_3(CO)_{10}$(dppbz) are presented in Figure 3.5.

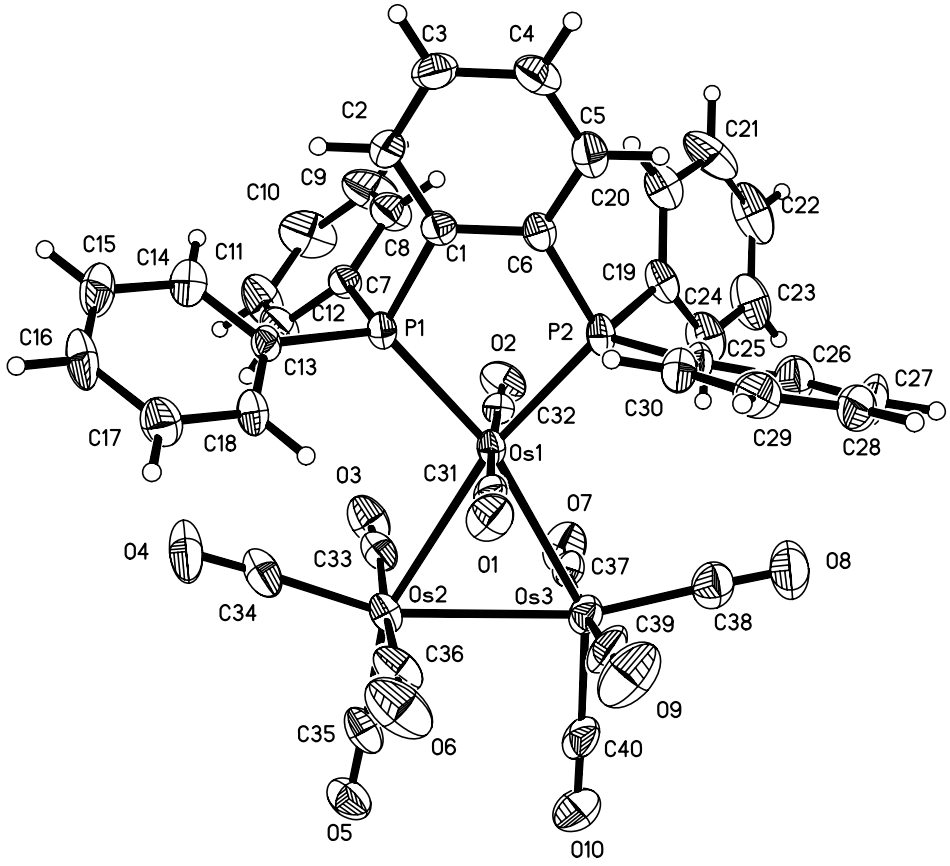

Figure 3.5 Thermal ellipsoid plot of 1,1-$Os_3(CO)_{10}$(dppbz) (**8c**) showing the thermal ellipsoids at the 50% probability level.

Table 3.3 Crystal and structure refinement data for 1,1-$Os_3(CO)_{10}$(dppbz) (**8c**).

Empirical formula	$C_{40}H_{24}O_{10}Os_3P_2$
Formula weight	1297.13
Temperature	213(2) K
Wavelength	0.71073 Å
Crystal system	Monoclinic
Space group	$P2_1/c$
Unit cell dimensions	a = 10.957(2) Å
	b = 20.174(3) Å α = 96.842(2)°.
	c = 17.488(3) Å
Volume	3838(1) $Å^3$
Formula units per cell (Z)	4
Density (calculated)	2.245 Mg/m^3
Absorption coefficient	10.048 mm^{-1}
Reflections collected	32208
Independent reflections	8915 [R(int) = 0.0661]
Completeness to theta = 28.27°	93.5%
Absorption correction	Empirical
Max. and min. transmission	0.9170 and 0.5006
Refinement method	Full-matrix least-squares on F^2
Data / restraints / parameters	8915 / 0 / 497
Goodness-of-fit on F^2	0.958
Final R indices [I > 2σ(I)]	R1 = 0.0399, wR2 = 0.0485
R indices (all data)	R1 = 0.0735, wR2 = 0.0534
Δp(max), Δp(min) ($e/Å^{-3}$)	1.412 and -1.047

Table 3.4 Selected bond lengths [Å] and bond angles [°] for 1,1-$Os_3(CO)_{10}$(dppbz) (**8c**).

Bond lengths

Os(1)-C(31)	1.919(6)	Os(1)-C(32)	1.920(6)
Os(1)-P(2)	2.279(6)	Os(1)-P(1)	2.2854(16)
Os(1)-Os(2)	2.915(5)	Os(1)-Os(3)	2.9182(5)
Os(2)-C(34)	1.896(7)	Os(2)-C(35)	1.909(7)
Os(2)-C(36)	1.917(7)	Os(2)-C(33)	1.946(7)
Os(2)-Os(3)	2.902(5)	Os(3)-C(38)	1.897(7)
Os(3)-C(40)	1.907(7)	Os(3)-C(39)	1.926(7)
Os(3)-C(37)	1.940(7)	P(1)-C(13)	1.831(6)
P(1)-C(7)	1.837(6)	P(1)-C(1)	1.844(6)
P(2)-C(25)	1.823(6)	P(2)-C(19)	1.830(6)
P(2)-C(6)	1.832(6)	C(1)-C(2)	1.389(7)
C(1)-C(6)	1.387(7)	C(3)-C(4)	1.372(8)
C(2)-C(3)	1.378(7)	P(1) ·· P(2)	3.09(2)

Bond angles

C(31)-Os(1)-P(2)	89.04(2)	C(32)-Os(1)-P(2)	90.1(2)
C(31)-Os(1)-P(1)	94.26(2)	C(32)-Os(1)-P(1)	88.5(2)
P(2)-Os(1)-P(1)	84.88(5)	C(31)-Os(1)-Os(2)	86.5(2)
C(32)-Os(1)-Os(2)	93.78(2)	P(2)-Os(1)-Os(2)	168.5(4)
P(1)-Os(1)-Os(2)	105.98(4)	C(31)-Os(1)-Os(3)	91.1(2)
C(32)-Os(1)-Os(3)	86.36(2)	P(2)-Os(1)-Os(3)	109.7(4)
P(1)-Os(1)-Os(3)	164.50(4)	Os(2)-Os(1)-Os(3)	59.8(9)
C(34)-Os(2)-C(35)	102.0(3)	C(34)-Os(2)-C(36)	89.7(3)
C(35)-Os(2)-C(36)	91.4(3)	C(34)-Os(2)-C(33)	90.6(3)
C(35)-Os(2)-C(33)	93.6(3)	C(36)-Os(2)-C(33)	174.8(3)
C(34)-Os(2)-Os(1)	99.72(2)	C(35)-Os(2)-Os(1)	158.1(2)
C(36)-Os(2)-Os(1)	90.87(2)	C(33)-Os(2)-Os(1)	84.1(2)

The molecular structure of 1,1-$Os_3(CO)_{10}$(dppbz) confirms the migration of the diphosphine ligand in 1,2-$Os_3(CO)_{10}$(dppbz) **8b** to a chelating dppbz ligand that is bound to a single osmium atom [Os(1)]. The mean Os-Os and Os-P bond lengths of 2.9075 Å and 2.2822 Å, respectively, are unremarkable with respect to those bond distances in 1,2-$Os_3(CO)_{10}$(cDPPEn) and other phosphine substituted osmium clusters.[13,14] The ten ancillary carbonyl groups are all linear in nature and display a slight twist of the axial groups that is much less pronounced than the twist observed in 1,2-$Os_3(CO)_{10}$(dppbz). The internuclear non-bonding P(1) ··· P(2) distance of 3.09(2) Å in chelating isomer is nearly 0.77 Å shorter than the internuclear non-bonding P(1) ··· P(2) distance in bridging isomer, in keeping with the trend reported for the free ligand whose internuclear P(1) ··· P(2) distance is 3.17(2) Å. The remaining bond distances and angles are unexceptional and require no comment.

3.1.3 Photochemical Activation of 1,1-$Os_3(CO)_{10}$(dppbz) (8b)

Photolysis of 1,1-$Os_3(CO)_{10}$(dppbz) at room temperature furnished the hydride cluster $HOs_3(CO)_9[\mu\text{-}PhP(C_6H_4)\{PPh(C_6H_4)\}]$ as the sole observable product. Irradiation of the dppbz-chelated cluster in toluene solution with near-UV light (366 nm) leads to the loss of one CO and formation of **9**, which was confirmed by ^{31}P NMR and IR spectroscopies. Photolysis of 1,1-$Os_3(CO)_{10}$(dppbz), followed by column chromatograph and recrystallization, furnished the hydride cluster as a yellow solid in high yield. The cluster $HOs_3(CO)_9[\mu\text{-}PhP(C_6H_4)\{PPh(C_6H_4)\}]$ was fully characterized in solution by IR and NMR spectroscopies and combustion analysis. The solid-state structure of **9** was also confirmed by X-ray crystallography. The carbonyl stretching bands of the terminal carbonyl ligands in **9** were observed at 2104 (vs), 2082 (s), 2062 (vs) 2040 (s), 2010 (s), and 1932 (s) cm^{-1} in CH_2Cl_2 solvent. The ^1H NMR spectrum of cluster **9** recorded in C_6D_6 shows a high-field triplet at -16.50 ppm ($J_{H\text{-}P}$ = 13 Hz), which is assigned to the bridging hydride group that spans the Os(1)-Os(2) vector of cluster **9** (*vide infra*). The presence of a first-order triplet resonance for the hydride indicates that it is coupled symmetrically to the two phosphorous atoms. Multiplets at δ 6.80-7.70 are readily assigned to the aromatic hydrogens of the dppbz ligand. The ^{31}P NMR spectrum displays a pair of inequivalent ^{31}P doublets at δ 28.50 and 40.50 ($J_{P\text{-}P}$ = 14 Hz). These spectroscopic data are fully consistent with the proposed structure for the hydride cluster.[15]

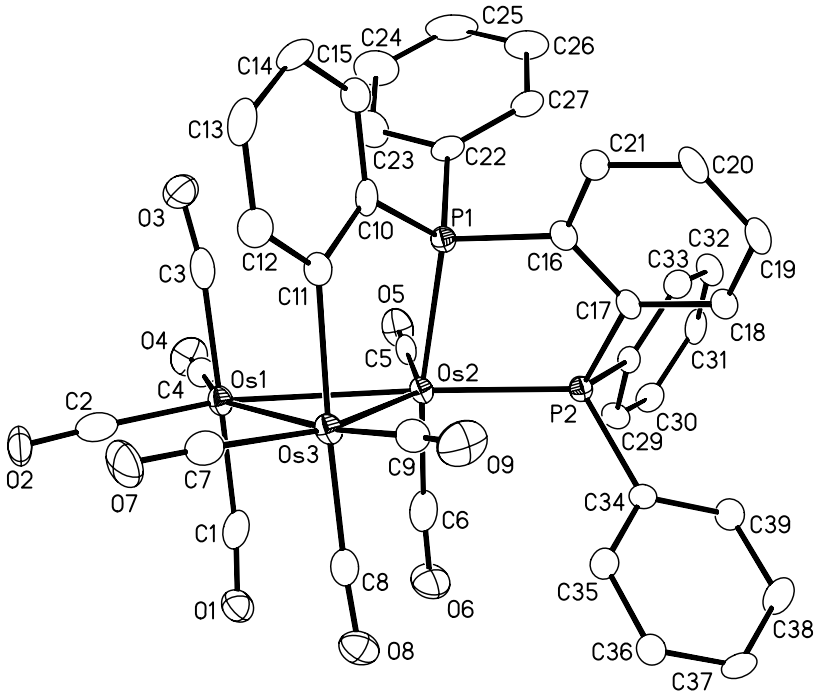

Figure 3.6 Thermal ellipsoid plot of the non-hydrogen atoms of the hydride cluster **9** showing the thermal ellipsoids at the 50% probability level. The CH_2Cl_2 solvent molecule has been omitted for clarity.

Table 3.5 Crystal data and structure refinement details for the hydride cluster **9**.CH_2Cl_2.

Empirical formula	$C_{40}H_{24}O_9Os_3P_2.\ CH_2Cl_2$
Formula weight	1354.05
Temperature	100(2) K
Wavelength	0.71073 Å
Crystal system	Orthorhombic
Space group	P b c a
Unit cell dimensions	a = 21.7445(2) Å
	b = 16.7738(2) Å
	c = 21.9364(2) Å
Volume	8001.0(1) $Å^3$
Formula units per cell (Z)	8
Density (calculated)	2.248 Mg/m^3
Absorption coefficient	9.773 mm^{-1}
Reflections collected	14706
Independent reflections	14832 [R(int) = 0.0000]
Completeness to theta = 26.50°	99.6%
Absorption correction	Semi-empirical from equivalents
Max. and min. transmission	0.5917 and 0.2026
Refinement method	Full-matrix least-squares on F^2
Data / restraints / parameters	14832 / 4 / 516
Goodness-of-fit on F^2	1.028
Final R indices [I > 2α(I)]	R1 = 0.0388, wR2 = 0.0748
R indices (all data)	R1 = 0.0697, wR2 = 0.0805
$\Delta p(max)$, $\Delta p(min)$ ($e.Å^{-3}$)	2.434 and -2.301

Table 3.6 Selected bond lengths [Å] and bond angles [°] for cluster **9.**

Bond lengths

Os(1)-C(2)	1.912(7)	Os(1)-C(1)	1.930(6)
Os(1)-C(4)	1.931(6)	Os(1)-C(3)	1.955(7)
Os(1)-Os(3)	2.880(4)	Os(1)-Os(2)	2.933(3)
Os(2)-C(5)	1.891(6)	Os(2)-C(6)	1.902(7)
Os(2)-P(2)	2.323(1)	Os(2)-P(1)	2.367(1)
Os(2)-Os(3)	2.994(4)	Os(3)-C(7)	1.874(7)
Os(3)-C(9)	1.900(6)	Os(3)-C(8)	1.935(6)
Os(3)-C(11)	2.184(6)	P(1)-C(10)	1.803(6)
P(1)-C(22)	1.828(6)	P(1)-C(16)	1.834(6)
P(2)-C(28)	1.817(5)	P(2)-C(17)	1.823(5)
P(2)-C(34)	1.837(5)	C(12)-C(13)	1.381(8)
C(10)-C(15)	1.404(8)	C(10)-C(11)	1.420(8)
C(11)-C(12)	1.421(7)	C(13)-C(14)	1.396(8)

Bond angles

C(2)-Os(1)-C(1)	89.3(2)	C(2)-Os(1)-C(4)	104.7(2)
C(1)-Os(1)-C(4)	93.0(2)	C(2)-Os(1)-C(3)	89.3(2)
C(1)-Os(1)-C(3)	178.0(2)	C(4)-Os(1)-C(3)	88.7(2)
C(2)-Os(1)-Os(3)	97.4(2)	C(1)-Os(1)-Os(3)	88.40(2)
C(4)-Os(1)-Os(3)	157.87(2)	C(3)-Os(1)-Os(3)	90.41(2)
C(2)-Os(1)-Os(2)	158.89(2)	C(1)-Os(1)-Os(2)	85.71(2)
C(4)-Os(1)-Os(2)	96.05(2)	C(3)-Os(1)-Os(2)	95.14(2)
Os(3)-Os(1)-Os(2)	62.03(8)	C(5)-Os(2)-C(6)	89.7(2)
C(5)-Os(2)-P(2)	97.09(2)	C(6)-Os(2)-P(2)	89.66(2)
C(5)-Os(2)-P(1)	95.14(2)	C(6)-Os(2)-P(1)	170.73(2)
P(2)-Os(2)-P(1)	81.94(5)	C(5)-Os(2)-Os(1)	89.99(2)
C(6)-Os(2)-Os(1)	90.31(2)	P(2)-Os(2)-Os(1)	172.92(4)
P(1)-Os(2)-Os(1)	97.55(4)	C(5)-Os(2)-Os(3)	146.96(2)
C(6)-Os(2)-Os(3)	98.20(2)	P(2)-Os(2)-Os(3)	114.87(3)
P(1)-Os(2)-Os(3)	81.95(3)	Os(1)-Os(2)-Os(3)	58.14(4)

The molecular composition the hydride cluster $HOs_3(CO)_9[\mu$-$PhP(C_6H_4)\{PPh\ (C_6H_4)\}]$ ascertains the activation of one of the aryl groups via an ortho metalation of the C(11)-H(11) bond. The Os-Os bond distances in **9** range from 2.888(4) Å [Os(1)-Os(3)] to 2.998(4) Å Os(2)-Os(3) and display a mean distance of 2.9362 Å that parallels those Os-Os single-bond distances reported for related Os_3 clusters.[2] Despite the fact that the bridging hydride was not located during the crystallographic refinement, its location may be confidently assigned to the Os(1)-Os(3) vector, based on bond-length alterations in the trimetallic core.[18] Here the formation of an edge-bridging hydride leads to an elongation of the Os(1)-Os(3) bond length relative to the other two Os-Os bonds. Both phosphorus atoms of the dppbz ligand coordinate to the Os(2) center in a chelating fashon and exhibit distinct axial and equatorial dispositions. The P(1)-Os(2)-P(2) bond angle of 81.94(5)° and the two Os-P distances of 2.323(1) Å [Os(2)-P(2)] and 2.367(1) Å [Os(2)-P(1)] exhibit values unremarkable to those angles and distances found in the related compounds.[1,2] The Os(3)-C(11) bond distance of 2.184(6) Å is in excellent agreement with those metal-carbon sigma bond distances found in di- and tri-nuclear osmium compounds containing an ortho-metalated aryl ligand.[19] The nine CO groups are linear and exhibit distances and angles consistent with such linkages. The remaining bond distances and angles are unexceptional and require no comment.

3.1.4 Reversible Ortho Metalation in 1,1-$Os_3(CO)_{10}$(dppbz)

The reactivity of the hydride cluster with CO was next investigated due to numerous reports on reversible ortho metalation in this family of metal clusters.[2] Thermolysis of the hydride cluster at 60-65 °C under 1 atm of CO regenerates the chelating cluster in quantitative yield. This control experiment demonstrates the putative cluster $Os_3(CO)_9$(dppbz) that is formed by reductive coupling of the C-H bond is effectively trapped by CO, confirming the reversible nature of the ortho-metalation step. The relationship that exists between the clusters 1,1-$Os_3(CO)_{10}$(dppbz), the π-complex, and $HOs_3(CO)_9[\mu\text{-}PhP(C_6H_4)\{PPh(C_6H_4)\}]$ is illustrated in Figure 3.2.

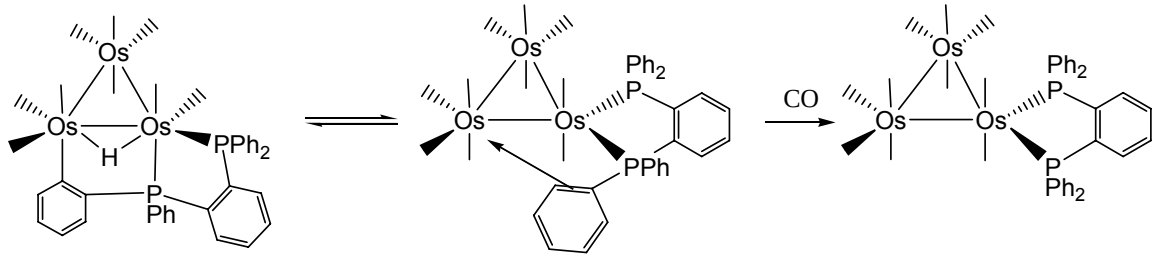

Scheme 3.2 Reversible ortho metalation of the chelating isomer (**8c**) to the hydride cluster (**9**).

3.1.5 Kinetic Data for Diphosphine Isomerization

The isomerization kinetics associated with the transformation of 1,2-$Os_3(CO)_{10}$(dppbz) to 1,1-$Os_3(CO)_{10}$(dppbz) was next investigated by UV-vis spectroscopy in toluene solution under 1 atm of CO. The UV-vis kinetic studies were conducted over the temperature range of 318-343 K, with the first-order rate constants reported in Table 3.7. The UV-vis rates were obtained through non-linear regression analysis by following the increase in the absorbance of the

365 nm band belonging to 1,1-$Os_3(CO)_{10}$(dppbz). Figure 3.7 shows the spectral changes that accompany the isomerization of 1,2-$Os_3(CO)_{10}$(dppbz) in toluene solution at 323 K, where the observed isosbestic points at 388 and 410 nm verify that the isomerization is kinetically well-behaved and not subject to significant material loss. Inspection of Figure 3.8 confirms the excellent fit between the least-squares regression curve and the absorbance data. The effect of added phosphine and CO on the isomerization reaction was also probed. Entries 3, 4 and 5 in Table 3.7 reveal that the experimentally measured rate constants under high CO pressure and in the presence of added PPh_3 (10 equiv), respectively, are indistinguishable, ruling out a dissociative process and the generation of a long-lived unsaturated intermediate.

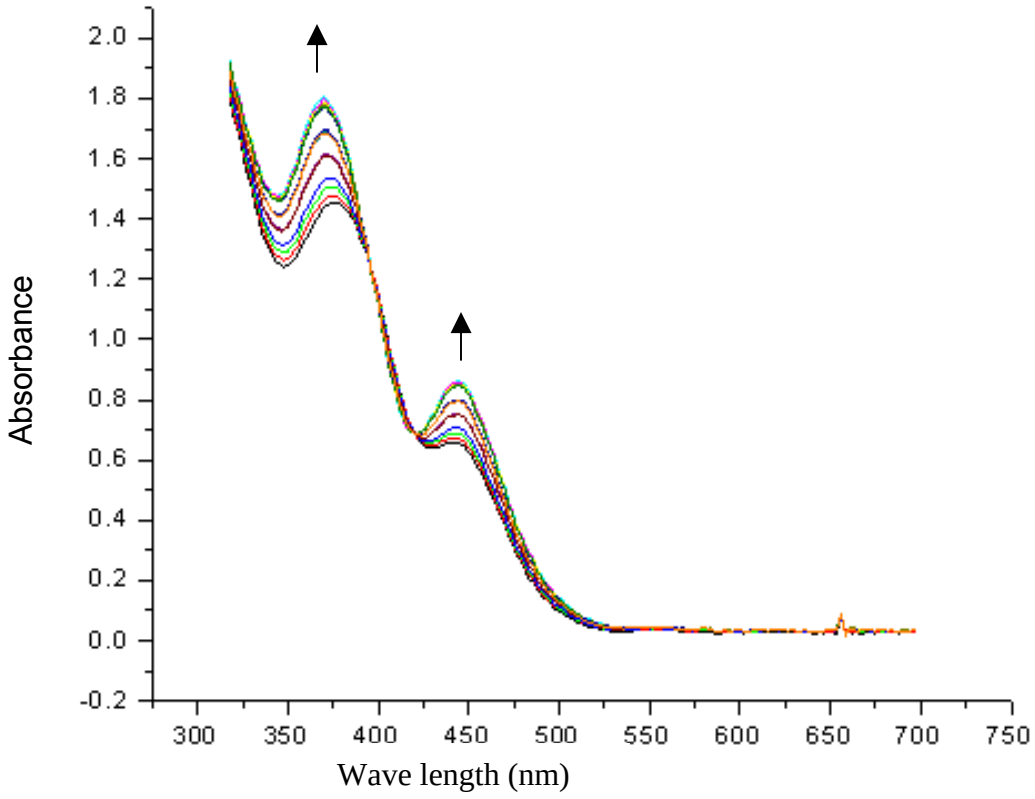

Figure 3.7 UV-vis spectral changes for the isomerization of 1,2-$Os_3(CO)_{10}$(dppbz) in toluene at 323 K.

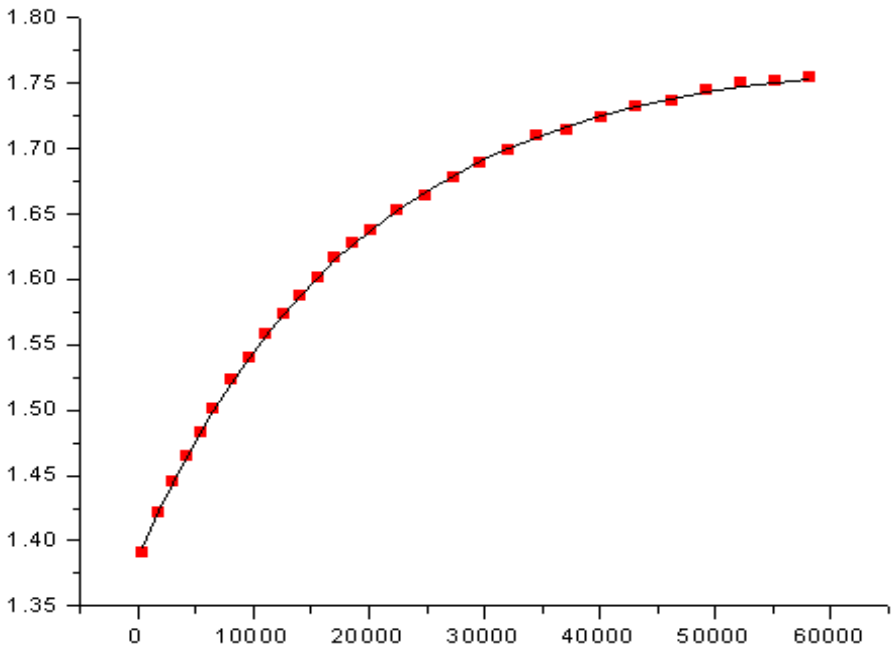

Figure 3.8 The absorbance versus time curve for the experimental data (■) with least-squares fit of k(——) for the UV-vis data reported in Figure 3.7.

Table 3.7 Kinetic data for the isomerization of 1,2-$Os_3(CO)_{10}$(dppbz) to 1,1-$Os_3(CO)_{10}$(dppbz).[a,b]

Temp (K)	Solvent	10^4k(s-1)	Method[d]	Trapping Ligand
318.0	Toluene	0.29 ± 0.08	UV-vis	-
323.0	Toluene	0.50 ± 0.07	UV-vis	-
323.0	Toluene	0.45 ± 0.10	UV-vis[c]	100 psi CO
323.0	Toluene	0.58 ± 0.09	UV-vis[c]	500 psi CO
323.0	Toluene	0.49 ± 0.08	UV-vis[d]	10 eq PPh_3
328.0	Toluene	1.01 ± 0.12	UV-vis	-
333.0	Toluene	1.41 ± 0.10	UV-vis	-
338.0	Toluene	2.63 ± 0.16	UV-vis	-
343.0	Toluene	3.66 ± 0.14	UV-vis	-

[a]All kinetic experiments were conducted under 1 atm of CO. [b]The extent of the isomerization was followed by monitoring the increase in the absorbance of the 365 nm band (UV-vis). [C]Reaction conducted under 100 and 500 psi CO. [d]Reaction conducted in the presence of 10 equivalents of PPh_3.

An Eyring plot of ln(k/T) versus T^{-1} (Figure 3.9) afforded the activation parameters [$\Delta H^{\ddagger}$ = 18.0(0.6) kcal/mol and $\Delta S^{\ddagger}$ = -11(1) eu] that are in close agreement with those data published on the diphosphine ligand isomerization in $Os_3(CO)_{10}$(cDPPEn) and $Os_3(CO)_{10}$(bpcd). The negative entropy of activation argues against a dissociative process involving the release of either a CO group or one arm of the dppbz ligand.

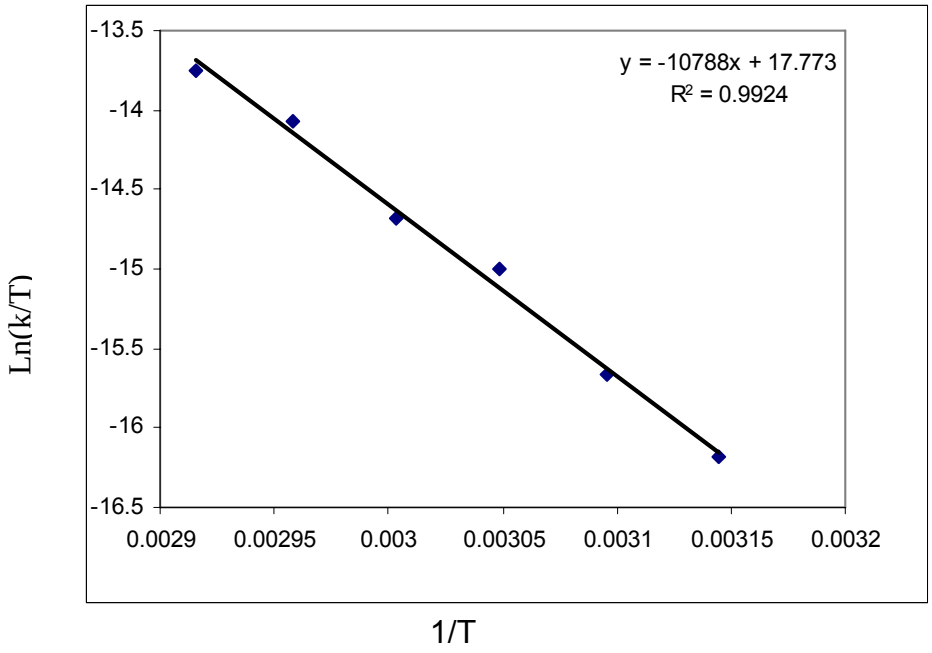

Figure 3.9 Eyring plot for the isomerization of 1,2-$Os_3(CO)_{10}$(dppbz)(**8b**) to 1,1-$Os_3(CO)_{10}$(dppbz)(**8c**).

The kinetic data for the isomerization of the ligand dppbz in **8b** → **8c** are consistent with the intramolecular migration or transit of one of the phosphine moieties across one of the Os-Os bonds by way of a μ-phosphine intermediate. Coupled with this phosphine transit is the simultaneous migration of two at the

equatorially situated CO ligands, as depicted in the merry-go-round process in Scheme 3.3.[2] It must be pointed out that the kinetic data do not rule out the participation of the doubly bridged cluster species $Os_3(CO)_9(\mu\text{-}CO)(\mu\text{-}dppbz)$ in the isomerization reaction. However, this route is not favored because the pairwise exchange of the CO/P groups across the osmium-osmium bond requires an additional turnstile rotation or permutation of the two CO groups and the two phosphorus groups at the osmium center in order to furnish the chelating isomer with equatorially disposed phosphine groups.

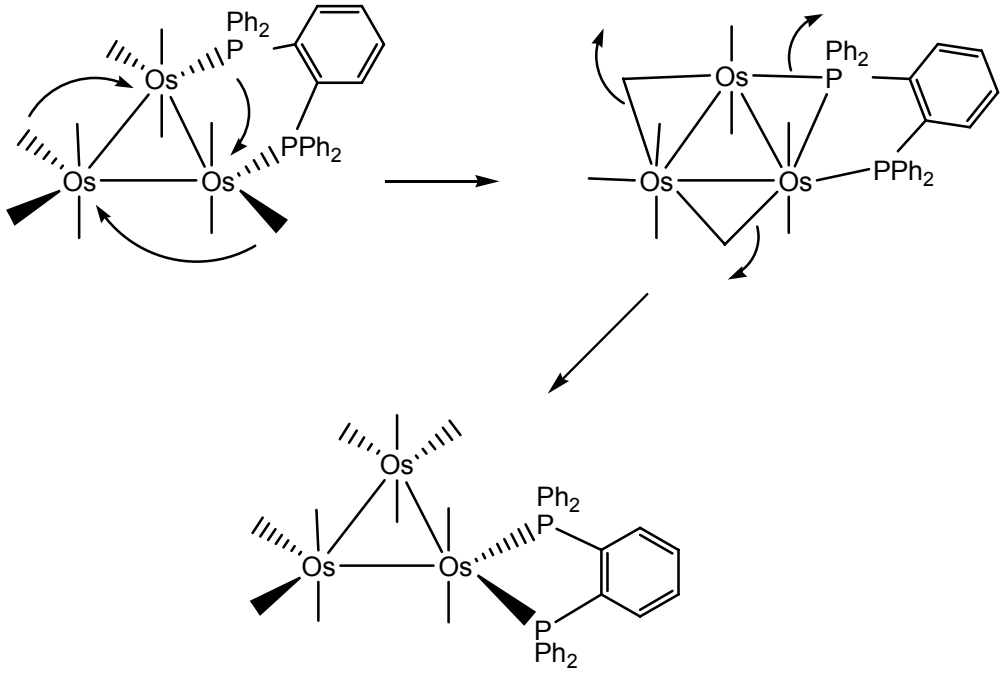

Scheme 3.3 Proposed merry-go-round mechanism for dppbz isomerization.

3.2 Conclusions

The reaction between the diphosphine ligand 1,2-bis(diphenylphosphino)-benzene (dppbz) and 1,2-$Os_3(CO)_{10}(MeCN)_2$ has been investigated at room temperature and found to produce the corresponding chelating cluster 1,1-$Os_3(CO)_{10}$(dppbz) as the major product. When the reaction is carried out at 0 °C, the bridging cluster is produced as the major product. It is established that the bridging cluster 1,2-$Os_3(CO)_{10}$(dppbz) undergoes a nondissociative isomerization of the ancillary dppbz ligand to give the chelated cluster 1,1-$Os_3(CO)_{10}$(dppbz). The isomerization kinetics and thermodynamics have been explored by UV-vis and ^{31}P NMR spectroscopic methods. Photochemical activation of the chelating cluster **8c** leads to the ortho metalation of one of the ancillary aryl groups to furnish the hydride-bridged cluster $HOs_3(CO)_9[\mu\text{-}PhP(C_6H_4)\{PPh(C_6H_4)\}]$ (**9**). The ortho-metalation reaction is reversible; simply heating the hydride cluster **9** under CO regenerates the dppbz-chelated cluster **8c**. All three clusters have been fully characterized by IR and NMR (^1H and ^{31}P) spectroscopies, and the solid-state structures established by X-ray crystallography. The mechanistic examination of other cluster-mediated ligand degradation reactions are worthy of future investigations.

3.3 Chapter References

1. (a) Fenske, D.; Becher, H.J. *Chem. Ber.* **1974**, *107*, 117. (b) Fenske, D.; Becher, H.J. *Chem. Ber.* **1975**, *108*, 2115. (c) Fenske, D.; Becher, H.J. *Chem. Ber.* **1979**, *112*, 363.

2. (a) Watson, W.H.; Wu, G.; Richmond, M.G. *Organometallics* **2006,** *25,* 930. (b) Watson, W.H.; Wu, G.; Richmond, M.G. *Organometallics* **2005,** *24,* 5431.
3. (a) Garrou, P.E.; *Chem. Rev.* 1981, *81*, 229. (b) Richmond, M.G.; Kochi, J.K. *Organometallics* **1987**, *6*, 254.
4. Watson, W.H.; Poola, B.; Richmond, M.G. *J. Chem. Crystallogr.* **2006**, *36*, 123.
5. Colthup, N.B.; Daly, L.H.; Wiberley, S.E. *Introduction to Infrared and Raman Spectroscopy*, 3rd Ed., Academic Press: New York, **1990**.
6. (a) Churchill, M.R; DeBoer, B. G. *Inorg. Chem.* **1977**, *16*, 878. (b) Bruce, M.I.; Pain, G.N.; Hughes, C.A.; Patrick, J.M.; Skelton, B.W.; White, A.H. *J. Organomet. Chem.* **1986**, *307*, 343.
7. (a) Adams, R.D.; Tanner, J.T. *Organometallics,* **1989**, *8*, 563. (b) Biradha, K.; Hansen, V.M.; Leong, W.K.; Pomeroy, R.K.; Zaworotko, M. *J. Clust. Sci*. **2000**, *11*, 285. (c) Deeming, A.J.; Stchedroff, M. *J. Chem. Soc., Dalton Trans.* **1998**, 3819.
8. Deeming, A.J.; Hassan, M.M.; Kabir, S.E.; Nordlander, E.; Tocher, D.A. *J. Chem. Soc., Dalton Trans.* **2004,** 3709.
9. Lauher, J.W. *J. Am. Chem. Soc.* **1986**, *108*, 1521.
10. Deeming, A.J.; Kabir, S.E. *J. Organomet. Chem.* **1988**, *340*, 359.
11. (a) Alex, R.F.; Einstein, F.W.B.; Jones, R.H.; Pomeroy, R.K. Inorg. Chem. **1987**, *26*, 3175. (b) Bruce, M.I.; Liddell, M.J.; Skawkataly, O.B.; Hughes, C.A.; Skelton, B.H.; White, A.H. *J. Organomet. Chem.* **1988**, *347*, 207.

12. Unpublished results.

13. Azam, K.A.; Hursthouse, M.B.; Kabir, S.E.; Malic, K.M.A.; Mottalib, M.A. *J. Chem. Crystallogr.* **1999**, *29*, 813.

14. Deeming, A.J. *J. Adv. Organomet. Chem*. **1986**, *26*, 1.

15. Watson, W.H.; Wiedenfeld, D.; Pingali, A.; Poola, B.; Richmond, M.G. *Polyhedron*, **2007**. In Press.

16. Watson, W.H.; Poola, B.; Richmond, M.G. *Polyhedron*, **2007**, In press.

17. Ejsmont, K.; Watson, W.H.; Liu, J.; Richmond, M.G.*J. Chem. Crystallogr.* **2003**, *33*, 541.

18. Mingos, D.M.P.; Wales, D.J. *Introduction to Cluster Chemistry*, Prentice-Hall: Englewood Cliffs, NJ, **1990.**

19. (a) Adams, R.D.; Cortopassi, J. *Cluster Sci.* **1995**, *6*, 437.

CHAPTER 4

REVERSIBLE ISOMERIZATION OF A DIPHOSPHINE LIGAND AND REGIOSPECIFIC C-H AND P-C BOND CLEAVAGE REACTIVITY IN THE TRIOSMIUM CLUSTER $Os_3(CO)_{10}$(bmf)

The reaction of bidentate phosphine ligands with the activated triosmium cluster $Os_3(CO)_{10}(MeCN)_2$ to furnish $Os_3(CO)_{10}L_2$ (L = ligand) has been investigated over the years with respect to the bonding mode adopted by the bidentate P-P ligand upon coordination.[1-3] Wishing to explore further the chemistry of triosmium cluster compounds with structurally diverse diphosphine ligands that posses conjugated π arrays and well-defined redox active ligands, and to study the effect of an unsymmetrical diphosphine ligand and its coordination chemistry with respect to the symmetrical ligands dppbz and bpcd, 3,4-bis(diphenylphosphino)-5-methoxy-2(5H)-furanone (bmf) has been prepared and the substitution chemistry of this ligand has been investigated with the triosmium cluster 1,2-$Os_3(CO)_{10}(MeCN)_2$. This ligand will allow one to probe for any regiochemistry associated with P-C bond cleavage due to the presence of inequivalent phosphine moieties.

The phosphine ligand bmf was first synthesized via the reaction of 3,4-dichloro-5-methoxy-2(5)H-furanone with Ph_2PK. The former chemical is readily prepared from mucochloric acid.[4] In a modified procedure, the 3,4-dichloro-5-methoxy-2(5)H-furanone was added dropwise to a solution containing Ph_2P^-, which in turn was prepared in situ from Ph_2PH and BuLi in THF at low temperature. Warming the reaction to ca. 0 °C and quenching the reaction at this

temperature yielded the bmf ligand in good yield. Schemes 4.1 and 4.2 illustrate the synthetic scheme and proposed stepwise mechanism for the synthesis of the 3,4-bis(diphenylphosphino)-5-methoxy-2(5H)-furanone used in these studies.

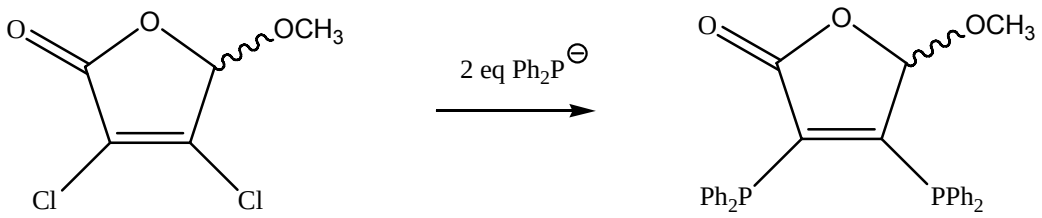

Scheme 4.1 Synthesis of 3,4-bis(diphenylphosphino)-5-methoxy-2(5H)-furanone

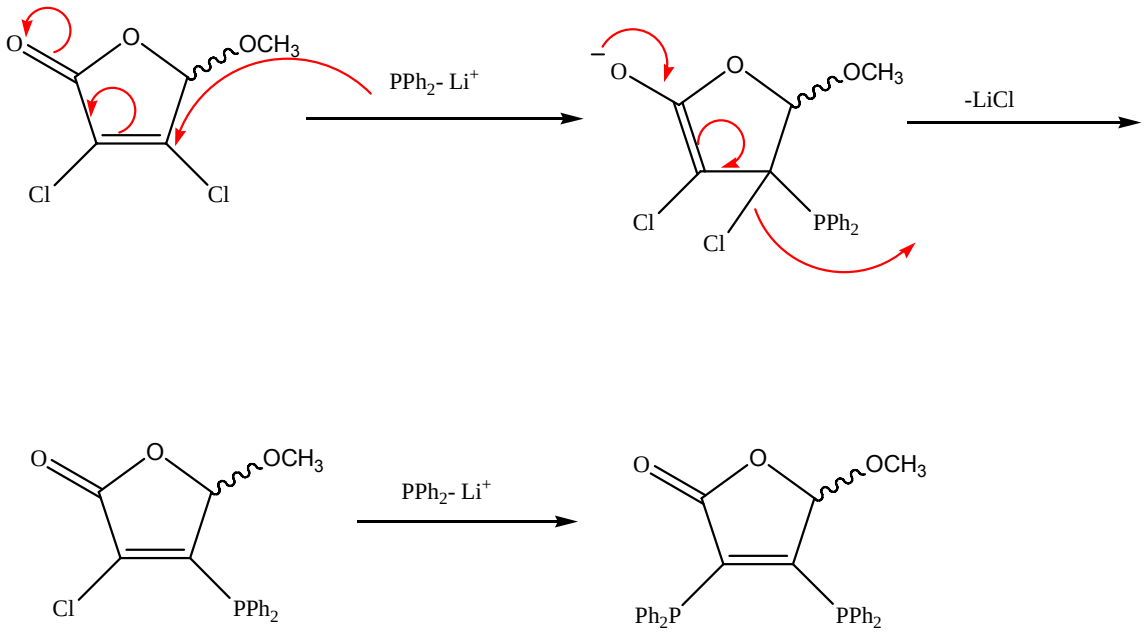

Scheme 4.2 Proposed mechanism for synthesis of 3,4-bis(diphenylphosphino)-5-methoxy-2(5H)-furanone (bmf).

Previous research from the Richmond lab has examined the substitution chemistry of the bmf ligand with the mixed-metal cluster $PhCCo_2MoCp(CO)_8$, where it was found that the initially formed cluster containing a bridging bmf ligand $PhCCo_2MoCp(CO)_6$(bmf) underwent P-C bond activation to give products with high regioselectivity and high diastereoselectiviy.[15] The detailed study related to the substitution chemistry of this chiral diphosphine ligand bmf with the activated trisomium cluster $Os_3(CO)_{10}(MeCN)_2$ is presented herein.

4.1 Results and Discussions

4.1.1 Reaction of 1,2-$Os_3(CO)_{10}$(MeCN) with the Ligand bmf

The reaction between activated cluster 1,2-$Os_3(CO)_{10}(MeCN)_2$ (**6**) and the unsaturated diphosphine ligand bmf proceeds rapidly with the complete consumption of **6** and the bmf ligand at room temperature. The ligand-bridged cluster 1,2-$Os_3(CO)_{10}$(bmf) (**10b**) is formed as the predominant product, along with minor amounts of $Os_3(CO)_{11}(\eta^1$-bmf), whose origin undoubtedly comes from the minor amount of mono(acetonitrile) derivative $Os_3(CO)_{11}$(MeCN) that accompanies the preparation of **6**.[5] This is markedly different from the substitution chemistry found with the dppbz ligand which furnishes a mixture of dppbz-substituted bridging, chelating and hydride clusters under similar conditions. Cluster **10b** was purified by column chromatography over silica gel and characterized in solution by IR and NMR spectroscopy. Particularly diagnostic in the characterization of **10b** were the high-field ^{31}P resonances at

-6.55 ppm and -18.25 ppm for the two non-equivalent phosphorus atoms on the bmf ligand, which support the bridging of adjacent osmium centers by the ancillary diphosphine ligand.[6]

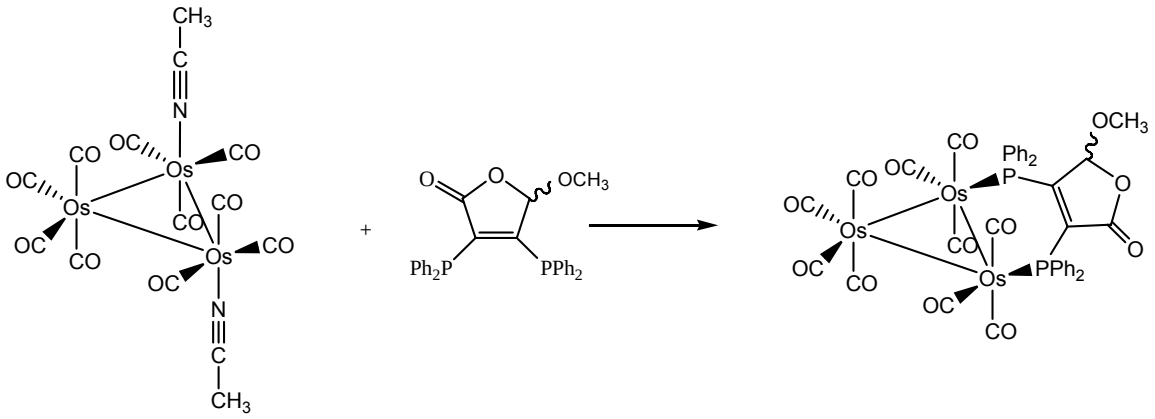

Scheme 4.3 The reaction between 1,2-$Os_3(CO)_{10}(MeCN)_2$ and bmf to give 1,2-$Os_3(CO)_{10}$(bmf).

The ^1H NMR spectrum of 1,2-$Os_3(CO)_{10}$(bmf) reveals that the three hydrogens of methoxy group and the lone methine hydrogen on the bmf ligand appear as singlets at 2.20 ppm and 4.35 ppm, respectively. A multiplet corresponding to the 20 aromatic hydrogens is observed at 6.70-7.80 ppm. The initial evidence for the transformation of bridging isomer to the chelating isomer came from a routine thermolysis study. Heating a sample of 1,2-$Os_3(CO)_{10}$(bmf) in toluene-d_8 in a sealed NMR tube at 85 °C overnight showed a decrease in intensity of the initial methoxy singlet and the presence of a new singlet at 2.80 ppm, corresponding to the methoxy group of the chelating isomer. The methine hydrogen associated with the chelating bmf ligand appears as a singlet at 4.80 ppm. The ^{31}P NMR showed two new singlets at 13.55 ppm and 18.45 ppm, whose large nuclear deshielding is consistent with the formation of chelating

diphosphine ligand.[6] Continued heating of this isomeric mixture for an extended period of time showed no change in the composition of the bridging and chelating isomers. An equilibrium value of 85:15 in favor of the chelating isomer (**10c)** was found at 85 °C. TLC examination of a parallel thermolysis reaction conducted in a Schlenk vessel showed a single spot for the equilibrium mixture of **10b** and **10c**, preventing the separation of the isomers.

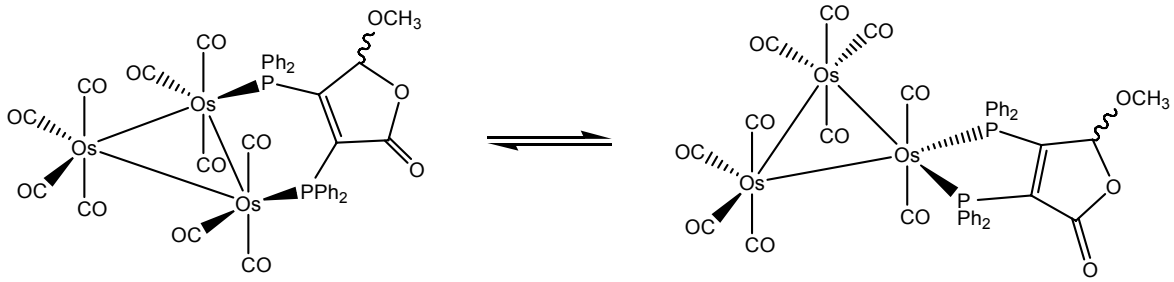

Scheme 4.4 Thermolysis of 1,2-$Os_3(CO)_{10}$(bmf) to yield 1,1-$Os_3(CO)_{10}$(bmf).

4.1.2 X- ray Diffraction Structures of the $Os_3(CO)_{10}$(bmf) Isomers

The solid-state structures of the bridging and chelating isomers of $Os_3(CO)_{10}$(bmf) were determined by X-ray crystallography. Single crystals of 1,2-$Os_3(CO)_{10}$(bmf) were grown by dissolving the compound in dichloromethane and layering the solution with hexane. In the case of cluster **10c**, that is not isolable as a distinct compound due to the reversible equilibrium, more care was required to obtain crystals of **10c** suitable for diffraction analysis. X-ray quality crystals of cluster **10c** were grown by the slow diffusion of diethyl ether into a toluene solution containing the isomeric mixture of **10b** and **10c**. In a very interesting observation, the diffraction data on the single crystal revealed that it consisted of both isomers in the same exact composition as observed in solution at 85 °C (85:15 in favor of **10c**). The crystal structure data for minor isomer were poor, and only the structure of the major isomer could be solved from the diffraction data with reasonable certainty. Single crystals of these clusters were found exist as discrete molecules in the unit cell with no unusually short inter- or intermolecular contacts. The X-ray data processing and collection parameters and selected bond distances and bond angles for both isomers of $Os_3(CO)_{10}$(bmf) are listed in Tables 4.1 through 4.4, respectively. The molecular configuration and the numbering scheme of 1,2- and 1,1-$Os_3(CO)_{10}$(bmf) are presented in the thermal ellipsoid plots shown in Figures 4.1 and 4.2, respectively.

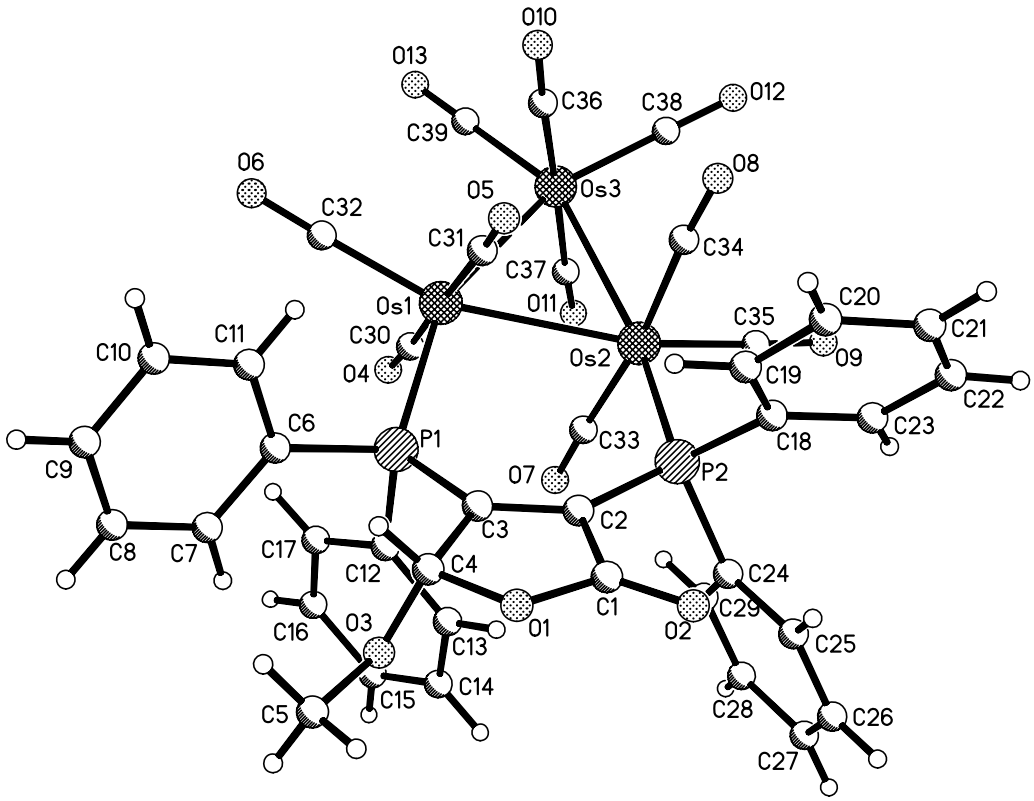

Figure 4.1 Thermal ellipsoid plot and numbering scheme of 1,2-$Os_3(CO)_{10}$(bmf) showing the thermal ellipsoids at the 50% probability level.

Table 4.1 Crystal data and structural refinement details for 1,2-$Os_3(CO)_{10}$(bmf).

Empirical formula	$C_{42}H_{27}O_{13}Os_3P_2$	
Formula weight	1372.18	
Temperature	295(2) K	
Wavelength	0.71073 Å	
Crystal system	Triclinic	
Space group	P-1	
Unit cell dimensions	a = 9.468(4) E	α = 75.473(7)°.
	b = 12.357(6) E	β = 79.960(8)°.
	c = 20.773(7) E	γ = 68.052(7)°.
Volume	2164.39(17) E^3	
Formula units per cell (Z)	2	
Density (calculated)	2.105 Mg/m^3	
Absorption coefficient	8.921 mm^{-1}	
Reflections collected	23746	
Independent reflections	11816 [R(int) = 0.0170]	
Coverage of independent reflections	95.2%	
Absorption correction	Semi-empirical from equivalents	
Max. and min. transmission	0.6640 and 0.2685	
Refinement method	Full-matrix least-squares on F^2	
Data / restraints / parameters	11816 / 0 / 530	
Goodness-of-fit on F^2	1.022	
Final R indices [I > 2σ(I)]	R1 = 0.0273, wR2 = 0.0659	
R indices (all data)	R1 = 0.0377, wR2 = 0.0704	
Δp (max), Δp (min) ($e.Å^{-3}$)	2.408 and -0.840	

Table 4.2 Selected bond lengths (Å) and bond angles (°) for 1,2-$Os_3(CO)_{10}$(bmf).

Bong lengths

Os(1)-C(32)	1.91(5)	Os(1)-C(31)	1.94(4)
Os(1)-C(30)	1.97(5)	Os(1)-P(1)	2.35(9)
Os(1)-Os(2)	2.86(2)	Os(1)-Os(3)	2.88(2)
Os(2)-C(35)	1.88(6)	Os(2)-C(33)	1.93(5)
Os(2)-C(34)	1.94(5)	Os(2)-P(2)	2.32(7)
Os(2)-Os(3)	2.87(3)	Os(3)-C(38)	1.90(5)
Os(3)-C(39)	1.91(6)	Os(3)-C(36)	1.93(5)
Os(3)-C(37)	1.93(5)	P(1)-C(12)	1.87(4)
P(1)-C(6)	1.83(4)	P(1)-C(3)	1.84(4)
P(2)-C(18)	1.86(5)	P(2)-C(24)	1.86(3)
P(2)-C(2)	1.84(4)	C(3)-C(4)	1.52(5)
C(1)-C(2)	1.51(6)	P(1) ·· P(2)	3.77(4)

Bong angles

C(32)-Os(1)-C(31)	92.4(2)	C(32)-Os(1)-C(30)	89.4(2)
C(31)-Os(1)-C(30)	175.8(9)	C(32)-Os(1)-P(1)	100.5(5)
C(31)-Os(1)-P(1)	90.2(3)	C(30)-Os(1)-P(1)	93.4(4)
C(32)-Os(1)-Os(2)	161.6(8)	C(31)-Os(1)-Os(2)	82.4(4)
C(30)-Os(1)-Os(2)	94.7(6)	P(1)-Os(1)-Os(2)	97.1(2)
C(32)-Os(1)-Os(3)	103.3(4)	C(31)-Os(1)-Os(3)	96.5(2)
C(30)-Os(1)-Os(3)	79.4(4)	P(1)-Os(1)-Os(3)	154.8(3)
Os(2)-Os(1)-Os(3)	60.1(6)	C(35)-Os(2)-C(33)	94.3(3)
C(35)-Os(2)-C(34)	90.1(3)	C(33)-Os(2)-C(34)	172.6(2)
C(35)-Os(2)-P(2)	96.7(9)	C(33)-Os(2)-P(2)	94.6(4)
C(34)-Os(2)-P(2)	90.9(4)	C(35)-Os(2)-Os(1)	159.2(9)
C(33)-Os(2)-Os(1)	80.3(6)	C(34)-Os(2)-Os(1)	93.7(5)
P(2)-Os(2)-Os(1)	104.1(3)	C(35)-Os(2)-Os(3)	100.9(8)
C(33)-Os(2)-Os(3)	93.9(5)	C(34)-Os(2)-Os(3)	79.4(4)
P(2)-Os(2)-Os(3)	160.7(3)	Os(1)-Os(2)-Os(3)	60.2(6)

The thermal ellipsoid plot of 1,2-$Os_3(CO)_{10}$(bmf) confirms that the diphosphine ligand is attached to the triosmium frame by way of coordination to the Os(1) and Os(2) atoms. The Os-Os bond distances range from 2.864(2) Å [Os(1)-Os(2)] to 2.885(2) Å [Os(1)-Os(3)] and display a mean distance of 2.875(2) Å. The Os-Os distances are normal relative to those distances found in other simple polynuclear osmium clusters.[17] The ten terminal carbonyl groups may be considered as linear with standard distances and angles. The two Os-P bond lengths of 2.35(9) Å [Os(1)-P(1)] and 2.32(7) Å [Os(2)-P(2)] are in excellent agreement with the average lengths reported for a variety of phosphine-substituted osmium compounds.[12] Coordination of the diphosphine ligand across the Os(1)-Os(2) bond leads to a significant stretching of the bmf ligand that leads to ground-state destabilization relative to chelating isomer 1,1-$Os_3(CO)_{10}$(bmf). The remaining bond distances and angles are unexceptional and require no comment.

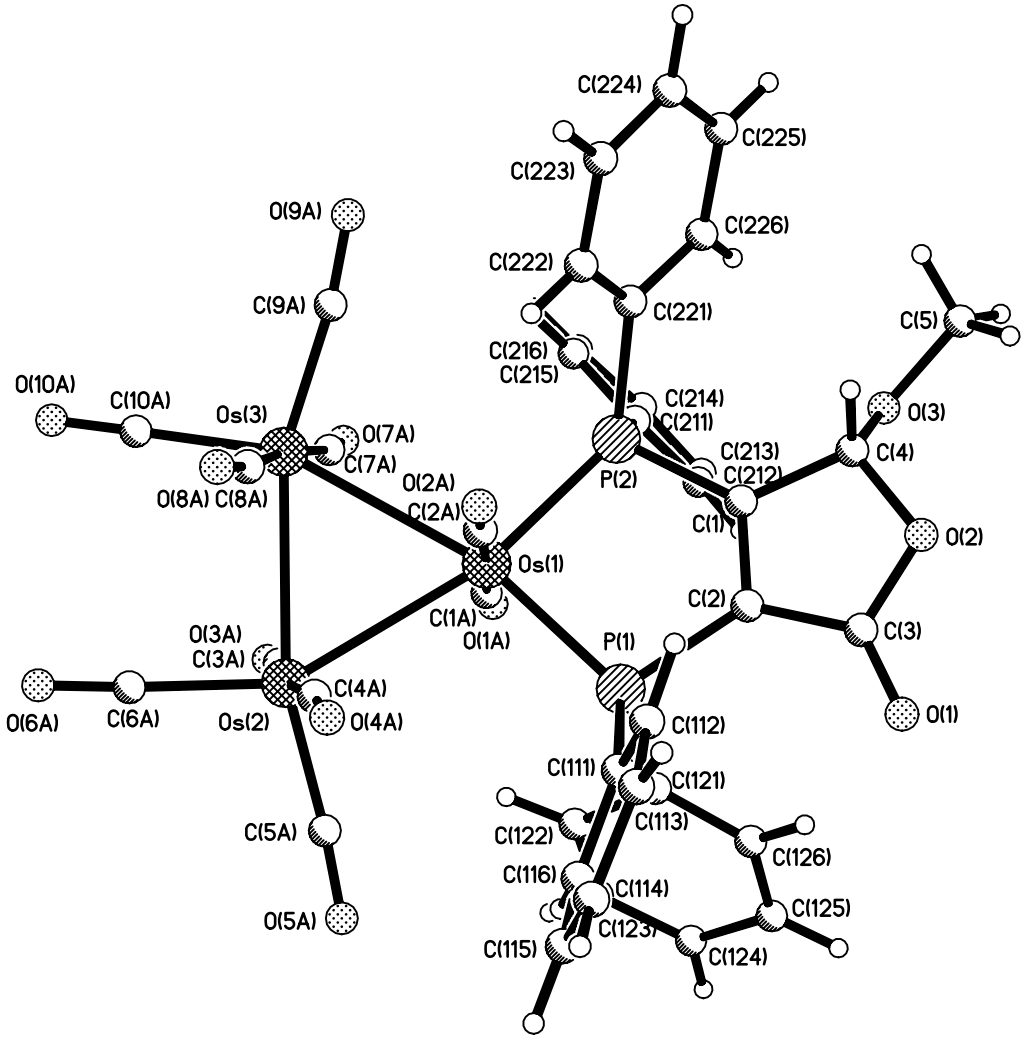

Figure 4.2 Thermal ellipsoid plot and numbering scheme of 1,1-$Os_3(CO)_{10}$(bmf) showing the thermal ellipsoids at the 50% probability level.

Table 4.3 Crystal data and structural refinement details for 1,1-$Os_3(CO)_{10}$(bmf).

Empirical formula	$C_{39}H_{24}O_{13}Os_3P_2$
Formula weight	1333.12
Temperature	100(2) K
Wavelength	0.71073 Å
Crystal size	0.16 x 0.15 x 0.14 mm^3
Crystal system	Monoclinic
Space group	P2(1)/c
Unit cell dimensions	a = 9.3489(6) Å
	b = 19.7355(2) Å β = 92.153(3)°
	c = 21.1817(3) Å
Volume	3905.4(4) $Å^3$
Formula units per cell (Z)	4
Density (calculated)	2.267 Mg/m^3
Absorption coefficient	9.884 mm^{-1}
Reflections collected	28291
Independent reflections	6873 [R(int) = 0.0647]
Coverage of independent reflections	100.0 %
Absorption correction	empirical multi-scan (SADABS)
Max. and min. transmission	0.3342 and 0.2957
Refinement technique	Full-matrix least-squares on F^2
Data / restraints / parameters	6873 / 1594 / 624
Goodness-of-fit on F^2	1.077
Final R indices [I > 2σ(I)]	R1 = 0.0750, wR2 = 0.1615
R indices (all data)	R1 = 0.0873, wR2 = 0.1667
Δp (max), Δp (min) ($e.Å^{-3}$)	6.587 and -1.552

Table 4.4 Selected bond lengths (Å) and bond angles (°) for 1,1-$Os_3(CO)_{10}$(bmf).

Bond lengths

Os1-C1A	1.936(8)	Os1-C2A	1.938(7)
Os1-P1	2.298(4)	Os1-P2	2.317(4)
Os1-Os3	2.899(9)	Os1-Os2	2.936(9)
Os2-C5A	1.916(7)	Os2-C6A	1.935(8)
Os2-C3A	1.934(6)	Os2-C4A	1.947(9)
Os2-Os3	2.882(9)	Os3-C10A	1.925(7)
Os3-C9A	1.954(6)	Os3-C8A	1.973(6)
Os3-C7A	1.998(1)	C1A-O1A	1.145(4)
Os2-C8A	2.895(6)	Os3-C8A	1.974(8)
Os2-C4	1.973(4)	Os3-C9A	1.987(5)
P1-C12	1.817(5)	P1-C11	1.866(5)
P1-C2	1.863(6)	P2-C21	1.827(6)
P2-C1	1.875(7)	P2-C22	1.848(6)
C1-C2	1.357(2)	C1-C4	1.515(7)
C2-C3	1.462(2)	C3-O1	1.194(9)
C11-C16	1.367(2)	C11-C12	1.407(5)
C(3)-C(4)	1.527(5)	P(1) ·· P(2)	3.174(4)

Bond angles

C1A-Os1-C2A	177.7(8)	C1A-Os1-P1	92.8(5)
C2A-Os1-P1	89.3(5)	C1A-Os1-P2	87.5(5)
C2A-Os1-P2	93.5(5)	P1-Os1-P2	88.8(1)
C1A-Os1-Os3	93.7(5)	C2A-Os1-Os3	84.0(5)
P1-Os1-Os3	163.5(5)	P2-Os1-Os3	106.6(6)
C1A-Os1-Os	84.3(5)	C2A-Os1-Os2	94.1(5)
P1-Os1-Os2	106.1(5)	P2-Os1-Os2	163.3(6)
Os3-Os1-Os2	59.6(2)	C5A-Os2-C6A	103.6(9)
C5A-Os2-C3A	91.8(8)	C6A-Os2-C3A	89.7(9)
C5A-Os2-C4	89.2(8)	C6A-Os2-C4A	97.6(9)
C3A-Os2-C4A	172.2(8)	C5A-Os2-Os3	164.6(6)
C6A-Os2-Os3	90.7(7)	C3A-Os2-Os3	82.7(5)
C4A-Os2-Os3	94.5(5)	C5A-Os2-Os1	106.2(6)
C6A-Os2-Os1	150.1(7)	C3A-Os2-Os1	92.3(5)
C4A-Os2-Os1	80.0(5)	Os3-Os2-Os1	59.9(2)
C10A-Os3-C9A	101.1(9)	C10-Os3-C8	91.5(9)
C9A-Os3-C8A	92.3(8)	C10A-Os3-C7A	94.0(9)

The thermal ellipsoid plot of 1,1-$Os_3(CO)_{10}$(bmf) confirms the migration of the diphosphine ligand in 1,2-$Os_3(CO)_{10}$(bmf) from an Os(1)-Os(2) bridged disposition to that where the ancillary ligand is bound to a single osmium atom OS(1). The mean Os-Os and Os-P bond lengths of 2.892(2) Å and 2.264(2) Å, respectively, are unremarkable with respect to those bond distances in other phosphine-substituted osmium clusters.[16] The ten ancillary carbonyl groups are all linear in nature and display a slight twist of the axial groups, much less pronounced than the twist observed in 1,2-$Os_3(CO)_{10}$(bmf). The internuclear non-bonding P(1) ··· P(2) distance of 3.17(2) Å in chelating isomer is nearly 0.60 Å shorter than the internuclear non-bonding P(1) ··· P(2) distance in bridging isomer, in keeping with the trend reported for the $Os_3(CO)_{10}$(dppbz) cluster isomers and other related osmium clusters containing a diphosphine ligand.[16] The remaining bond distances and angles are unexceptional and require no comment.

4.1.3 Synthesis of Hydride Bridged-Clusters from 1,1-$Os_3(CO)_{10}$(bmf)

The photochemical reactivity of cluster **10c** was examined due to the reported photochemical activation of diphosphine ligands at sundry metal cluster through ortho metalation.[7,8] The Richmond group has previously demonstrated photoefficient CO loss and C-H bond activation of an ancillary aryl ligand in the diphosphine-chelated clusters 1,1-$Os_3(CO)_{10}$(bpcd) and 1,1-$Os_3(CO)_{10}$(bmi) to give hydride-bridged clusters $HOs_3(CO)_9[\mu\text{-}Ph_2PC{=}C(PhP\{C_6H_4\})C(O)CH_2C(O)]$ and $HOs_3(CO)_9[\mu\text{-}Ph_2PC{=}C(PhP\{C_6H_4\})C(O)N(p\text{-tolyl})C(O)]$, respectively.[8] Irradiation of an isomeric mixture of clusters **10b** and **10c** using 366 nm light leads to the loss of one CO ligand and ortho metalation of one of the phenyl ligands to give an 80:20 mixture of the hydride clusters **11a** and **11b**. In an interesting observation, the chelating isomer selectively undergoes CO loss to yield the hydride-bridged clusters **11a** and **11b**, with the bridging isomer unaffected by photolysis. This demonstrates that the ortho-metalation reaction is isomer selective. The controlled thermolysis of the resulting isomeric hydride clusters at 80 °C under 1 atm CO regenerates cluster **10c** in quantitative yield, as determined by NMR spectroscopy. These observations strongly support the equilibria depicted in scheme 4.5. Depending on the amount of **10b** initially present, good yields of the ortho-metalation products could be achieved by a combination of prolonged photolysis or thermolysis. This protocol allows for the conversion of the bridging isomer to the chelating isomer **10c**. The hydride clusters were isolated free of any starting materials by column chromatography and were recrystallized to afford the isomeric hydrides as an air sensitive red

solid. Unfortunately, the two hydride clusters could not be separated from each other since their R_f values were identical.

The hydride clusters were characterized in solution by IR and NMR spectroscopies. The ^{31}P NMR spectrum revealed the existence of not one but a diastereomeric mixture of two hydride-bridged clusters in a 80:20 mixture. This isomeric mixture is presumed to derive from proximal and distal methoxy groups relative to the ortho-metalated aryl group that is oriented *β* to the furanone carbonyl group.

The observation of high-field AB quartets centered at -16.20 ppm and -15.90 ppm by ^{1}H NMR provides unequivocal evidence for the presence of two isomeric hydride species. The high-field location of these resonances supports the existence of edge-bridged cluster hydrides. Two singlets corresponding to distinct methoxy moieties at 2.72 ppm and 2.84 ppm were recorded in the ^{1}H NMR spectrum, with the later chemical shift ascribed to the minor isomer (**11b**). The lone methine hydrogen on the bmf ligand was observed as a singlet at 4.70 ppm and 4.80 ppm for the major and minor isomers, respectively. The aromatic hydrogens for the isomeric mixture appear from 6.60 – 7.80 ppm.

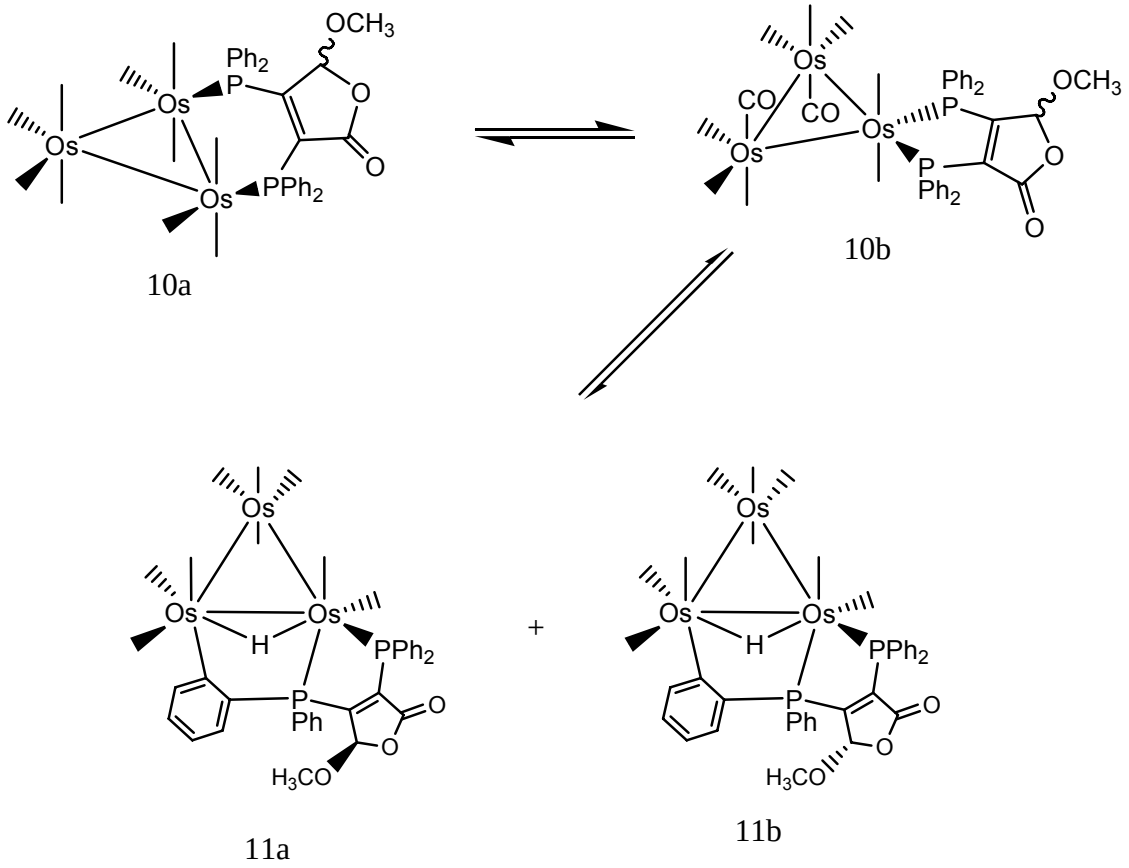

Scheme 4.5 Reversible ligand isomerization and ortho-metalation reactivity of phenyl group β to the furanone carbonyl group in 1,1-$Os_3(CO)_{10}$(bmf).

4.1.4 Thermal Activation of 1,1-$Os_3(CO)_{10}$(bmf) and Characterization of the P-CB Bond Activation Products

Thermolysis of the cluster 1,1-$Os_3(CO)_{10}$(bmf) (thermally equilibrated sample) or the hydride-bridged clusters **11a** and **11b** at elevated temperatures provided evidence for the irreversible activation of the bmf ligand. Thermolysis at 130 °C in toluene, with periodic removal of the liberated CO, furnishes a diastereomeric mixture of the P-C bond activated clusters $HOs_3(CO)_9(\mu_3\text{-}C_6H_4)[\mu_2,\eta^1\text{-}PPhC{=}C(PPh_2)C(O)OCH(CH_3)]$ (**12a** and **12b**) in good yield (scheme 4.5). TLC and NMR examination of the crude reaction mixture revealed the presence of P-C bond activation products, along with a small amount of bmf chelated cluster **10c**. The new clusters **12a** and **12b** were subsequently isolated as pure compounds by column chromatography and fully characterized in solution and by X-ray diffraction analysis in the case of major isomer. Particularly informative was the ^{31}P NMR spectrum of the mixture of **12a** and **12b** that revealed the existence of a diastereomeric mixture of the benzyne-substituted cluster in an 80:20 mixture. The ^{31}P NMR spectrum of **12a** revealed two ^{31}P doublets at 9.40 ppm and -78.50 ppm, with the latter resonence readily assigned to a phosphido moiety that spans the two non-bonded osmium centers.[9] **12b** showed two ^{31}P doublets at 8.50 ppm and -74.20 ppm in the ^{31}P NMR spectrum, where the latter doublet represents the phosphido moiety in cluster **12b**. The ^{1}H NMR data for the benzyne-substituted cluster **12a** reveal resonances at -16.20 ppm (AB quartet 1H), 3.10 ppm (s, 3H), and 5.50 ppm (s, 1H) for the bridging hydride, methoxy group and the methine hydrogen associated with furanone ring,

respectively. The minor benzyne isomer exhibited resonances at -16.00 ppm (AB quartet, 1H), 2.70 ppm (s, 3H) and 4.80 ppm (s, 1H) for the same relative assignments.

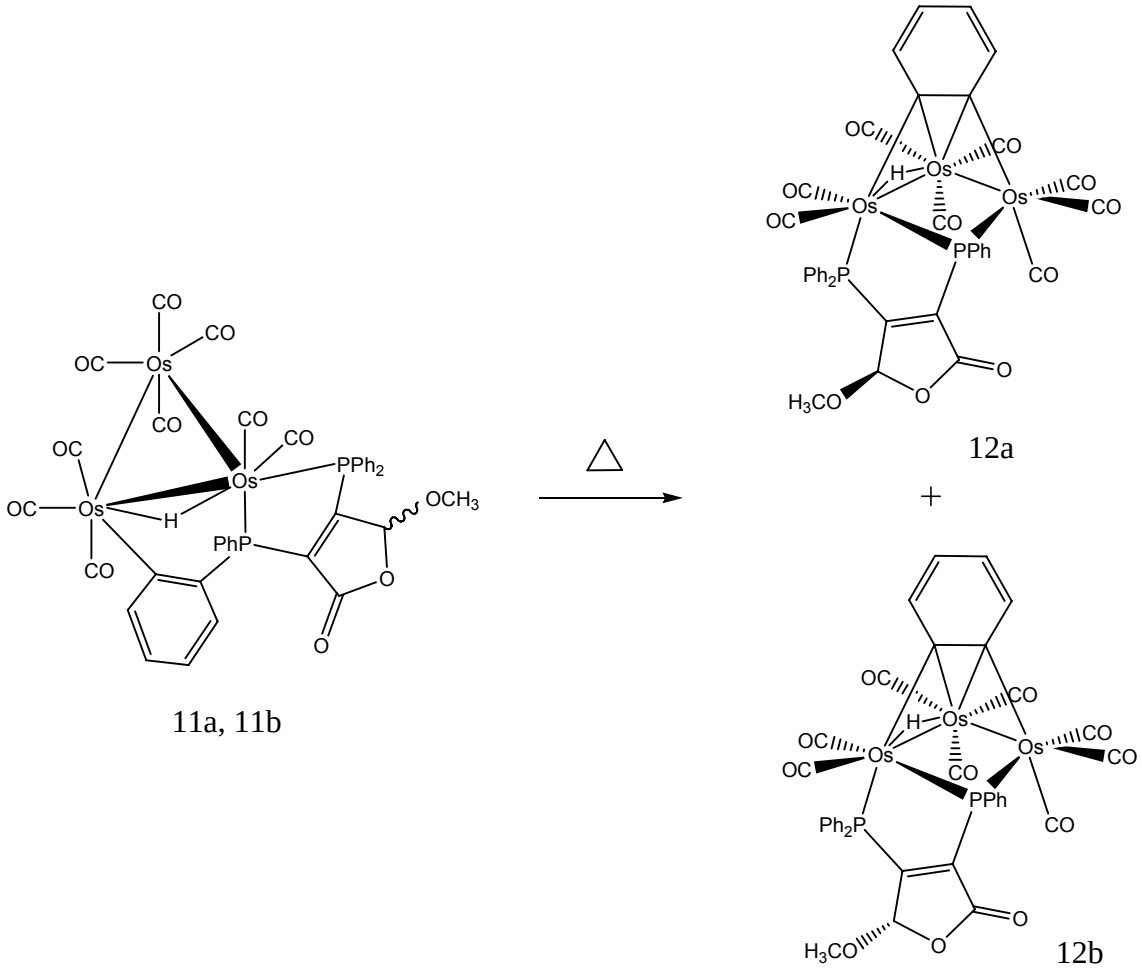

Scheme 4.6 Thermal activation of the hydride clusters **11a** and **11b**

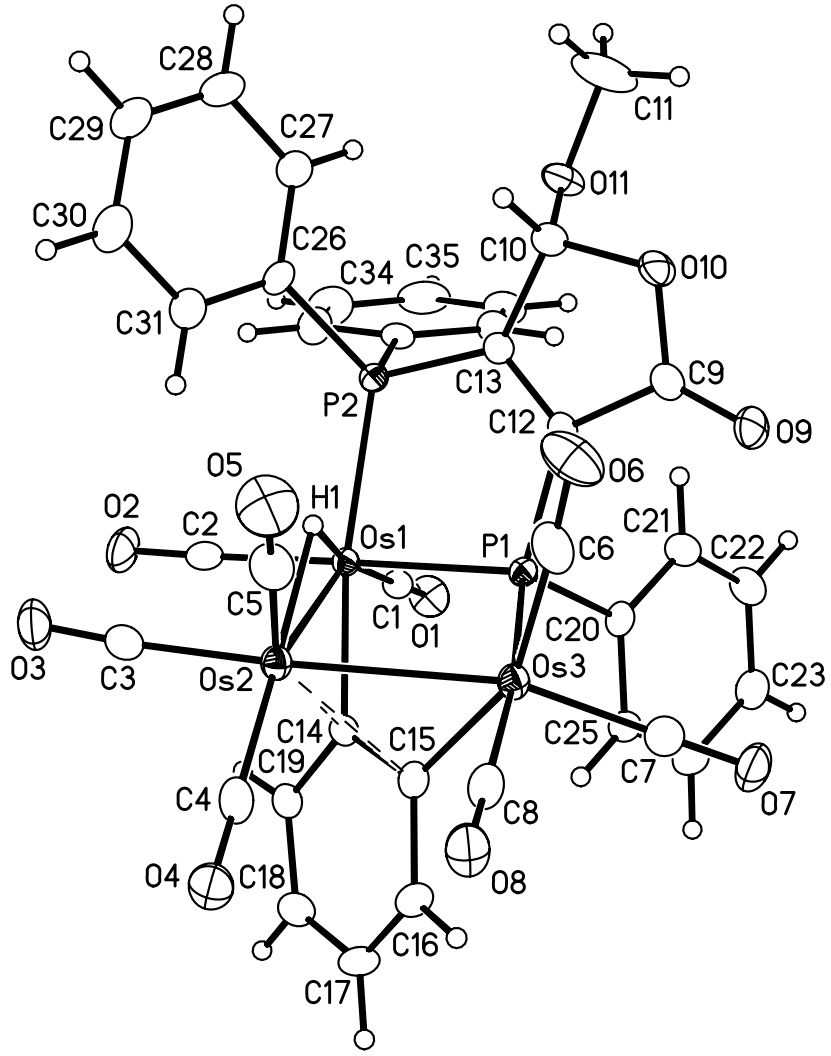

Figure 4.3 Thermal ellipsoid plot of $HOs_3(CO)_9(\mu_3\text{-}C_6H_4)[\mu_2,\eta^1\text{-}PPhC{=}C(PPh_2)C(O)OCH(OCH_3)]$ (**12a**) showing the thermal ellipsoids at the 50% probability level.

Table 4.5 Crystal data and structure refinement for **12a .**

Empirical formula	$C_{37}H_{24}O_{11}Os_3P_2$
Formula weight	1277.10
Temperature	100(2) K
Wavelength	0.71073 Å
Crystal system	Triclinic
Space group	P -1
Unit cell dimensions	a = 10.3986(5) Å α = 74.68(9)°.
	b = 11.3464(5) Å β = 72.59(9)°.
	c = 17.0559(7) Å γ = 84.10(9)°.
Volume	1851.3(4) $Å^3$
Formula units per cell (Z)	2
Density (calculated)	2.291 Mg/m^3
Absorption coefficient	10.416 mm^{-1}
Reflections collected	23179
Independent reflections	8182 [R(int) = 0.0249]
Coverage of independent reflections	99.8%
Absorption correction	Semi-empirical from equivalents
Max. and min. transmission	0.5738 and 0.2422
Refinement method	Full-matrix least-squares on F^2
Data / restraints / parameters	8182 / 0 / 483
Goodness-of-fit on F^2	1.049
Final R indices [I > 2σ(I)]	R1 = 0.0174, wR2 = 0.0433
R indices (all data)	R1 = 0.0193, wR2 = 0.0440
Δp (max), Δp (min) ($e.Å^{-3}$)	1.529 and -0.962

Table 4.6 Selected bond lengths [Å] and bond angles [°] for **12a.**

Bond lengths

Os(1)-C(1)	1.897(3)	Os(1)-C(2)	1.91(3)
Os(1)-C(14)	2.158(3)	Os(1)-P(2)	2.34(8)
Os(1)-P(1)	2.378(8)	Os(1)-Os(2)	2.93(9)
Os(1)-H(1)	1.81(4)	Os(2)-C(5)	1.89(4)
Os(2)-C(3)	1.91(3)	Os(2)-C(4)	1.91(3)
Os(2)-C(14)	2.31(3)	Os(2)-C(15)	2.37(3)
Os(2)-Os(3)	2.82(2)	Os(2)-H(1)	1.89(4)
Os(3)-C(6)	1.92(4)	Os(3)-C(7)	1.92(4)
Os(3)-C(8)	1.93(3)	Os(3)-C(15)	2.14(3)
Os(3)-P(1)	2.38(8)	P(1)-C(12)	1.81(3)
P(1)-C(20)	1.82(3)	P(2)-C(32)	1.81(3)
P(2)-C(26)	1.82(3)	P(2)-C(13)	1.82(3)

Bond angels

C(1)-Os(1)-C(2)	91.24(8)	C(1)-Os(1)-C(14)	95.73(2)
C(2)-Os(1)-C(14)	97.07(7)	C(1)-Os(1)-P(2)	92.84(9)
C(2)-Os(1)-P(2)	94.75(9)	C(14)-Os(1)-P(2)	165.23(9)
C(1)-Os(1)-P(1)	91.75(9)	C(2)-Os(1)-P(1)	176.81(1)
C(14)-Os(1)-P(1)	81.51(8)	P(2)-Os(1)-P(1)	86.23(3)
C(1)-Os(1)-Os(2)	147.03(9)	C(2)-Os(1)-Os(2)	93.23(1)
C(14)-Os(1)-Os(2)	51.31(8)	P(2)-Os(1)-Os(2)	119.26(2)
P(1)-Os(1)-Os(2)	83.65(6)	C(1)-Os(1)-H(1)	170.4(2)
C(2)-Os(1)-H(1)	96.5(7)	C(14)-Os(1)-H(1)	89.0(2)
P(2)-Os(1)-H(1)	80.8(8))	P(1)-Os(1)-H(1)	80.6(2)
Os(2)-Os(1)-H(1)	38.4(8)	C(5)-Os(2)-C(3)	97.73(5)
C(5)-Os(2)-C(4)	93.04(5)	C(3)-Os(2)-C(4)	91.36(4)
C(5)-Os(2)-C(14)	156.91(3)	C(3)-Os(2)-C(14)	98.32(3)
C(4)-Os(2)-C(14)	103.06(3)	C(5)-Os(2)-C(15)	133.28(4)
C(3)-Os(2)-C(15)	128.78(3)	C(14)-Os(2)-C(15)	36.05(7)
C(4)-Os(2)-C(15)	82.88(3)	C(5)-Os(2)-Os(3)	86.74(7)

Unequivocal evidence for the presence of the benzyne moiety and an open cluster core in the major isomer **12a** was provided by the X-ray diffraction structure of the same (Figure 4.3). Cluster **12a** contains 50 valence electrons, which is two electrons in excess of the electron-precise count of 48 valence electrons for saturated triangular Os_3 clusters, accounting for the observed polyhedral opening of the metallic frame.[10] The benzyne ligand is composed of the atoms C(14)-C(19) and functions as a typical four-electron, face-capping ligand where the two Os-C σ bonds Os(1)-C(14) 2.310(3) Å and (Os(3)-C(15) 2.143(3) Å and the Os-C π bonds Os(2)-C(14) 2.310(3) Å and Os(2)-C(25) 2.372(3) Å are similar in distance to those distances found in other benzyne-substituted osmium clusters.[11-13] The phosphido ligand, which is defined by the P(1) atom, is equatorially situated and serves to tether the nonbonded Os(1) and Os(3) atoms. The internulear Os(1) ··· Os(3) distance of 3.719(3) Å clearly precludes any direct bonding interactions between these metal centers. The phosphorus atom P(2) behaves as a normal phosphine ligand and is bound in an η^1 fashion to the Os(1) center. The Os-Os bond distances ranges from 2.827(2) to 2.935(2) Å. The bridged hydride ligand was refined during the X-ray data refinement and was found to span the Os(1) and Os(2) vector.

4.2 Kinetic Measurements on the Diphosphine Ligand Isomerization in $Os_3(CO)_{10}$(bmf)

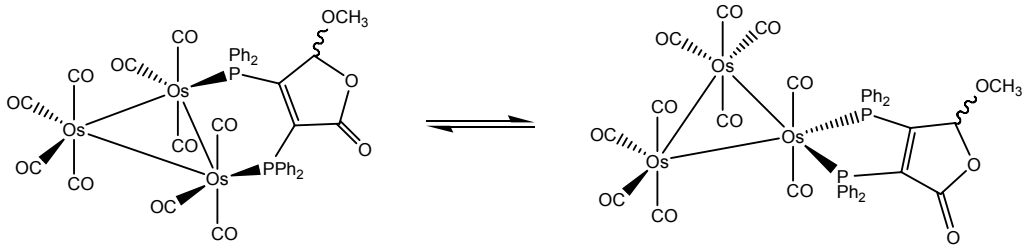

10b **10c**

Scheme 4.7 Isomerization of 1,2- to 1,1-$Os_3(CO)_{10}$(bmf).

The isomerization reaction involving the ancillary bmf ligand in clusters **10b** and **10c** was investigated by both UV-vis and ^{1}H NMR spectroscopy, with the latter analytical method providing unequivocal evidence for the reversible equilibrium between **10b** and **10c**. The approach to equilibrium for the conversion of the bridging isomer to chelating isomer was monitored by ^{1}H NMR spectroscopy in toluene-d_8 at 358 K, with Figure 4.4 showing the smooth decay and growth peaks for the consumption and formation of clusters **10b** and **10c**, respectively. Here the singlet at 2.20 ppm corresponding to the methoxy hydrogens of the bridging isomer is consumed at the expense of the singlet at 2.82 ppm, which belongs to the methoxy moiety of the chelating isomer. Paralleling these changes in the intensity of the methoxy groups is the decrease in intensity of the methine hydrogen at 4.35 ppm for the bridging isomer and an increase in the intensity of the related methine hydrogen for the chelating isomer at 4.80 ppm. The peak at 1.26 ppm represents the internal standard, *t*-butyl benzene.

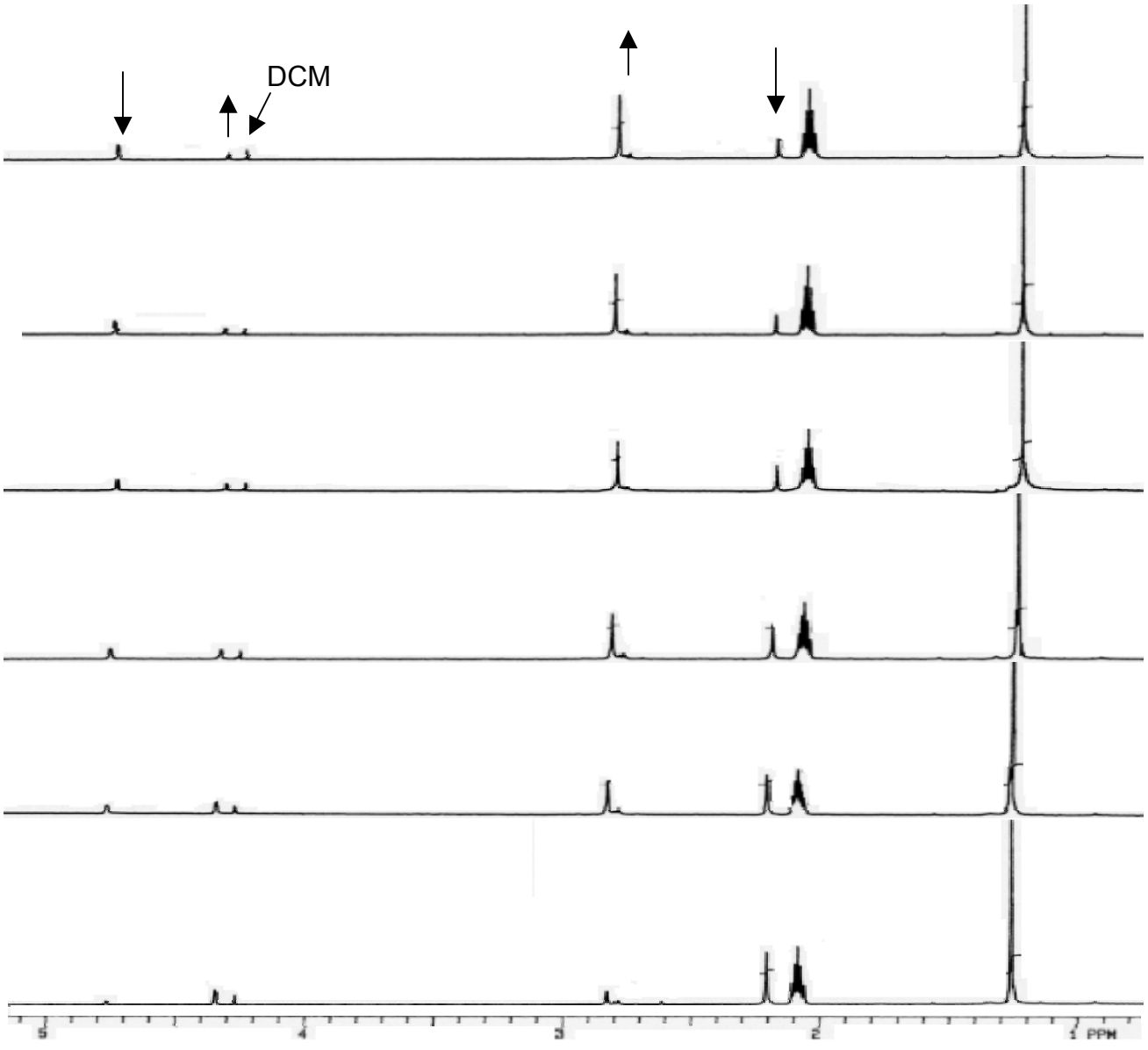

Figure 4.4 Representative ^{1}H NMR spectra recorded at 358 K for the approach to the equilibrium from **10b** to **10c.**

Nonlinear regression analysis of the ^{1}H NMR data depicted in Figure 4.4 afforded the rate constant to equilibrium, which is identical to the rate constant calculated by UV-vis spectroscopy at the same temperature. The values for k_1 and k_{-1} for the reversible first-order process were computed with the aid of the equations[17]: $k_1 = k_e/[1+K_{eq}^{-1}]$, $k_{-1} = k_e/[1+K_{eq}]$.

The kinetics for the isomerization reaction were also studied by UV-vis spectroscopy in toluene solution under 1 atm of CO over the temperature range of 358 - 383 K by following the increase in the absorbance of the 365 nm band. The UV-vis spectral changes for the thermolysis of **10b** in toluene at 368 K are shown in Figure 4.5, where clearly defined isosbestic points at 386 and 462 nm are observed to accompany the reaction. The excellent fit between the least-squares regression curve and the absorbance data (Figure 4.6) confirms that the isomerization is well-behaved and free from kinetic complications. The amount of hydride cluster present in the UV-vis experiments is predicted to be negligible. The equilibrium in Scheme 4.6 mandates the suppression of the hydride cluster for reactions carried out under high concentrations of CO relative to cluster **10c**. A conservative 10-fold concentration excess of CO relative to the bridging and chelating clusters **10b,c** is predicted from the available solubility data for CO in toluene.[14] The rate constants for the approach to equilibrium (K_{eq}), along with the values of k_1 and k_{-1}, as computed with the tablulated K_{eq} values for **10b** to **10c**, are given in Table 4.2. Entries 3 and 4 in Table 4.7 confirm that the reaction rate measured under standard conditions (entry 3: 1 atm CO) is not significantly

different from the rate measured under 100 psi CO (entry 4). The effect of added PPh_3 (10 equiv) was examined and similar results were obtained. Collectively, these data rule out a dissociative process and the generation of a long-lived unsaturated intermediate. Eyring plots of $\ln(k_1/T)$ and $\ln(k_{-1}/T)$ versus T^{-1} allowed for the determination of the isomerization activation parameters for the forward and reverse reaction directions for the equilibrium between **10b** and **10c**. The calculated values of $\Delta H^{\ddagger}$= 26.9(0.7) kcal/mol, and $\Delta S^{\ddagger}$= 6(1) eu for forward isomerization (**10b** to **10c**) and $\Delta H^{\ddagger}$= 27.9(0.7) kcal/mol, and $\Delta S^{\ddagger}$= 6(1) eu for the reverse reaction (**10c** to **10b**) reveal that the entropy of activation is small in both directions, arguing against a dissociative mechanism involving the release of one of the PPh_2 moieties from the cluster frame to generate an unsaturated Os_3 cluster having a pendent η^1-diphosphine moiety.

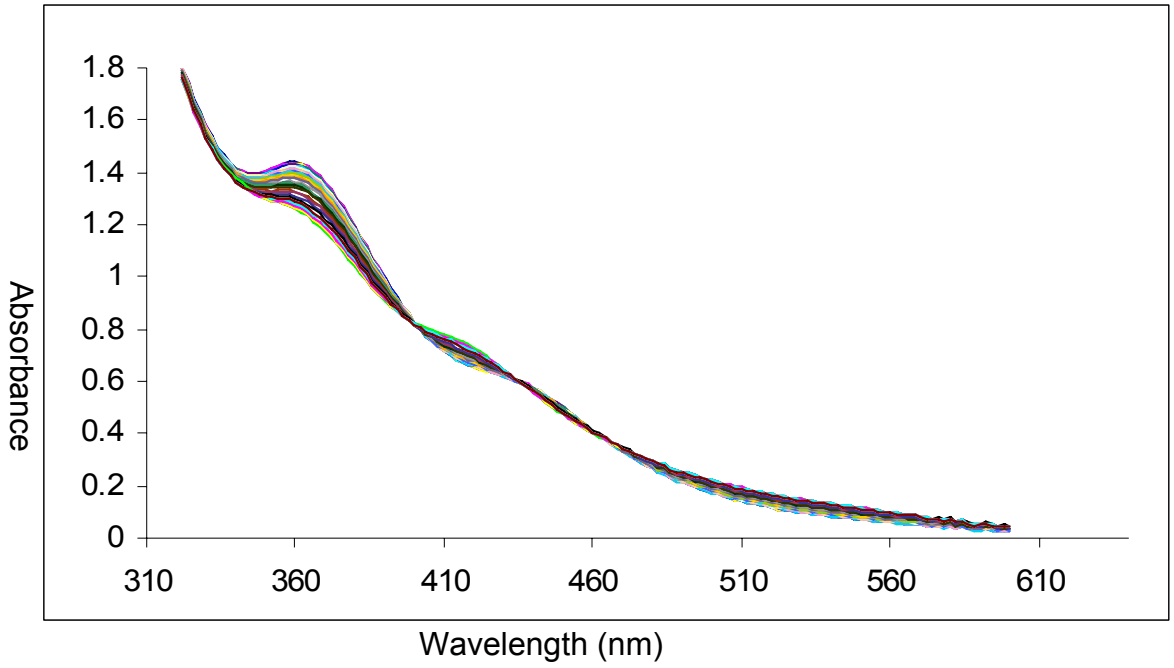

Figure 4.5 UV-vis spectral changes for the isomerization of **10b** to **10c.**

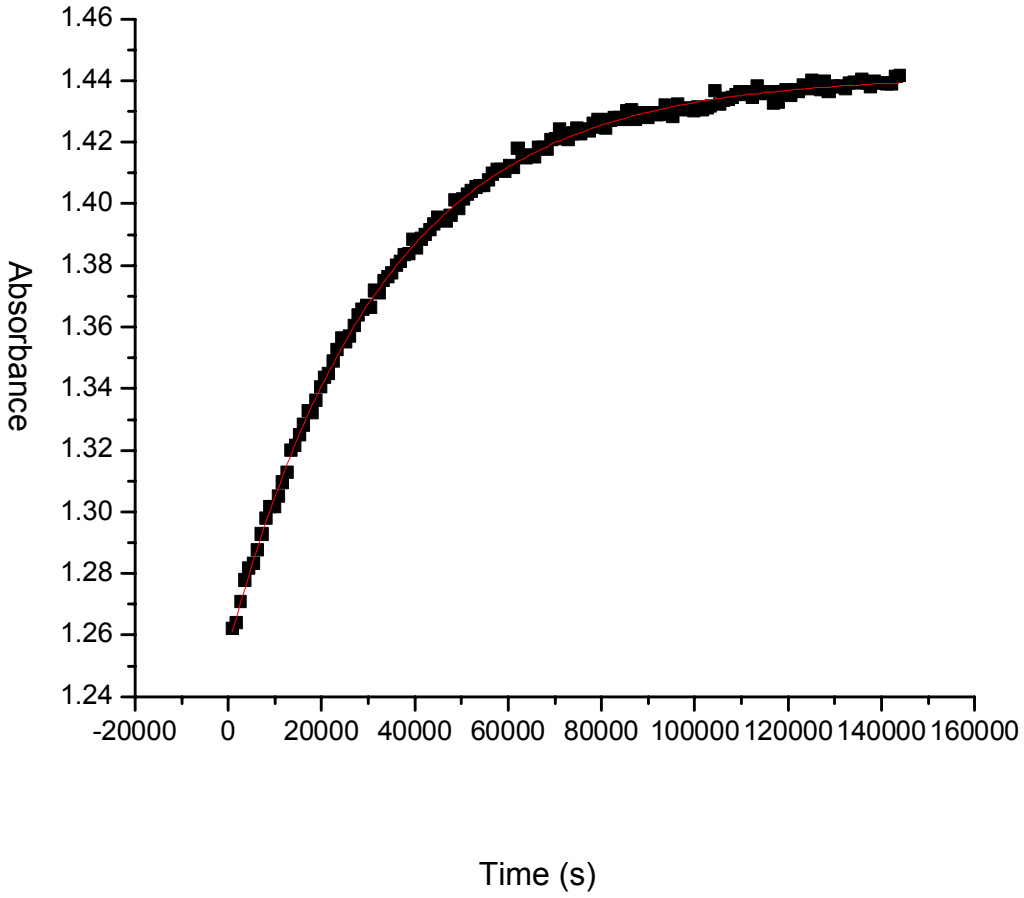

Figure 4.6 The absorbance versus time curve (■) and the least-squares fit of k(—**)** for the spectroscopic data in Figure 4.5.

Table 4.7 Kinetic data for the isomerization of 1,2-$Os_3(CO)_{10}$(bmf) (**10b**) to 1,1-$Os_3(CO)_{10}$(bmf) (**10c**).[a]

Temp (K)	Solvent	10^4 k_e[b] (s^{-1})	10^4 k_1 (s^{-1})	10^4 k_{-1} (s^{-1})	Method
358	Toluene	0.30 ± 0.04	0.26 ± 0.03	0.04 ± 0.03	UV-vis
358	Toluene (D)	0.19± 0.04	0.16 ± 0.03	0.03± 0.02	^{1}H NMR
363	Toluene	0.70± 0.04	0.59 ± 0.03	0.11± 0.03	UV-vis
363	Toluene	0.70 ± 0.07	0.59 ± 0.06	0.11± 0.06	UV-vis/100 psi CO[c]
368	Toluene	1.19± 0.06	1.01 ± 0.06	0.18 ± 0.06	UV-vis
368	Toluene	0.89± 0.04	0.76 ± 0.04	0.13 ± 0.04	UV-vis/ 10eq PPh_3[d]
373	Toluene	1.83± 0.10	1.55 ± 0.09	0.27 ± 0.09	UV-vis
383	Toluene	6.11± 0.14	5.19 ± 0.12	0.91 ± 0.12	UV-vis

[a]All kinetic experiments were conducted under 1 atm of CO unless otherwise noted. [b]The extent of the isomerization was followed by monitoring the increase in the absorbance of the 365 nm band (UV-vis) or the decrease in the initial intensity of the methoxy singlet at δ 2.20 for 1,2-$Os_3(CO)_{10}$(bmf) (NMR). [c]Reaction conducted in the presence of 100 psi CO. [d]Reaction conducted in the presence of 10 equivalents of PPh_3.

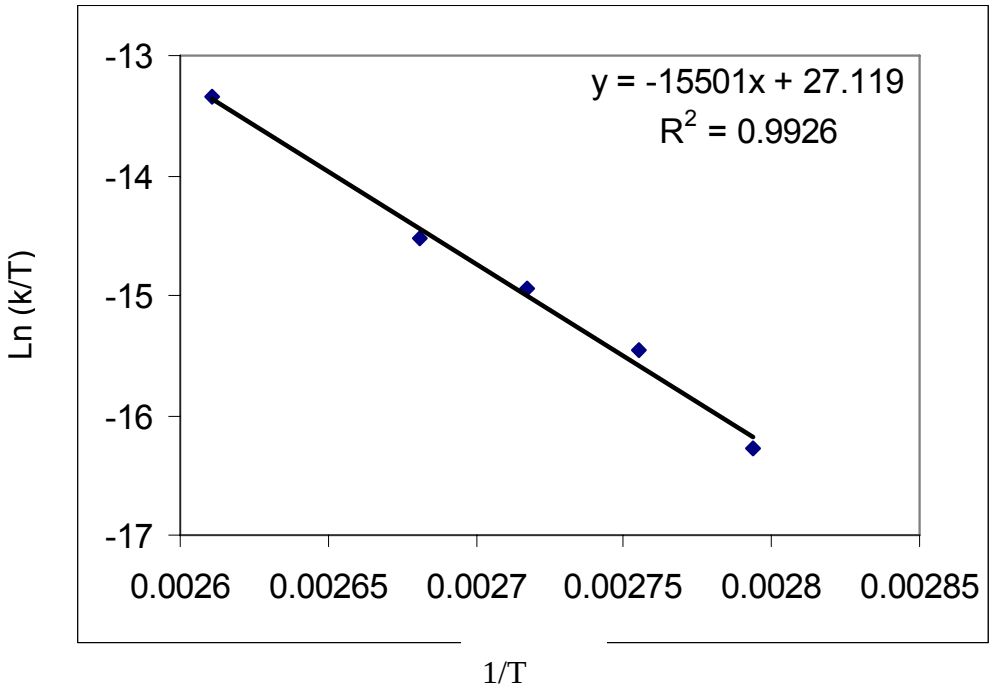

Figure 4.7 Eyring Plot for the isomerization of 1,2-$Os_3(CO)_{10}$(bmf)(**10b**) to1,1-$Os_3(CO)_{10}$(bmf)(**10c**).

4.3 Conclusions

The triosmium cluster 1,2-$Os_3(CO)_{10}(MeCN)_2$ reacts with the diphosphine ligand 3,4-bis(diphenylphosphino)-5-methoxy-2(5)H-furanone (bmf) at 25 ºC to give the bmf-bridged cluster 1,2-$Os_3(CO)_{10}$(bmf) (**10b**) in high yield. Heating **10b** leads to an equilibrium with the chelating isomer 1,1-$Os_3(CO)_{10}$(bmf) (**10c**). The molecular structure of each isomer has been crystallographically determined, and the kinetics for the isomerization have been investigated by UV-vis and ^{1}H NMR spectroscopy. The reversible nature of the diphosphine isomerization has been confirmed by NMR and UV-vis measurements, and the forward (k_1) and reverse (k_{-1}) first-order rate constants for the bridge-to-chelate isomerization (**10b** to **10c**) have been determined. Thermolysis of cluster **10c** (>110 ºC) leads to regiospecific activation of C-H and P-C bonds, producing the hydrido clusters $HOs_3(CO)_9[\mu\text{-}PPh_2C{=}C\{PPh(C_6H_4)\}CH(OMe)OC(O)]$ (**11a** and **b**) and the benzyne clusters $HOs_3(CO)_8(\mu_3\text{-}C_6H_4)[\mu\text{-}PPhC{=}C(PPh_2)CH(OMe)\ OC(O)]$ (**12a** and **b**). Clusters **11** and **12**, which exist as a pair of diastereomers, have been fully characterized in solution by IR and NMR spectroscopy, and the molecular structure of **12b** (major diastereomer) has been determined by X-ray crystallography.

4.4 Chapter References

1. Pöe, A.J.; Sekhar, V.C. *J. Am. Chem. Soc.* **1984**, *106*, 5034.
2. Deeming, A.J.; Donovan-Mtunzi, S.; Kabir, S.E. *J. Organomet. Chem.* **1984**, *276*, C65; **1987**, *333*, 253. (b) Deeming A.J.; Stchedroff, M. *J. Chem. Soc., Dalton Trans.* **1988**, 3819.
3. Cartwright, S.; Clucas, J.A.; Dawson, R,H,; Foster, D.F; Harding, M.M.; Smith, A.K. *J. Organomet. Chem.* **1986**, *302*, 403.
4. (a) Fenske, D.; Becher, H.J. *Chem. Ber.* **1975,***108,* 2115. (b) *Chem. Ber.* **1974**, *107*, 117. (c) Fenske, D. *Chem. Ber*. **1979**, *112*, 363.
5. Dahlinger, K.; Pöe, A.J.; Sayal, P.K.; Sekhar, V.C. *J. Chem. Soc., Dalton Trans.* **1986**, 2145.
6. (a) Churchill, M.R.; Lashewycz, R.A.; Shapley, J.R. Richter, S.I. *Inorg. Chem.* **1980**, *19*, 1277. (b) Garrou, P.E. *Chem. Rev.* **1981**, *81*, 229. (c) Richmond, M.G.; Kochi, J.K. *Inorg. Chem.* **1987**, *6*, 254.
7. (a) Watson, W.H.; Wu, G.; Richmond, M.G. *Organometallics*, **2006**, *25*, 930. (b) Watson, W.H.; Wu, G.; Richmond, M.G. *Organometallics*, **2005**, *24*, 5431.
8. Watson, W.H.; Poola, B.; Richmond, M.G. *J. Organomet. Chem.* **2006**, *691*, 4676.
9. Carty, A.J.; MacLaughlin, S.A.; Nucciarone, D. In *Phosphorus-31 NMR Spectroscopy in Stereochemical Analysis*; Verkade, J.G.; Quin, L.D. Eds.; VCH: New York, **1987**.

10. Mingo, D.M.P.; Wales, D.J.; *Introduction to Cluster Chemistry*; Prentice Hall: Englewood Cliffs, NJ, 1990**.**

11. Kabir, S.E.; Miah, M.A.; Sarker, N.C.; Hossain, G.M.G.; Hardcastle, K.I.; Nordlander, E.; Rosenberg, E. *Organometallics* **2005**, *24*, 3315.

12. (a) Goudsmit, R.J.; Johnson, B.F.G.; Lewis, J.; Raithby, P.R.; Rosales, M.J. *J. Chem. Soc., Dalton Trans.* **1983**, 2257. (b) Chen, G.; Deng, M.; Lee, C.K.; Leong, W.K. *Organometallics* **2002**, *21*, 1227.

13. (a) Leong, W.K.; Chen, G. *Organometallics* **2001**, *20*, 2280. (b) Tay, C.T.; Leong, W.K. *J. Organomet. Chem.* **2001**, *625*, 231.

14. (a) Van Raaij, E.U.; Schmulbach, C.D.; Brintzinger, H.H. *J. Organomet. Chem.* **1987**, *328*, 275. (b) Bascikos, L.; Bunn, A.G.; Wayland, B.B.; *Can. J. Chem.* **2001**, *79*, 854.

15. Bott, S.G.; Yang, K.; Richmond, M.G. *J. Organomet. Chem.* **2006**, *691*, 3771.

16. (a) Azam, K.A.; Hursthouse, M.B.; Kabir, S.E.; Malic, K.M.A.; Mottalib, M.A. *J. Chem. Crystallogr.* **1999**, *29*, 813. (b) Deeming, A.J. *J. Adv. Organomet. Chem*. **1986**, *26*, 1.

17. (a) Churchill, M.R; DeBoer, B. G. *Inorg. Chem.* **1977**, 16, 878. (b) Bruce, M.I.; Pain, G.N.; Hughes, C.A.; Patrick, J.M.; Skelton, B.W.; White, A.H. *J. Organomet. Chem.* **1986**, *307*, 343.

CHAPTER 5

EXPERIMENTAL

5.1 Materials

5.1.1 Solvents and Reagents

All reaction and NMR solvents were distilled from an appropriate drying agent under argon. All distilled solvents were stored under argon in Schlenk vessels equipped with Teflon stopcocks.[1] The cluster $H_4Ru_4(CO)_{12}$ was prepared from $Ru_3(CO)_{12}$,[2] and the clusters 1,2- and 1,1-$H_4Ru_4(CO)_{10}$(dppe) were synthesized according to the procedures reported by Shapley and Churchill.[3] The $Os_3(CO)_{12}$ used in the synthesis of $Os_3(CO)_{10}(MeCN)_2$ was prepared from high-pressure carbonylation of OsO_4 using a 500 mL Parr 4571 series autoclave.[4] The activated cluster 1,2-$Os_3(CO)_{10}(MeCN)_2$ was synthesized by following the known procedure.[5] The ligand bpcd was synthesized from 4,5-dichloro-4-cyclopenten-1,3-dione using the known procedure by Fenske and Becher.[6] The $Ph_2P(TMS)$ used in the synthesis of bpcd ligand was prepared according to the published procedure.[7] The OsO_4 was purchased from Engelhard Chemical Co, and the chemicals dppe, PPh_3, *p*-N,N'-dimethylaminobenzaldehyde $Me_3NO{\bullet}xH_2O$, were purchased from Aldrich Chemical Co. The $Me_3NO{\bullet}xH_2O$ was dried by azeotropic distillation from benzene, and the remaining chemicals were used as received.

5.1.2 Instrumentation

The IR spectral data were recorded on a Nicolet 20 SXB FT-IR spectrometer in sealed 0.1 mm NaCl cells, using PC control and OMNIC software. The ^{1}H and ^{31}P NMR spectra were recorded at 200 and 121 MHz,

respectively, on a Varian Gemini-200 and Varian 300-VXR spectrometers. The reported ^{31}P chemical shift data, which were recorded in the proton-decoupled mode, are referenced to external H_3PO_4 (85%), whose chemical shift was set at δ = 0. The UV-vis spectroscopic data were collected on Hewlett-Packard 8452A diode array spectrometer. The photolysis experiments were carried out with GE Blacklight bulbs having a maximum output of 366 ± 20 nm.[11] The GE blacklight bulbs used in the study were configured with a variable-temperature customized UV-vis cell holder that was connected to a VWR constant temperature circulator, which allowed regulation of the reaction temperature within ±0.5 °C. The combustion analyses were performed by Atlantic Microlab, Norcross, GA.

5.2. Synthesis of Compounds

5.2.1 Reaction of 4-N,N'-dimethylaminobenzaldehyde with bpcd

To 0.20 g (0.43 mmol) of bpcd in 30 mL of DCM was added under argon flush 0.63 g (0.45 mmol) of 4-N,N'-dimethylaminobenzaldehyde, 5 g of molecular sieves and 5 mL of methanol. The reaction solution was stirred overnight at room temperature and was then examined by TLC analysis, which revealed the consumption of the starting materials and the presence of new yellow spot (R_f = 0.65 in 1:1 DCM/hexanes). At this point, the solution was filtered to remove molecular sieves, followed by removal of the solvents in vacuo. The desired product was isolated by column chromatography over silica gel using 8:2 DCM/hexanes as the eluent. Yield 0.18 g (70%). IR (CH_2Cl_2): *v*(CO) 1772 (w, sym dione), 1709 (s, antisym dione) cm^{-1}. ^1H NMR ($CDCl_3$): δ 2.30 (s, 6H, Me), 6.80-7.50 (m, 24H, aromatics). ^{31}P NMR ($CDCl_3$): δ -22.00 (s).

5.2.2 Synthesis of $H_4Ru_4(CO)_{10}$[(Z)-Ph_2CH=$CHPPh_2$]

Me_3NO Activation: To 0.10 g (0.13 mmol) of $H_4Ru_4(CO)_{12}$ and 59 mg (0.15 mmol) of (Z)-Ph_2PCH=$CHPPh_2$ in a large Schlenk flask was added 20 mL of CH_2Cl_2 under argon, followed by 21 mg (0.28 mmol) of Me_3NO. The solution was stirred for 1 h at room temperature, after which the solution was examined by TLC in CH_2Cl_2/hexane (1:1), which revealed the presence of a new orange spot (R_f = 0.65) that was ascribed to cluster 1, in addition to a small amount of unreacted starting cluster (R_f = 0.90) and (Z)-Ph_2PCH=$CHPPh_2$ (R_f = 0.85). The solvent was removed under vacuum and the solid residue was purified by column chromatography over silica gel employing CH_2Cl_2/hexane (1:1) as the eluent. Yield: 61 mg (41%). IR (CH_2Cl_2): ν(CO) 2073 (s), 2044 (vs), 2021 (vs), 2003 (s), 1985 (sh) cm^{-1}. ^1H NMR ($CDCl_3$): δ 6.95-7.58 (m, 22 H, aryl and vinyl), -15.34 (b, 3H), -18.70 (b, 1H). ^{31}P NMR ($CDCl_3$; 298 K): δ 72.20 (s).

Thermolysis Reaction: To a Schlenk tube under argon was charged 50 mg (0.067 mmol) of $H_4Ru_4(CO)_{12}$ and 29 mg (0.070 mmol) of (Z)-Ph_2PCH=$CHPPh_2$, and then the Schlenk tube was charged with 20 mL of 1,2-dichloroethane (DCE). The vessel was sealed and heated at 75 $^{\circ}$C overnight. Upon cooling to room temperature, the solution was analyzed by TLC, which showed the presence of unreacted starting cluster, diphosphine ligand, and the desired product **1**, along with some unknown material at the origin. This origin material did not move with the above solvent system and its characterization was not pursued. Cluster **1** was isolated as previously described in a ca. 40% yield.

5.2.3 Synthesis of $H_4Ru_4(CO)_{10}$(dbpcd)

Me_3NO Activation: To a Schlenk tube under argon flush was added 0.10 g (0.13 mmol) of $H_4Ru_4(CO)_{12}$, 88 mg (0.15 mmol) of dbpcd, and 21 mg (0.28 mmol) of Me_3NO, after which 20 mL of CH_2Cl_2 was syringed into the vessel and the reaction was stirred for ca. 1 hr at room temperature. TLC examination of the reaction solution using CH_2Cl_2/hexane (1:1) showed the presence of cluster 2 (R_f = 0.37). The desired orange-colored cluster was subsequently isolated by column chromatography over silica gel using a 3:2 CH_2Cl_2/hexane mixture as the eluent. Yield: 59 mg (38%). IR (CH_2Cl_2): *v*(CO) 2072 (s), 2045 (vs), 2024 (vs), 2007 (s), 1975 (m), 1748 (w, symm dione), 1719 (s, antisymm dione) cm^{-1}. ^1H NMR ($CDCl_3$): δ 3.2 (s, 6H, Me), 7.40-7.70 (m, 24H, aryl) -16.15 (b, 3H), -18.75 (b, 1H). ^{31}P NMR ($CDCl_3$; 298 K): δ 48.40 (s).

Thermolysis Reaction: This reaction was carried out in DCE solvent with 50 mg (0.067 mmol) of $H_4Ru_4(CO)_{12}$ and 44 mg (0.075 mmol) of bpcd. The reaction vessel was heated at ca. 75 °C overnight and the work-up was identical to that described above. Yield: 27 mg (35%).

5.2.4. Synthesis of 1,2-$Os_3(CO)_{10}$(dppbz) from 1,2-$Os_3(CO)_{10}(MeCN)_2$

To 0.25 g (0.27 mmol) of 1,2-$Os_3(CO)_{10}(MeCN)_2$ in 30 mL of CH_2Cl_2 under argon flush was added 0.14 g (0.31 mmol) of dppbz in one portion. The reaction was stirred at room temperature for ca. 3 h, at which time TLC analysis confirmed the complete consumption of starting cluster and the formation of a single yellow spot at R_f = 0.50 (1:1 CH_2Cl_2/hexane) corresponding primarily to 1,1-$Os_3(CO)_{10}$(dppbz) (**8c**, 60%) and minor amounts of 1,2-$Os_3(CO)_{10}$(dppbz)

(**8b**, 20%) and the hydride-bridged cluster $HOs_3(CO)_9[\mu\text{-}(PPh_2)C{=}C\{PPh(C_6H_4)\}C_4H_4]$ (**9**, 20%) (as established by NMR spectroscopy). The dppbz-substituted clusters **8b**, **8c** and **9** were obtained by flash column chromatography over alumina using a 1:1 mixture of CH_2Cl_2/hexane as the eluent. Carrying out the reaction at 0 °C yielded 1,2-$Os_3(CO)_{10}$(dppbz) (**8b**, 75%) as a major product along with minor amounts of 1,2-$Os_3(CO)_{10}$(dppbz) (**8c**, 15%) and the hydride-bridged cluster $HOs_3(CO)_9[\mu\text{-}(PPh_2)C{=}C\{PPh(C_6H_4)\}C_4H_4]$ (**9**, 10%). Spectroscopic data for **8b**: IR (CH_2Cl_2): *v*(CO) 2092 (s), 2041 (m), 2013 (s), 2004 (m), 1973(w) cm^{-1}. ^1H NMR ($CDCl_3$): δ 6.70-7.50 (m, 24H, aromatics). ^{31}P NMR ($CDCl_3$): δ 8.50 (s).

5.2.5 Synthesis of 1,1-$Os_3(CO)_{10}$(dppbz)

The synthesis of 1,1-$Os_3(CO)_{10}$(dppbz) was quantitatively achieved by heating a mixture containing 1,2-$Os_3(CO)_{10}$(dppbz), 1,1-$Os_3(CO)_{10}$(dppbz), and $HOs_3(CO)_9[\mu\text{-}(PPh_2)C{=}C\{PPh(C_6H_4)\}C_4H_4]$ at 60 °C in toluene under 1 atm of CO for 24 hr. At the end of thermolysis, the solvent was removed under vacuum and the residue separated by column chromatography over alumina using 1:1 DCM/hexane. The crude product was recrystallized using dichloromethane. Typical yields of recrystallized 1,1-$Os_3(CO)_{10}$(dppbz) were on the order of 90%. Spectroscopic data for **8c**: IR (CH_2Cl_2): *v*(CO) 2094 (s), 2040 (s), 2012 (s), 2001 (m), 1971 (m) cm^{-1}. ^1H NMR ($CDCl_3$): δ 6.70-7.60 (m, 24H, aromatic). ^{31}P NMR ($CDCl_3$): δ 26.50 (s). Anal. Calcd (found) for $C_{40}H_{24}Os_3O_{10}P_2$: C, 37.03 (39.81); H, 1.86 (1.84).

5.2.6. Synthesis of $HOs_3(CO)_9[\mu\text{-}(PPh_2)C{=}C\{PPh(C_6H_4)\}C_4H_4]$

To a small Schlenk storage vessel was added 0.10 g (0.036 mmol) of cluster **8c** and 25 mL of toluene, after which the vessel was sealed and subjected to three freeze-pump-thaw degas cycles. The vessel was next placed between two GE Blacklights for the period of 5 to 7 days. The CO that accompanies the formation of hydride cluster (**9**) was periodically removed by additional freeze-pump-thaw degas cycles to drive the reaction to completion. At the end of photolysis, the crude reaction solution containing cluster **9** was passed over a short pad of alumina and recrystallized from CH_2Cl_2/hexane to furnish a yellow solid in 90% yield (90 mg). IR (CH_2Cl_2): *v*(CO) 2075 (s), 2038 (vs), 2013 (s) 1997 (s), 1967 (m) cm^{-1}. ^1H NMR ($CDCl_3$): δ -16.80 (AB quartet, hydride, $J_{P\text{-}H}$ = 12.3 Hz), δ 6.70-7.80 (m, 23H, aromatic). ^{31}P NMR (Toluene-d_8): δ 28.50 ppm (d, $J_{p\text{-}p}$ =11 Hz), 40.50 ppm (d, $J_{p\text{-}p}$ = 13). Anal. Calcd (found) for $C_{39}H_{24}Os_3O_9P_2$: C, 36.91 (37.41); H, 1.91 (2.12).

5.2.7. Synthesis of 1,2-$Os_3(CO)_{10}$(bmf)

To a Schlenk flask containing 25 mL of dichloromethane and 0.25 g (0.27 mmol) of $Os_3(CO)_{10}(MeCN)_2$ was added 0.15 g (0.30 mmol) of bmf under argon flush, after which the solution was stirred for two hours at ambient temperature. TLC examination at this time revealed the consumption of the starting cluster and formation of a major red spot (R_f = 0.45 with 3:2 DCM/hexane). The solvent was stripped under vacuum and the residue separated by column chromatography over silica gel using 60% dichloromethane in hexane to give 1,2-$Os_3(CO)_{10}$(bmf). Yield: 0.22 g (60%) IR (CH_2Cl_2): *v*(CO) 2090 (vs), 2042 (s), 2011 (vs) 2007 (vs),

1976 (m) 1772 (s, furanone) cm^{-1}. ^{1}H NMR ($CDCl_3$): δ 2.22 (s, 3H), 4.35(s, 1H), 6.70-7.80 (m, 20H, aromatic). ^{31}P NMR (C_6D_6): δ -6.00 (s), -18.00(s). Anal. Calcd (found) for $C_{39}H_{24}Os_3O_{13}P_2$: C, 35.14 (34.77); H, 1.81 (1.82).

5.2.8. Isomerization of 1,2-$Os_3(CO)_{10}$(bmf) to 1,1-$Os_3(CO)_{10}$(bmf)

A Schlenk tube was charged with 0.20 g (0.15 mmol) of 1,2-$Os_3(CO)_{10}$(bmf) and 20 mL of toluene that was saturated with CO. The solution was then heated at 90 °C for the period of 24 h, after which time the solvent was removed under vacuum and the residue was separated by column chromatography over silica gel using 60% DCM in hexane to give 0.16 g (0.12 mmol) of 85:15 equilibrium mixture of 1,1-$Os_3(CO)_{10}$(bmf) and 1,2-$Os_3(CO)_{10}$(bmf). IR (CH_2Cl_2): *v*(CO) 2095 (vs), 2046 (vs), 2014 (vs) 2005 (vs), 1991 (m), 1977 (m) 1771 (s, furanone) cm^{-1}. ^{1}H NMR ($CDCl_3$): δ 2.82 (s, 3H), 4.74(s, 1H), 6.50-7.50 (m, 20H, aromatic). ^{31}P NMR (C_6D_6): δ 13.00 (s), 18.00(s).

5.2.9. Synthesis of $HOs_3(CO)_9$[μ-(PPh_2)C=C{$PPh(C_6H_4)$}$CH(OCH_3)OC(O)$]

To a 0.20 g sample of the thermally equilibrated 1,1-$Os_3(CO)_{10}$(bmf) and 1,2-$Os_3(CO)_{10}$(bmf) clusters was added 40 mL of dichloromethane in a Schlenk tube, followed irradiation with two Black lights for 7 days. The CO that accompanies the formation of hydride cluster was periodically removed by freeze-pump-thaw degas cycles to drive the reaction to completion. The sample was also briefly heated at 90 °C to drive the bridging isomer to chelating isomer during the course of this reaction. At the end of 7 days, the solvent was removed under vacuum and the residue was separated by column chromatography over silica gel using 60% dichloromethane in hexane to give inseparable mixture of

two diastereomers (80:20) of $HOs_3(CO)_9[\mu\text{-}(PPh_2)C{=}C\{PPh(C_6H_4)\}CH(CH_3)OC(O)]$ at 90% yield (0.18 g). IR (CH_2Cl_2): *v*(CO) 2087 (vs), 2071 (vs), 2044 (vs) 2019 (vs), 1985 (m), 1774 (s, furanone) cm^{-1}. ^1H NMR ($CDCl_3$): δ 2.72, 2.84 (s, 3H), 4.70, 4.80 (s, 1H), -16.20, -15.90 (AB q, μ2-hydride), 6.70-8.00 (m, 40H, aromatic). Anal. Calcd (found) for $C_{38}H_{24}Os_3O_{12}P_2$: C, 34.97 (34.61); H, 1.85 (1.86).

5.2.10. Synthesis of $HOs_3(CO)_9(\mu_3\text{-}C_6H_4)$ [μ_2,.^{1}-PPhC=C(PPh$_2$)CH(CH$_3$)OC(O)]

0.10 g (0.07 mmol) of cluster mixture of 1,1-$Os_3(CO)_{10}$(bmf) and 1,2-$Os_3(CO)_{10}$(bmf) was charged to a screw-capped NMR tube, followed by 0.7 mL of toluene-d_8. The NMR tube was heated at 120 °C and the progress of reaction was monitored by ^1H and ^{31}P NMR spectroscopy. Upon complete consumption of the starting cluster mixture, the solvent was removed under vacuum and the residue was separated by column chromatography over silica gel suing 60% dichloromethane in hexane. Yield: 95% (0.09 g). IR (CH_2Cl_2): *v*(CO) 2074 (vs), 2040 (vs), 2028 (vs) 2004 (vs), 1988 (m), 1770 (s, furanone) cm^{-1}. ^1H NMR ($CDCl_3$): δ 3.10, 2.70 (s, 3H), 5.50, 4.80 (s, 1H), -16.20, -16.00 (ABq, hydride ligand), δ 6.70-7.90 (m, 40H, aromatic). ^{31}P NMR (C_6D_6): δ -74.20, -78.50 (phosphido, d), 8.00 (d), 9.40 (d).

5.3. Kinetic Studies

5.3.1 Isomerization of $H_4Ru_4(CO)_{10}$(dppe) by UV-vis Spectroscopy

The UV-vis studies were carried out using a cluster concentration of ca. 10^{-4} M using 1.0 cm quartz UV-visible cells that were equipped with a high-vacuum Teflon stopcock to facilitate handling on the vacuum line. Fresh

solutions of 1,2-$H_4Ru_4(CO)_{10}$(dppe) were prepared either under argon or CO and used immediately before each kinetic measurement. All samples for UV-vis kinetic experiments were saturated with CO prior to heating. The Hewlett-Packard 8452A diode array spectrometer employed in our studies was configured with a variable-temperature cell holder and was connected to a VWR constant temperature circulator, allowing for the quoted temperatures to be maintained within ±0.5 °C. The UV-vis kinetics were monitored by following the decrease of the 300 nm absorbance band as a function of time typically for 4-6 half-lifes. The rate constants for the approach to equilibrium (k_e) were determined by non-linear regression analysis using the single exponential function:

$$A(t) = A_\alpha + \Delta A \times e(-k_e t) \quad (\mathbf{1})$$

5.3.2 Isomerization of $H_4Ru_4(CO)_{10}$(dppe) by ^{31}P NMR Spectroscopy

The ^{31}P NMR kinetics and equilibration experiments were carried out in 5 mm NMR tubes equipped with a J-Young valve for easy admission of argon. All NMR samples were freshly prepared by dissolving 50 mg of 1,2-$H_4Ru_4(CO)_{10}$(dppe) in 0.7 mL of dichloromethane-d_2, followed by deoxygenation via three freeze-pump-thaw cycles and final admission of CO to the tube. The NMR samples were heated in a VWR constant temperature circular bath. Samples for analysis were removed at the desired time and quenched in an ice/water bath immediately before NMR analysis. The relative molar ratio of 1,2- and 1,1-$H_4Ru_4(CO)_{10}$(dppe) was calculated on the basis of the integration values of each species relative to the total integration value of the both the isomers. The

data were analyzed and the rate to equilibrium (k_e) determined by non-linear regression analysis with Origin® software using a single exponential function.

5.3.3 Isomerization of $H_4Ru_4(CO)_{10}$(dppe) by ^1H NMR with Trapping Ligand

The ^1H NMR kinetic experiment was carried out in a 5 mm NMR tube. The NMR sample was prepared fresh by dissolving 40 mg of 1,2-$H_4Ru_4(CO)_{10}$(dppe) cluster and an internal standard (*tert*-butylbenzene) in 0.7 mL of dichloromethane-d_2. After three freeze-pump-thaw degassing cycles, the tube was flame sealed under vacuum. The NMR sample was heated in a VWR constant temperature circulator at the desired temperature regulated within ±0.5 °C. The extent thermolysis reaction was quenched by immersion of the NMR tube into an external ice bath prior to NMR analysis. The relative molar ratios of bridging and chelating isomers were calculated based on the integral value of the hydride ligand peak of each species relative to the internal standard. The first-order rate constants were determined by non-liner regression analysis.

5.3.4. Isomerization of $Os_3(CO)_{10}$(dppbz) and $Os_3(CO)_{10}$(bmf) by UV-vis Spectroscopy

The UV-vis kinetic studies were conducted by preparing a stock solution of 1,2-$Os_3(CO)_{10}$(P-P), having a concentration of ca. 1.0 x 10^{-4} M, prepared by dissolving ca. 6 mg of cluster in 50 mL of CO-saturated toluene under CO atmosphere. The stock solution, when not in use, was stored in the dark and under CO. All of the samples for UV-vis kinetic experiments were saturated with CO prior to heating to suppress the formation of the hydride-bridged cluster. The techniques used in the rate measurements are similar to those outlined in section

5.3.1.

5.3.5 Isomerization of $Os_3(CO)_{10}$(dppbz) and $Os_3(CO)_{10}$(bmf) in the Presence of Trapping Ligands by UV-vis Spectroscopy

A stock solution of 1,2-$Os_3(CO)_{10}$(P-P) (ca. 1.0 x 10^{-4} M) in 40 mL of benzene solution was treated with a measured excess of trapping ligand (PPh_3, $P(OEt)_3$). The solution containing only the trapping ligand was used as the blank for all the UV-vis measurements. The stock solution when not in use was stored in the dark and under argon. The kinetics were monitored by following the increases in the absorbance increase of the 1,1-isomer as a function of time for at least 3 half-lifes.

5.3.6 Isomerization of $Os_3(CO)_{10}$(bmf) by ^{1}H NMR Spectroscopy

The ^{1}H NMR kinetic and equilibration experiments were carried our in 5 mm NMR tubes equipped with a J-Young valve for the easy admission of CO gas. All NMR samples were prepared by dissolving 0.050 g of 1,2-$Os_3(CO)_{10}$(bmf) and a known molarity of internal standard (t-butyl benzene) in 0.7 mL of tolune-d_8, followed by deoxygenation by three freeze-pump-thaw degas cycles, after which 1 atm of CO was added to the tube. The NMR samples were heated in a VWR constant temperature circulator bath. Samples for the analysis were removed at the desired time and quenched in an external ice/water bath immediately before NMR analysis. The relative molar ratio of 1,2-$Os_3(CO)_{10}$(bmf) and 1,1-$Os_3(CO)_{10}$(bmf) was calculated on the basis of integral values of each species relative to the integral values of the internal standard (t-butyl benzene). The data were analyzed and the rate to equilibrium (k_e) determined by non-linear

regression analysis with Origin® software using a single exponential function (equation 1)

5.4. X-ray Crystallography

5.4.1 1,2-$Os_3(CO)_{10}$(dppbz)

Single crystals of 1,2-$Os_3(CO)_{10}$(dppbz).CH_2Cl_2 were grown from a CH_2Cl_2 solution containing a 75:15:10 mixture of bridging, chelating and hydride-bridged clusters, respectively, that had been layered with hexane. A suitable orange-red crystal was selected and the Mo Kα radiation used was monochromatized by a crystal of graphite. The reported X-ray data were collected on a Bruker SMART™ 1000 CCD-based diffractometer at 213 K. The frames were integrated with the available SAINT software package using a narrow-frame algorithm,[8] and the structure was solved and refined using the SHELXTL program package.[9] The molecular structure was checked by using PLATON,[10] and solved by direct methods with all nonhydrogen atoms refined anisotropically. All carbon-bound hydrogen atoms were assigned calculated positions and allowed to ride on the attached heavy atom, unless otherwise noted. Refinement converged at R = 0.014 and R_w = 0.032 for 8375 independent reflections with $I > 2\sigma(I)$.

5.4.2 1,1-$Os_3(CO)_{10}$(dppbz)

Single crystals of 1,1-$Os_3(CO)_{10}$(dppbz) suitable for X-ray diffraction analysis were grown from a dichloromethane solution of pure 1,1-$Os_3(CO)_{10}$(dppbz) that had been layered with hexane. An orange-yellow crystal of dimensions 0.29 x 0.23 x 0.21 mm^3 was selected and the Mo Kα radiation

used was monochromatized by a crystal of graphite. Intensity data were collected at 213 K in the variable scan speed mode on a bruker SMART^{TM} 1000 CCD-based diffractometer. The frames were integrated with the SAINT software package using a narrow-frame algorithm, and the structure was solved and refined using the SHELXTL program package. The hydrogen atoms were assigned calculated positions and allowed to ride on the attached heavy atom. Refinement converged at R = 0.0399 and R_w = 0.0485 for 8915 independent reflections with I>2σ(I).

5.4.3 $HOs_3(CO)_9[\mu\text{-}(PPh_2)C{=}C\{PPh(C_6H_4)\}C_4H_4]$ (9)

Single crystals of $HOs_3(CO)_9[\mu\text{-}(PPh_2)C{=}C\{PPh(C_6H_4)\}C_4H_4].CH_2Cl_2$ suitable for X-ray diffraction analysis were grown from a dichloromethane solution containing pure **9** that has been layered with ether. A yellow crystal of dimensions 0.24 x 0.17 x 0.06 mm^3 was selected. The X-ray data for were collected on an APEX II CCD-based diffractometer 100 K. The frames were integrated with the available SAINT and APEX II[12] software packages using a narrow-frame algorithm, and the structure was solved and refined using the SHELXTL program package[13]. The molecular structures were checked using PLATON[10], and all non-hydrogen atoms were refined anisotropically. All carbob-bound hydrogen atoms were assigned calculated positions and allowed to ride on the attached heavy atom. Despite the inability to locate the lone bridging hydride group during data refinement, the significantly different Os···Os bond distances allow to confidently assign the bridging hydride group to the longer

Os(1)·····Os(3) vector. The refinement for **9** converged at R = 0.0388 and R_w = 0.0748 for 14832 independent reflection with I > 2σ(I).

5.4.4 1,2-$Os_3(CO)_{10}$(bmf)

Single crystals of 1,2-$Os_3(CO)_{10}$(bmf) suitable for X-ray diffraction analysis were grown from a dichloromethane solution of pure 1,2-$Os_3(CO)_{10}$(bmf) that had been layered by toluene. A red crystal of dimensions 0.20 x 0.10 x 0.05 mm^3 was selected. Intensity data were collected at 295 K in the variable scan speed mode on an APEX II CCD-based diffractometer. The frames were integrated with the SAINT and APEX II software packages using a narrow-frame algorithm, and the structure was solved and refined using the SHELXTL program package. The hydrogen atoms were assigned calculated positions and allowed to ride on the attached heavy atom. Refinement converged at R = 0.0273 and R_w = 0.0659 for 11816 independent reflections with I > 2σ(I).

5.4.5 1,1-$Os_3(CO)_{10}$(bmf)

The single crystals of 1,1-$Os_3(CO)_{10}$(bmf) suitable for X-ray diffraction analysis were grown from a toluene solution containing a 85:15 mixture of 1,1-$Os_3(CO)_{10}$(bmf) and 1,2-$Os_3(CO)_{10}$(bmf) that had been layered with hexane. An orange crystal of dimensions 0.16 x 0.15 x 0.14 mm^3 was selected and the X-ray intensity data were measured at 100 K on a Bruker SMART APEX CCD area detector system equipped with a graphite monochromator and a Mo Kσ fine-focus sealed tube. It was observed that the crystal shows co-crystallization of both 1,2- and 1,1-$Os_3(CO)_{10}$(bmf). The structure of major major isomer (1,1-$Os_3(CO)_{10}$(bmf) ca. 85%) was solved and refined using the Bruker SHELXTL

(Version 6.1) software package and all non hydrogen atoms were refined anisotropically. The hydrogen atoms were assigned calculated positions and allowed to ride on the attached heavy atom. Refinement converged at R = 0.0750 and R_w = 0.1615 for 6873 independent reflections with I > 2σ(I).

5.4.6 $HOs_3(CO)_9(\mu_3\text{-}C_6H_4)$ [μ_2,.^{1}-PPhC=C(PPh_2)CH(OCH_3)OC(O)]

The single crystals of $HOs_3(CO)_9(\mu_3\text{-}C_6H_4)[\mu_2,\eta^1\text{-}PPhC{=}C(PPh_2)CH(CH_3)OC(O)]$ suitable for X-ray diffraction analysis were grown from a slow evaporation of a toluene/hexane solution containing $HOs_3(CO)_9(\mu_3\text{-}C_6H_4)[\mu_2,\eta^1\text{-}PPhC{=}C(PPh_2)CH(CH_3)OC(O)]$. A yellow-brown crystal was selected and the X-ray data for were collected on an APEX II CCD-based diffractometer at 215 K. The frames were integrated with the available SAINT and APEX II software packages using a narrow-frame algorithm, and the structure was solved and refined using the SHELXTL program package. The molecular structures were checked using PLATON, and all non-hydrogen atoms were refined anisotropically. The refinement was converged at R = 0.0174 and Rw = 0.0433 for 8182 independent reflection with I > 2σ(I).

5.5 Chapter References

1. Shriver, D.F. *The Manipulation of Air-Sensitive Compounds*, McGraw-Hill: New York, 1969.
2. Bruce, M.I.; Williams, M. L. *Inorg. Synth.* **1990**, *28*, 219.
3. Churchill, M.R.; Lashewycz, R.A.; Shapley, J.R.; Richter, S.I. *Inorg. Chem.* **1980**, *19*, 1277.
4. Drake, S.R.; Loveday, P.A. *Inorg. Synth.* **1990**, *28*, 230.

5. Nicholls, J.N.; Vargas, M.D. *Inorg. Synth.* **1989**, *26*, 289.
6. Fenske, D.; Becher, H.J. Chem. Ber. **1974**, *107*, 117.
7. Kuchen, W.; Buchward, H. *Chem. Ber.* **1959**, *92*, 227.
8. Saint Version 6.02; Bruker Analytical X-ray Systems, Inc., Madison, WI, 1997-1999.
9. SHELXTL Version 5.1; Bruker Analytical X-ray Systems, Inc., Madison, WI, 1998.
10. Spek, A.L. PLATON-A Multipurpose Crystallographic Tool; Utrecht University, Utrecht, The Netherlands, 2001.
11. Calvert, J.G.; Pitts, J.N. *Photochemistry*; Wiley: New York, 1966. (b) Parker, C.A. *Proc. R. Soc. London Ser. A* **1953**, *220*, 104
12. APEX2 Version 2.02, Bruker Analytical X-ray Systems, Inc. Copyright 2005, Madison, WI.
13. SHELXTL Version 6.14, Bruker Analytical X-ray Systems, Inc. Copyright 2003, Madison, WI.